# Perturbative analysis of operators under improved gradient flow in lattice QCD

**Störungstheoretische Analyse von Operatoren unter verbessertem Gradient Flows in Gitter-QCD**

Master thesis by Simon Stendebach (Student ID: 2702458)

Date of submission: 24.03.2022

1. Review: Prof. Guy D. Moore
2. Review: Prof. Jens Braun

Darmstadt

TECHNISCHE UNIVERSITÄT DARMSTADT

Physics Department
Institut für Kernphysik

## Erklärung zur Abschlussarbeit gemäß §22 Abs. 7 APB TU Darmstadt

Hiermit versichere ich, Simon Stendebach, die vorliegende Masterarbeit gemäß §22 Abs. 7 APB der TU Darmstadt ohne Hilfe Dritter und nur mit den angegebenen Quellen und Hilfsmitteln angefertigt zu haben. Alle Stellen, die Quellen entnommen wurden, sind als solche kenntlich gemacht worden. Diese Arbeit hat in gleicher oder ähnlicher Form noch keiner Prüfungsbehörde vorgelegen.
Mir ist bekannt, dass im Falle eines Plagiats (§38 Abs. 2 APB) ein Täuschungsversuch vorliegt, der dazu führt, dass die Arbeit mit 5,0 bewertet und damit ein Prüfungsversuch verbraucht wird. Abschlussarbeiten dürfen nur einmal wiederholt werden.
Bei einer Thesis des Fachbereichs Architektur entspricht die eingereichte elektronische Fassung dem vorgestellten Modell und den vorgelegten Plänen.

Darmstadt, 24.03.2022

Simon Stendebach

## Abstract

Quantum Chromodynamics, the study of quarks, gluons and their interaction, is a field yet to be fully understood. The strength of the coupling makes perturbative predictions less reliable than those of weakly coupled Quantum Electrodynamics. Therefore, based on the path integral formalism, lattice calculations were introduced and proven to be a powerful tool. However, the numerical results come with systematic deviations from the physical world that make it hard to extrapolate to the continuum limit. These can be reduced by choosing the lattice action and observable cleverly. Furthermore, lattice results are often very noisy, again making it hard to extract information. Gradient flow has proven to be a useful tool to resolve this problem. Its lattice formulation again suffers from systematic deviations that can be reduced via a more elaborate definition, the Zeuthen flow. In lattice studies, this improved gradient flow is used to measure color-electric as well as color-magnetic correlators which are expectation values of components of the QCD gauge field strength tensor. They contain information about propagation of heavy quarks in the quark-gluon plasma. Lattice perturbation theory is used in this work to derive their leading order behaviour which allows for easier extrapolation to the continuum and zero flow. In addition, the action density which can be used to measure the gauge coupling on the lattice is expanded in the lattice spacing for various combinations of action, flow and operator to both simplify continuum extrapolation and to see which combinations are to be preferred.

## Contents


**1. Introduction** **1**

**2. Quantum Chromodynamics in the path integral formalism** **1**
2.1. Path integral approach to quantization . . . 2
2.1.1. Euclidean time . . . 2
2.2. QCD in the continuum . . . 2
2.2.1. Local SU(3) gauge symmetry . . . 3
2.2.2. The continuum QCD action . . . 3

**3. QCD on the lattice** **4**
3.1. The gluonic action on the lattice . . . 4
3.2. Fourier transforms on the lattice . . . 7

**4. Symanzik improvement of the lattice gluon action** **8**
4.1. An introductory toy example . . . 8
4.2. Improving the lattice gluon action . . . 9

**5. Perturbation theory** **10**
5.1. Feynman diagrams . . . 12
5.2. Feynman rules for gluons . . . 12
5.3. Perturbative lattice QCD . . . 13
5.3.1. Feynman rules for lattice QCD . . . 15

**6. Gradient flow** **15**
6.1. Perturbation theory of gradient flow . . . 17
6.2. Gradient flow on the lattice . . . 18
6.2.1. Improved gradient flow . . . 19
6.2.2. Solving the the lattice flow equation to leading order . . . 20

**7. Color-electric and color-magnetic correlation functions on the lattice** **21**
7.1. Thermal baths as a time cut-off . . . 21
7.2. Relevance of color-electric and color-magnetic correlators for heavy quark behaviour in the QGP . . . 22
7.3. Leading order analysis of color-electric and -magnetic correlators under flow . . . 24
7.3.1. Flowed color-electric correlator in leading order perturbation theory . . . 25
7.3.2. Flowed color-magnetic correlator in leading order perturbation theory . . . 26

**8. Lattice deviations of action density** **28**
8.1. Definitions of the action density on the lattice . . . 29
8.2. Expansion of action density in the lattice spacing . . . 30

**9. Conclusion and Outlook** **32**

**A. Expansion of Wilson and Lüscher-Weisz action to leading order** **34**

**B. Expansion of $G_E$ and $G_B$ on the lattice** **35**
B.1. Analytical solution for $G_E$ and $G_B$ on the lattice with Wilson action and flow . . . 39

**C. Action density integrations and notation** **40**
C.1. Notation of lattice momenta . . . 41
C.2. Analytical solution for Wilson-Wilson-Wilson . . . 41

**D. Derivation of naive and improved clover kernel** **42**

## 1. Introduction

Quantum Chromodynamics (QCD), the theory of strongly interacting particles such as quarks, gluons and their dynamics, is a highly fascinating field due to plenty of non-trivial phenomena such as confinement and the running coupling. At the beginning of the century, at the Relativistic Heavy Ion Collider of the Brookhaven National Laboratory, a new phase of strong-interacting matter, the quark-gluon plasma (QGP) was discovered after its existence has been speculated for years. At extreme conditions such as high temperatures and pressure, quarks can propagate freely instead of being bound in hadrons. The QGP can be modeled by hydrodynamics to describe the propagation of heavy quarks. Hydrodynamics requires input parameters such as the momentum diffusion coefficient which, according to heavy quark effective theory, can be determined by analysing color-electric and -magnetic correlation functions of the gluon fields. Hence, these observables are the main subject of this work. Color-electric and -magnetic fields are components of the QCD field strength tensor and, in a classical picture, describe the force acting on a quark. In contrast to the weakly coupled Quantum Electrodynamics, perturbation theory often fails because the coupling in QCD is too large. Therefore, another approach to determine correlators had to be developed: Introducing a lattice, space-time is discretised, and by considering the path integral approach to quantization, correlation functions of operators can be computed non-perturbatively.

Discretization of the quark and gluon fields is neither trivial nor unique. Therefore, one has to be careful to find an approach that is best suited for the considered problem. Since the lattice approach is an approximation, systematic deviations from the continuum occur. These vanish in the continuum limit. However, approaching it with finer and finer lattices is computationally very costly and hence not always feasible. The lattice artefacts can be reduced by taking advantage of the fact that the discretization is not unique, more precisely, by choosing lattice action and operators in a clever way. This way, the continuum extrapolation is more accessible. In addition, correlation functions obtained by lattice calculations do not always have a good signal-to-noise ratio which makes it hard to extract physical information. Resolving this problem by brute force, namely increasing the number of configurations generated to measure the correlation function, is computationally costly, so further methods had to be developed. One of them is gradient flow, a tool that smears fields and suppresses ultraviolet contributions in a gauge-invariant way. In the continuum, gradient flow is defined with a heat equation but has to be discretized as well to make use of it on the lattice. Again, this is not unique and lattice artefacts can be reduced with the proper discretization. This leads to Zeuthen flow, an improved version of lattice gradient flow. Obviously, gradient flow changes correlation functions. It is therefore necessary to extrapolate to no flow. To simplify this procedure, it is helpful to determine correlation functions measured on the lattice to leading order in lattice perturbation theory. While the leading order correlators bear little physical insight by themselves, they can be used for tree-level improvement, that is normalising the lattice data with the perturbative result which simplifies extrapolation not only to zero flow but also to the continuum.

Another issue in lattice measurements that needs resolving is determining the gauge coupling since it is not an input parameter. Using gradient flow, this can be done by measuring the action density. Knowing its leading order perturbative behaviour or at least its expansion coefficients in the lattice spacing can facilitate the extraction of the gauge coupling from the measured observable and help to find the most practical definition of the action density on the lattice.

The goal of this work is to derive leading order correlation functions of QCD operators on a lattice under gradient flow. The key methods are introduced in the following sections. First, the path integral approach to quantization as well as continuum QCD will be introduced in Sect. 2. In Sect. 3, this theory will be adapted to the lattice, followed by Sect. 4 where improvement of lattice theories, especially QCD, is explained. In Sect. 5, perturbation theory is outlined. Emphasis is on Sect. 5.3 which describes the applications and Feynman rules of perturbative lattice QCD. Sect. 6 introduces gradient glow, first in the continuum, then its different realizations on the lattice in Sect. 6.2. In Sect. 6.2.2, it is outlined how to solve the lattice flow equation to leading order and how it influences propagators. Sect. 7 finally explains the role of color-electric and color-magnetic correlation functions to the QGP. Their leading order contributions under Zeuthen flow - the main results of this work - are presented in Sect. 7.3. Sect. 8 introduces the action density, its role in lattice calculations and how to calculate its expansion coefficients in the lattice spacing under lattice perturbation theory and gradient flow. Some of these coefficients are then listed in Sect. 8.2, another result of this work. Finally, Sect. 9 summarizes this work and gives an outlook about possible further developments.

## 2. Quantum Chromodynamics in the path integral formalism

Quantum Chromodynamics is the theory of the strong interaction and the particles it couples to, quarks and gluons. Like all quantum field theories, it can be described in the path integral formalism. How this is done will be discussed in the following section. The path integral approach allows for lattice studies of QCD as well as emphasizes parallels to statistical mechanics. For some theories such as Quantum Electrodynamics the path integral approach is a mere alternative to other formulations such as perturbation theory. For QCD however, this is not always valid, so the path integral formalism is of paramount importance there.

## 2.1. Path integral approach to quantization

Consider a free scalar field $\phi(x)$ where $x$ is a point in Minkowski space-time. Information about the theory and physical quantities are stored in correlation functions $\langle\phi(x_1)\phi(x_2)...\phi(x_n)\rangle$ which are vacuum expectation values. The dynamics of the field are described by its Lagrangian density $\mathcal{L}(\phi(x))$ or, equivalently, by the action $S[\phi]$. The action is the space-time integral over the Lagrangian density,

$$S[\phi] = \int \mathrm{d}^4x \mathcal{L}(\phi(x)), \tag{2.1}$$

and is hence a functional that depends on the field's configuration, meaning on the combination of values on every space-time point $x$. In classical physics, Hamilton's principle holds: The only contributing configuration $\phi_{\text{class}}$ is the one where the action is extremal,

$$\delta S[\phi_{\text{class}}] = 0. \tag{2.2}$$

In quantum field theories, that does not hold: Each configuration contributes to correlation functions with the weight of its contribution depending on its action. The correlation function is then given by the weighted average over all possible configurations:

$$\begin{aligned} \langle\phi(x_1)\phi(x_2)...\phi(x_n)\rangle &= Z^{-1}\int \mathcal{D}\phi e^{iS[\phi]}\phi(x_1)\phi(x_2)...\phi(x_n), \\ Z &= \int \mathcal{D}\phi e^{iS[\phi]}, \end{aligned} \tag{2.3}$$

where $Z$ acts as a normalization constant to ensure $\langle 1\rangle = 1$ and $\exp iS[\phi]$ is the weight factor. The integration measure $\mathcal{D}\phi = \prod_y \mathrm{d}\phi(y)$ in Eqs. (2.3) is to be understood symbolically as $y$ runs over all of space-time so there is an infinite number of factors involved. In fact, the path integral is usually derived as the limit of a finite number of steps. The integration measure therefore implies considering every possible value at each point. At first glance, this seems like an overwhelming task, as one needs to consider infinitely many values at an infinite number of points. Analytically, this is indeed only possible for a few select cases such as the harmonic oscillator, so numerical methods are necessary [1].

### 2.1.1. Euclidean time

Having a closer look at Eq. (2.3), one might notice another problem. The weight $\exp iS[\phi]$ is a periodic function of $S$, meaning that configurations that have large actions won't be suppressed. This makes numerical calculations a whole lot more complicated as one can't neglect any exotic configurations. The solution to this problem is a Wick rotation: One rotates the real time coordinate $t$ into imaginary time via

$$t \to \tau = -it. \tag{2.4}$$

This transforms Minkowski space-time into Euclidean space-time, so all metric tensors $g_{\mu\nu}$ are replaced by $\delta_{\mu\nu}$. Substituting Eq. (2.4) into $S[\phi]$, a new Euclidean action $S_E[\phi]$ is obtained. The relation between both is

$$iS[\phi] = -S_E[\phi]. \tag{2.5}$$

Considering now the weight in the path integral, configurations with large Euclidean action are exponentially suppressed if $S_E$ is positive definite. This renders Monte Carlo simulations to calculate Euclidean correlation functions feasible by choosing an appropriate probability distribution [2]. Additionally, a similarity between quantum field theories and statistical mechanics can be observed: One might consider the normalization factor $Z$ in Eq. (2.3) as the partition function of a canonical ensemble. This allows methods from statistical mechanics to be used in QFT studies. A few more details on that can be found in Sect. 7.1. Furthermore, Euclidean space-time has major applications in equilibrium physics as well as the study of thermal ensembles. Euclidean space-time will be considered in this work if not stated otherwise, therefore, the index $E$ for the action will be dropped.

## 2.2. QCD in the continuum

In the theory of strong interaction, Quantum Chromodynamics, multiple fields are at play: The matter field $\Psi$, its conjugate $\overline{\Psi}$ as well as a gauge field $A_\mu$. While the former describe quarks, the latter describes gluons which mediate the strong force. The quark field has four Dirac, six flavour and three colour components which results in a total of 72 components. Meanwhile, the gluon field has four Lorentz and eight free colour-anticolour components, making 32 total [3].

### 2.2.1. Local SU(3) gauge symmetry

The following discussion will be based on the standard textbooks Refs. [1, 3] albeit in Euclidean instead of Minkowski space-time. An important property of QCD is a local SU(3) gauge symmetry in colour space, which can be used to construct the action $S_{\text{QCD}}[\Psi, A_\mu]$. SU(3) is the group of all unitary $3 \times 3$ matrices with determinant 1. As it is a Lie group, its elements $G$ can be described by

$$G = e^{i \sum_{A=1}^{8} \epsilon^A T^A}, \tag{2.6}$$

where the generators $T^A$ are a basis of the Lie algebra in the fundamental representation and $\epsilon^A$ are their coefficients. The Lie algebra $\mathfrak{su}(3)$ is eight-dimensional - this is why the sum in the exponent of Eq. (2.6) runs from 1 to 8 - and equivalent to traceless hermitian $3 \times 3$ matrices. The fundamental representation of the $T^A$ is

$$T^A = \lambda^A/2, \tag{2.7}$$

where $\lambda^A$ are the Gell-Mann matrices. This specific but not unique choice of representation results in a normalization of

$$\text{Tr}(T^A T^B) = \frac{1}{2}\delta^{AB}. \tag{2.8}$$

In addition, the commutator relation

$$[T^A, T^B] = \sum_{C=1}^{8} i f^{ABC} T^C \tag{2.9}$$

holds, where $f^{ABC}$ is the total anti-symmetric SU(3) structure constant. It is independent of the group's representation. The structure constant may be used to define another representation of the group, the adjoint representation with generators

$$(t^A)^{BC} = -i f^{ABC}. \tag{2.10}$$

Hence, the $t^A$ are $8 \times 8$ matrices. Eq. (2.9) shows that QCD is non-abelian: Different group elements do not commute, so their order is important. This adds a lot of complexity to the theory. Sums over repeated colour indices will be understood in the following and not be written down as explicitly as in Eqs. (2.6) and (2.9). While the quark fields transform according to

$$\Psi(x) \to G(x)\Psi(x), \tag{2.11}$$

$$\overline{\Psi}(x) \to \overline{\Psi}(x)G^\dagger(x) \tag{2.12}$$

under a gauge transformation represented by $G(x) \in$ SU(3), the gluon fields are Lie-algebra valued and transform as

$$A_\mu(x) \to G(x)A_\mu(x)G^\dagger(x) + i(\partial_\mu G(x))G^\dagger(x). \tag{2.13}$$

Note that the SU(3) group elements depend on $x$: Each point in space-time is transformed differently, so it is a local gauge transformation and not a global one.

### 2.2.2. The continuum QCD action

The need of local SU(3), CPT (charge, parity and time) and Lorentz invariance is the guiding principle behind the determination of the action. It was first formulated in Ref. [4]. The terms that fulfil these requirements can be found using Eqs. (2.11) to (2.13) and by making sure they are covariant. It is convenient to split the action in a fermionic part describing the quark fields and its interaction with the gluons and a purely gluonic part. The former is

$$S_F^{\text{cont}}[\Psi, A] = \sum_{f=1}^{6} \int \mathrm{d}^4x \overline{\Psi}^{(f)}(x)\Big(\gamma_\mu D_\mu + m^{(f)}\Big)\Psi^{(f)}(x) \tag{2.14}$$

with $f$ being the flavour index, the gamma matrices $\gamma^\mu$, the covariant derivative $D_\mu = \partial_\mu + ig_0 A_\mu(x)$ and the strong coupling $g_0$. The gluonic part of the action is

$$S_g^{\text{cont}}[A] = \frac{1}{2}\int \mathrm{d}^4x \,\text{Tr}\, F_{\mu\nu}(x)F_{\mu\nu}(x) = \frac{1}{4}\int \mathrm{d}^4x F^A_{\mu\nu}(x)F^A_{\mu\nu}(x) \tag{2.15}$$

with

$$F_{\mu\nu}(x) = \partial_\mu A_\nu(x) - \partial_\nu A_\mu(x) + ig_0[A_\mu(x), A_\nu(x)] \tag{2.16}$$

being the gluon field strength tensor and $F^A_{\mu\nu}(x)$ being its colour components as defined by expanding in the Lie algebra basis according to $F_{\mu\nu}(x) = F^A_{\mu\nu}(x)T^A$. Summation over Lorentz indices is to be understood in Eqs. (2.14) and (2.15) and will be in the following if not stated otherwise. Note that in Euclidean space-time it does not matter whether Lorentz indices are super- or subscripted. The last term in the field strength tensor is a necessity to ensure gauge invariance as SU(3) group elements do not

commute and therefore does not emerge in abelian theories. It is straightforward to check that these expressions are invariant under the transformations Eqs. (2.11) to (2.13) as well as CPT conjugation. Additionally, they are covariant and therefore invariant under Lorentz transformations. The total QCD action is then given by

$$S_{\text{QCD}}^{\text{cont}}[\Psi, A] = S_F^{\text{cont}}[\Psi, A] + S_g^{\text{cont}}[A]. \tag{2.17}$$

In this work, the focus will be the gluonic part of the action. Having a closer look at Eq. (2.15), one can see that the commutator in $F_{\mu\nu}$ adds terms that are cubic and quartic in the gluon field to the action, meaning that there is three- and four-gluon coupling. That is a major difference between QCD and abelian theories such as quantum electrodynamics (QED) as those do not have the commutator in the field strength tensor. Unlike photons - the gauge bosons in QED -, gluons have a self-interaction with each other due to these additional terms. These interactions have major consequences on the theory's phenomenology, for example the running coupling where the coupling constant's value $g_0$ decreases with the energy scale.

## 3. QCD on the lattice

The actions obtained in Sect. 2.2 can now be used to calculate correlation functions. If $\Gamma[\Psi, \overline{\Psi}, A]$ is a functional of the quark and gluon fields, its vacuum expectation value is then, generalizing Eqs. (2.3),

$$\begin{aligned} \left\langle \Gamma[\Psi, \overline{\Psi}, A] \right\rangle &= Z^{-1} \int \mathcal{D}\Psi \mathcal{D}\overline{\Psi} \mathcal{D}A e^{-S_{\text{QCD}}[\Psi, \overline{\Psi}, A]} \Gamma[\Psi, \overline{\Psi}, A], \\ Z &= \int \mathcal{D}\Psi \mathcal{D}\overline{\Psi} \mathcal{D}A e^{-S_{\text{QCD}}[\Psi, \overline{\Psi}, A]}. \end{aligned} \tag{3.1}$$

The integration measures contain all flavour, colour, Dirac and Lorentz components, so a large number of fields has to be considered. As this cannot be solved analytically, one needs to resort to numerical methods. However, there is an infinite number of configurations each defined on a set with an infinite number of points, hence infinite integrations have to be performed. Obviously, this is not feasible for computers. Perturbation theory as will be described in Sect. 5 is furthermore not always reliable for QCD. Many phenomena such as confinement - the fact that only colour-neutral states such as protons, neutrons or pions are observed - cannot be described this way, so a different approach is needed. For this, a lattice with sites $n$ and spacing $a$ is now introduced as first proposed by K. Wilson in Ref. [5]. The actual physical position of a site is then $x = an$. Considering a finite volume with boundary conditions, only a finite number of lattice sites exists and hence a finite amount of integrations is necessary to calculate correlation functions, making Monte Carlo simulations feasible. The idea is to calculate observables for smaller and smaller $a$ so that continuum physics can be extrapolated from fine enough lattices. However, the action on the lattice is different from the one in the continuum because notions such as the derivative are only defined in the continuum and look different on the lattice. This will be discussed hereafter, following the standard textbooks Refs. [6, 7, 8]. Obviously, in the continuum limit $a \to 0$, the continuum action $S_{\text{QCD}}^{\text{cont}}$ should be obtained. The choice of a lattice action is not unique as there are plenty possible discretizations that have the same continuum limit. In this work, the fermionic part of the action is of no importance, so it will not be discussed in detail. However, some aspects of it can be mentioned to motivate the pure-gauge lattice action, which will be derived in this section.

### 3.1. The gluonic action on the lattice

The quark fields $\Psi(n)$ reside on the lattice sites. The continuum fermion action Eq. (2.14) contains terms such as $\overline{\Psi}\gamma_\mu \partial_\mu \Psi$. A naive discretization of the derivative $\partial_\mu \Psi$ is the right-handed lattice derivative

$$\partial_\mu^R \Psi(n) = \frac{\Psi(n + \hat{\mu}) - \Psi(n)}{a} \tag{3.2}$$

with the vector $\hat{\mu}$ of length $a$ pointing to the next neighbour in $\mu$ direction. Hence, by substituting $\partial_\mu$ by $\partial_\mu^R$, one expects to find terms such as $\overline{\Psi}(n)\gamma_\mu \Psi(n + \hat{\mu})$ in the lattice fermion action. As the gamma matrix plays no role in the following, it will be ignored. The bilinear form $\overline{\Psi}(n)\Psi(n + \hat{\mu})$ is not invariant under the local SU(3) transformations Eqs. (2.11) and (2.12) as it transforms to

$$\overline{\Psi}(n)\Psi(n + \mu) \to \overline{\Psi}(n) G^\dagger(n) G(n + \hat{\mu}) \Psi(n). \tag{3.3}$$

Consequently, this term is not suitable for a lattice action as local SU(3) invariance is again required. To compensate for this, one introduces a new degree of freedom $U_\mu(n) \in$ SU(3) that resides on the path connecting both neighbouring lattice sites $n$ and $n + \hat{\mu}$ as illustrated in Fig. 1. It is referred to as link variable or simply link. If one inserts it in the considered bilinear form, it gives

$$\overline{\Psi}(n) U_\mu(n) \Psi(n + \hat{\mu}). \tag{3.4}$$

Now one can define the link variable's transformation as

$$U_\mu(n) \to G(n) U_\mu(n) G^\dagger(n + \hat{\mu}). \tag{3.5}$$

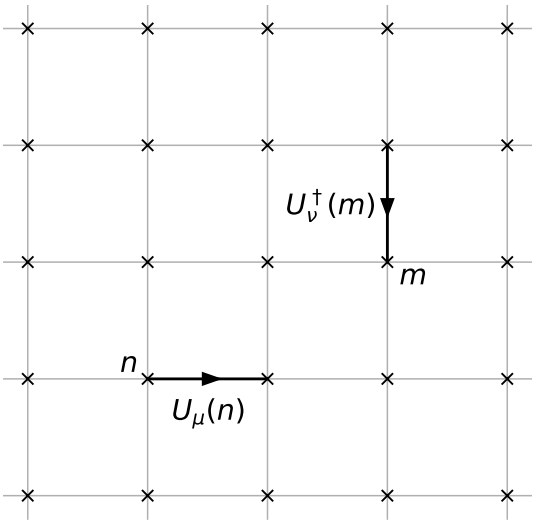


Figure 1: Representation of two link variables $U_\mu(n)$ and $U_\nu^\dagger(m)$. They are SU(3) group elements and connect two lattice sites.

When transforming Eq. (3.4), the group elements then cancel, so this term is gauge invariant and a suitable candidate for the lattice fermion action. From this consideration, it also follows that

$$U_{-\mu}(n+\hat{\mu}) = U_\mu^\dagger(n). \tag{3.6}$$

The link variables $U_\mu(n)$ are closely related to the continuum gauge field $A_\mu$ as will be explained now. In the continuum, it is known that the Schwinger line integral

$$U(x,y) = e^{ig_0 \int_x^y \mathrm{d}z_\mu A_\mu(z)} \tag{3.7}$$

transforms according to

$$U(x,y) \to G(x)U(x,y)G^\dagger(y) \tag{3.8}$$

which is the continuum equivalent of Eq. (3.5) and thus seems like the continuum analogue to the link. On the lattice, one can replace the integral in the Schwinger line integral by the factor $aA_\mu(n)$, therefore, the link variable can be identified as

$$U_\mu(n) = \exp iag_0 A_\mu(n). \tag{3.9}$$

Indeed, performing a small $a$ expansion,

$$U_\mu(n) \approx 1 + iag_0 A_\mu(n), \tag{3.10}$$

the continuum limit of Eq. (3.4) yields a term that corresponds to the fermion-gluon coupling in Eq. (2.14). This consideration illustrates that the link variables $U_\mu(n)$ play the role of the gluon field $A_\mu$, but there is a major structural difference: The link is a SU(3) group element while the continuum field is part of the corresponding Lie algebra. To justify that despite this difference the links are indeed the right choice to describe the gauge degree of freedom in a rigorous way, one needs to deep dive into the mathematical foundations of gauge theory and understand what gauge fields truly are. In a topological sense, they are connections on a principle bundle, that is they describe how the colour value - or in the QED case the phase - changes when particles move through position space. This property is called parallel transport. The links do the same on the lattice, so they are the right discretization of the gluon field. For more details on the topological background of gauge theories, consider Refs. [9, 10].

It is now necessary to construct a gauge invariant action that describes the dynamics of the link variables. It is supposed to approach the continuum gluon action Eq. (2.15) in the limit $a \to 0$. To achieve this, consider an arbitrary closed path $\mathcal{C}_n$ starting and ending on site $n$ on the lattice, see Fig. 2. Now define the product of link variables,

$$U(\mathcal{C}_n) = \prod_{(m,\mu)\in\mathcal{C}_n} U_\mu(m), \tag{3.11}$$

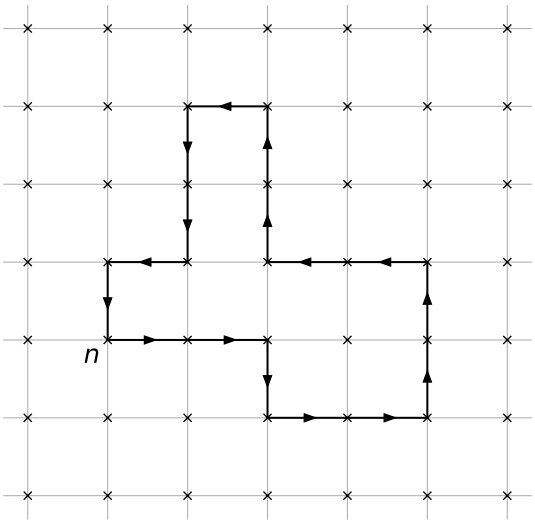


Figure 2: An arbitrary closed path on the lattice. The product of the links along the path can be used to construct a lattice action.

along this path. Note that this is still an element of SU(3). Its trace in colour space is invariant under SU(3) transformations according to Eq. (3.5) and the cyclicity of the trace. Hence, it might be suitable for the action. Indeed, using Eq. (3.10) and

$$\lim_{a\to 0} \frac{f(n+\hat{\mu}) - f(n)}{a} = \partial_\mu f(n), \tag{3.12}$$

the action

$$S_{\mathcal{C}}[U] = \frac{2c_{\mathcal{C}}}{g_0^2} \sum_{\mathcal{C}_n} \mathrm{Re}\,\mathrm{Tr}(1 - U(\mathcal{C}_n)) \tag{3.13}$$

where the sum runs over all paths $\mathcal{C}_n$ of type $\mathcal{C}$ gives the appropriate continuum limit with a correctly chosen coefficient $c_{\mathcal{C}}$. The overall factor 2 is convention. Note that technically, the operation $1 - U(\mathcal{C}_n)$ is not defined since the second term is a SU(3) object where no sum is defined. However, the trace is taken and the linearity of the trace for matrices justifies this somewhat sloppy notation. This will come up repeatedly in this work, so whenever SU(3) elements are summed, the trace will be taken at some point later on. The simplest path is a square in the $\mu - \nu$ plane, the so-called plaquette $P$ with

$$P_{\mu\nu}(n) = U(P_n) = U_\mu(n) U_\nu(n+\hat{\mu}) U_\mu^\dagger(n+\hat{\nu}) U_\nu^\dagger(n). \tag{3.14}$$

Choosing $c_P = 1$ yields the so-called Wilson action

$$\begin{aligned} S_P[U] &= \frac{2}{g_0^2} \sum_{P_n} \mathrm{Re}\,\mathrm{Tr}(1 - U(P_n)) \\ &= \frac{1}{g_0^2} \sum_{\substack{n\mu\nu \\ \mu\neq\nu}} \mathrm{Re}\,\mathrm{Tr}(1 - P_{\mu\nu}(n)) \end{aligned} \tag{3.15}$$

which is the easiest possible choice for a lattice gauge action. The factor 2 disappears in the second step since the plaquette is oriented and it is sufficient to sum over all squares with $\mu < \nu$. The sum in the second line of Eq. (3.15), however, also accounts for pairs $\mu > \nu$, so an additional factor of $1/2$ is necessary. Another, slightly more complex path is the rectangle $R$ with

$$R_{\mu\nu}(n) = U(R_n) = U_\mu(n) U_\mu(n+\hat{\mu}) U_\nu(n+2\hat{\mu}) U_\mu^\dagger(n+\hat{\mu}+\hat{\nu}) U_\mu^\dagger(n+\nu) U_\nu^\dagger(n). \tag{3.16}$$

Plugging this into Eq. (3.13) again defines a lattice action $S_R$ with the proper continuum limit. Both paths are shown in Fig. 3. Note that for the rectangle, unlike the plaquette, it is necessary to consider both cases $\mu < \nu$ as well as $\mu > \nu$ as rectangles that extend for two lattice units in the $\mu$ direction give a different contribution than those that extend for two lattice units in the $\nu$ direction. The reason why more complicated paths can be helpful will be explained in Sect. 4.

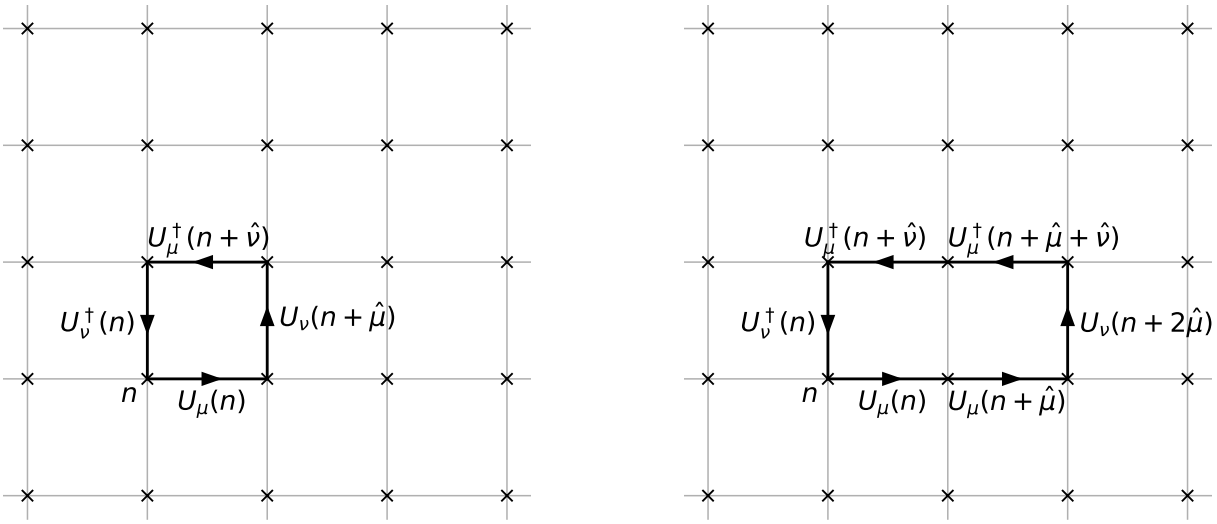


(a) Plaquette

(b) Rectangle

Figure 3: The path of the plaquette and the rectangle on the lattice and the contributing link variables

The fact that in the continuum, the gluon degrees of freedom are the algebra-valued fields $A_\mu$, while on the lattice, they are the group-valued link variables $U_\mu$, has consequences for the path integral. On the lattice, one needs to integrate over all possible links instead of fields. The group is a compact manifold, so conveniently, the integration range is reduced. For integration on a group, one needs an appropriate gauge invariant measure. In the SU(3) case, this is the Haar measure. Gauge invariance yields another simplification on the lattice: Configurations that only differ by a local transformation give the same contribution to a correlator. In consequence, it is sufficient to consider only one of the equivalent configurations in the path integral which can be achieved by fixing the value of some link variables, making less integrations necessary - varying the remaining, unfixed links is enough.

## 3.2. Fourier transforms on the lattice

Similar to the continuum, it is often helpful to perform lattice calculations in momentum space. Hence, lattice Fourier transforms of the gluon fields need to be defined. As distances smaller than $a$ cannot be resolved, the lattice causes a momentum cut-off

$$-\frac{\pi}{a} < p_\mu \leqslant \frac{\pi}{a} \tag{3.17}$$

to the so-called Brillouin zones BZ. Consequently, the finite lattice spacing acts as a regulator. At finite volume and lattice size $L$, the Fourier transforms include sums $a^{-4}\sum_p$ as the only allowed momenta are

$$(k_n)_\mu = \frac{2\pi n_\mu}{L}, \quad n_\mu = -\frac{L}{2a}+1, ..., 0, ..., \frac{L}{2a} \tag{3.18}$$

due to boundary conditions. In perturbation theory however, an infinite volume is assumed, therefore these sums transition into momentum integrals $\int_{\mathrm{BZ}} \frac{\mathrm{d}^4 p}{(2\pi)^4} \equiv \int_p$. This abbreviation will be frequently used in this work, even in the continuum case, where the integration range is replaced by $\mathbb{R}^4$. The gluon field's Fourier transform may now be defined as

$$A_\mu(a) = \int_p e^{ipa(n+\hat{\mu}/2a)} \tilde{A}_\mu(p). \tag{3.19}$$

Emphasis is on the displacement $ip_\mu a/2$ in the exponent. It essentially redefines the center of the links being in between two lattice sites instead of being exactly on one. This has two advantages: First of all, a phase factor will be cancelled in numerous calculations.

In addition, a redefinition of the link location removes deviations from the continuum limit that are of odd order. This will come in handy in Sect. 4. Lastly, the momentum delta function on the lattice is given by

$$\delta^{(4)}(p) = \frac{a^4}{(2\pi)^4} \sum_n e^{ipan}. \tag{3.20}$$

It is periodic in $p$ with periodicity $2\pi/a$. This is in agreement with the fact that momentum integrals extend only over a single Brillouin zone - larger momenta are redundant. The periodicity will additionally manifest itself in momentum integrals as trigonometric functions.

## 4. Symanzik improvement of the lattice gluon action

The discretization of space-time has many advantages such as momentum regularization and opening the door for Monte Carlo simulation. However, it comes at the price of lattice artefacts in calculated correlation functions since the lattice formulation of QCD differs from the continuum one as seen in the previous section. These artefacts should vanish with $a \to 0$, but the true continuum limit can never be achieved, and considering small $a$ is computationally very costly as the number of considered lattice sites then increases. Therefore, it is sensible to keep discretization errors as small as possible. Improvement for lattice theories was first introduced by K. Symanzik in Refs. [11, 12]. How it works for gauge theories is the topic of this section and the general idea will be introduced using a toy example.

### 4.1. An introductory toy example

Approximations for the derivative are not unique - different ones can still have the same continuum limit. They differ by the considered points. First, define the common difference quotient

$$\tilde{\partial}^1 f(0) = \frac{f(a) - f(-a)}{2a} \tag{4.1}$$

for an analytical function $f$. To check how it differs from the derivative, one inserts the Taylor expansion

$$f(a) = f(0) + af'(0) + \frac{a^2}{2} f''(0) + \frac{a^3}{6} f'''(a) + \mathcal{O}(a^4), \tag{4.2}$$

which gives

$$\tilde{\partial}^1 f(0) = f'(0) + \frac{a^2}{6} f'''(0) + \mathcal{O}(a^4), \tag{4.3}$$

so the derivate and difference quotient differ dominantly by $\mathcal{O}(a^2)$. To remove this discretization artefact, one considers another approximation for the derivative, for example

$$\begin{aligned} \tilde{\partial}^2 f(0) &= \frac{f(2a) - f(-2a)}{4a} \\ &= f'(0) + \frac{2a^2}{3} f'''(0) + \mathcal{O}(a^4). \end{aligned} \tag{4.4}$$

In the second step, the Taylor expansion was employed again. Now one searches for a linear combination $\tilde{\partial} \equiv c_1\tilde{\partial}^1 + c_2\tilde{\partial}^2$ where the dominating deviation is of $\mathcal{O}(a^4)$. Inserting Eqs. (4.3) and (4.4) into the definition of $\tilde{\partial}$ and demanding

$$\tilde{\partial} f(0) = f'(0) + \mathcal{O}(a^4) \tag{4.5}$$

yields

$$c_1 + c_2 = 1, \tag{4.6}$$

$$\frac{1}{6}c_1 + \frac{2}{3}c_2 = 0. \tag{4.7}$$

The solution $c_1 = 4/3,\ c_2 = -1/6$ defines an approximation $\tilde{\partial}$ for the derivative that is free of $\mathcal{O}(a^2)$ cut-off effects. The first deviation is of $\mathcal{O}(a^4)$, so the continuum limit is obtained faster if $a$ decreases. This is precisely what was to be achieved.

## 4.2. Improving the lattice gluon action

The general considerations from Sect. 4.1 can be translated into the gauge field case by taking advantage of the fact that the lattice action is not unique. One therefore constructs a linear combination of different approximations of the continuum gluon action $S_g^{\text{cont}}$ to remove lattice artefacts of lower order. As in the toy example, these actions involve lattice sites at different distances from a considered point. Two candidates that fulfil these properties were already presented in Sect. 3.1, the Wilson plaquette and the rectangle action. These can be used to construct an action where the leading order deviation from the continuum limit is suppressed. To do this, there are two different approaches: The first one is similar to the toy example, defining an approximation and inserting continuum expressions. In the gauge field case, this corresponds to plugging the Schwinger line integral Eq. (3.7) into the plaquette or rectangle action. This method was followed in Ref. [13]. Another, in this case simpler approach is to use the lattice expression Eq. (3.9) but transforming to momentum space. The latter approach was used in Ref. [14] and will also be followed here. In this work, only contributions in leading order of $g_0$ will be considered. In this approximation and for the considered purposes, QCD is equivalent to abelian theories such as QED, and they only differ by a colour factor of $8$ as this is the dimension of the Lie algebra $\mathfrak{su}(3)$.

First, consider the Wilson action, Eq. (3.15). As a product of group elements, a closed path can be written as

$$U(\mathcal{C}_n) = e^{iag_0 A_\mathcal{C}(n)} \tag{4.8}$$

with $A_\mathcal{C}(n)$ being algebra-valued. Inserting this into Eq. (3.13) and expanding the exponential in $a$ gives

$$\begin{aligned} S_\mathcal{C}[U] &= 2c_\mathcal{C} \sum_{\mathcal{C}_n} \frac{a^2}{2} \operatorname{Tr} A_\mathcal{C}(n)^2 + \mathcal{O}(g_0^2) \\ &= \frac{c_\mathcal{C} a^2}{2} \sum_{\mathcal{C}_n} A_\mathcal{C}^B(n) A_\mathcal{C}^B(n) + \mathcal{O}(g_0^2), \end{aligned} \tag{4.9}$$

where $A_\mathcal{C}^B(n)$ is the colour component according to $A_\mathcal{C}(n) = T^B A_\mathcal{C}^B(n)$. In the last step, the orthonormalization of Lie algebra basis elements, Eq. (2.8), was used. Note that odd powers of the Taylor expansion vanish since the real part is taken. Following this consideration, one needs to calculate $A_\mathcal{C} = A_P, A_R$ for the plaquette and the rectangle respectively. To do so, one requires the Baker-Campbell-Hausdorff formula

$$e^X e^Y = \exp\left(X + Y + \frac{1}{2}[X,Y] + \frac{1}{12}[X,[X,Y]] - \frac{1}{12}[Y,[X,Y]] + ...\right) \tag{4.10}$$

for matrices $X, Y$. It can be used in

$$\begin{aligned} P_{\mu\nu}(n) &= e^{iag_0 A_\mu(n)} e^{ig_0 a A_\nu(n+\hat{\mu})} e^{-iag_0 A_\mu(n+\hat{\nu})} e^{-iag_0 A_\nu(n)} \\ &= \exp iag_0\big(A_\mu(n) + A_\nu(n+\hat{\mu}) - A_\mu(n+\hat{\nu}) - A_\nu(n) + \mathcal{O}(g_0)\big). \end{aligned} \tag{4.11}$$

In the first step, Eqs. (3.9) and (3.14) were combined. In the second step, the Baker-Campbell-Hausdorff formula was used. Note that to leading order, the commutators are neglected as they are of $\mathcal{O}(g_0)$. This is the reason why for this purpose, leading order QCD is equivalent to QED. From Eq. (4.11), one can now read off

$$A_P(n) = A_\mu(n) + A_\nu(n+\hat{\mu}) - A_\mu(n+\hat{\nu}) - A_\nu(n) + \mathcal{O}(g_0) \tag{4.12}$$

and analyse lattice cut-off effects. Transforming into momentum space gives

$$A_P(n) = a \int_p e^{ipan} e^{i(p_\mu + p_\nu)a/2} \tilde{f}_{\mu\nu}(p), \tag{4.13}$$

$$\tilde{f}_{\mu\nu}(p) = i(\hat{p}_\mu \tilde{A}_\nu(p) - \hat{p}_\nu \tilde{A}_\mu(p)), \tag{4.14}$$

$$\hat{p}_\mu = \frac{2}{a} \sin \frac{p_\mu a}{2}. \tag{4.15}$$

In Eq. (4.14), the lattice gluon field strength tensor in momentum space was defined while Eq. (4.15) defines the lattice momentum. It is, as foreshadowed in Sect. 3.2, periodic in $p$ and will feature prominently in this work. Inserting this into Eq. (4.9) gives

$$S_P[U] = \frac{1}{4} \sum_{\mu\neq\nu} \int_p \tilde{f}_{\mu\nu}^B(p) \tilde{f}_{\mu\nu}^B(-p) \tag{4.16}$$

with $c_P = 1$ as before. Obviously, the lattice momenta contain the discretization artefacts. The same procedure can be done for the rectangle. One finds

$$A_R(n) = 2a \int_p e^{ipan} e^{i(p_\mu + p_\nu/2)a} \cos \frac{p_\mu a}{2} \tilde{f}_{\mu\nu}(p) + \mathcal{O}(g_0) \tag{4.17}$$

and, with $c_R = 1$,

$$S_R[U] = 2 \sum_{\mu \neq \nu} \int_p \cos^2 \frac{p_\mu a}{2} \tilde{f}^B_{\mu\nu}(p) \tilde{f}^B_{\mu\nu}(-p) + \mathcal{O}(g_0). \tag{4.18}$$

With this normalization, the rectangle action would not have the right continuum limit by itself. One now demands that the small $a$ expansion of a linear combination

$$\begin{aligned} S_{\text{impr}}[U] &= r_P S_P[U] + r_R S_R[U] \\ &= \frac{1}{4} \sum_{\mu \neq \nu} \int_p (r_P + 8 r_R \cos^2 \frac{p_\mu a}{2}) \tilde{f}^B_{\mu\nu}(p) \tilde{f}^B_{\mu\nu}(-p) + \mathcal{O}(g_0) \\ &= \frac{1}{4} \sum_{\mu \neq \nu} \int_p \Big[ (r_P + 8 r_R) - a^2 p^2 (\frac{1}{6}(r_P + 8 r_R) + 2 r_R) \Big] \tilde{F}^B_{\mu\nu}(p) \tilde{F}^B_{\mu\nu}(-p) + \mathcal{O}(a^4, g_0) \end{aligned} \tag{4.19}$$

is free of terms quadratic in the lattice spacing. The expansion returns the continuum field strength tensor as defined in Eq. (2.16) in momentum space. In the last step, both the explicit cosine as well as the sine in the lattice field strength tensor were expanded in $a$. Also note the absence of odd powers due to the relocation of the links to the middle between two lattice sites. To obtain the continuum limit free of $\mathcal{O}(a^2)$ artefacts, one needs

$$r_P + 8 r_R = 1, \tag{4.20}$$

$$\frac{1}{6}(r_P + 8 r_R) + 2 r_R = 0. \tag{4.21}$$

Solving this set of linear equations gives the solution $r_P = 5/3, r_R = -1/12$. In conclusion, it was shown that to leading order, the improved Lüscher-Weisz action

$$S_{\text{LW}}[U] = S_{\text{impr}}[U] = \frac{5}{3} S_P[U] - \frac{1}{12} S_R[U] \tag{4.22}$$

both returns the continuum limit and approaches it faster since the leading order artefacts are of $\mathcal{O}(a^4)$ instead of $\mathcal{O}(a^2)$. In principle, it can be pushed back even further to $\mathcal{O}(a^6)$. For this, paths with length $8a$ need to be included in the action. Furthermore, in the presented consideration, one could also use actions from other loops of length $6a$ such as so-called chairs ('bent' rectangles) or parallelograms. However, these are not planar and to leading order, rectangles are sufficient as was shown before. Additionally, in lattice gauge theory, not only the action but also the observables are discretised. Therefore, they are intrinsically cut-off dependent and can to be improved as well. Examples of lattice observables are considered in Sects. 7 as well as 8. Improvement is possible for the fermionic part of the lattice action as well, see for example Ref. [15], but that is not of interest for this work.

## 5. Perturbation theory

As discussed above, the lattice is a powerful tool to make predictions about quantum field theories. Another framework to calculate correlation functions is perturbation theory. The idea is to expand them in powers of the coupling constant. This way, one can try to improve the predictions order by order. The success of this method is dependent on the convergence behaviour of the emerging series. Obviously, this only works for small coupling constants, such as the electron charge $e$ in QED. However, this is not necessarily true for the strong coupling constant $g_0$ in QCD. In fact, it depends on the energy scale and decreases with rising energy or smaller distances [16]. This effect is called asymptotic freedom as particles start behaving almost free for high energies. Therefore, perturbation theory in QCD is only feasible for high energy processes. In this section, perturbation theory in the continuum is outlined first. Afterwards, lattice perturbation theory and its applications are explained.

Following Ref. [1] but transforming to Euclidean space-time, the path integral formalism is a practical starting point to discuss perturbation theory. Consider an interacting scalar theory with

$$S[\phi] = S_0[\phi] + S_{\text{int}}[\phi] = \int \mathrm{d}^4 x \left[ \int \mathrm{d}^4 y \phi(x) M(x,y) \phi(y) + \lambda \phi(x)^3 \right] \tag{5.1}$$

where $S_0$ is the free action, $S_{\text{int}}$ the interacting action and $\lambda$ is a small coupling constant. A correlation function is then

$$\langle \phi(x_1) ... \phi(x_n) \rangle = Z^{-1} \int \mathcal{D}\phi e^{-S_{\text{int}}[\phi]} e^{-S_0[\phi]} \phi(x_1) ... \phi(x_n). \tag{5.2}$$

Now, a mathematical trick is introduced, that is the generating functional

$$\mathcal{Z}_0[J] = \int \mathcal{D}\phi e^{-S_0[\phi] + \int \mathrm{d}^4 x \phi(x) J(x)}, \tag{5.3}$$

$$\mathcal{Z}[J] = \int \mathcal{D}\phi e^{-S_{\text{int}}[\phi]} e^{-S_0[\phi] + \int \mathrm{d}^4 x \phi(x) J(x)} \tag{5.4}$$

with a source $J$. A free, non-interacting correlation function can be written as

$$\begin{aligned}\langle\phi(x_1)...\phi(x_n)\rangle_0 &= \frac{1}{\mathcal{Z}_0[0]}\int\mathcal{D}\phi\frac{\delta}{\delta J(x_1)}...\frac{\delta}{\delta J(x_n)}e^{-S_0[\phi]+\int \mathrm{d}^4x\phi(x)J(x)}\Big|_{J=0}\\ &= \frac{1}{\mathcal{Z}_0[0]}\frac{\delta}{\delta J(x_1)}...\frac{\delta}{\delta J(x_n)}\mathcal{Z}_0[J]\Big|_{J=0}.\end{aligned} \tag{5.5}$$

In the second step one took advantage of the interchangeability of the integral and the derivative. This expression is helpful because the free generating function can actually be computed analytically since the integral in Eq. (5.3) is gaussian. It is

$$\mathcal{Z}_0[J] = Ae^{\frac{1}{2}\int \mathrm{d}^4x\mathrm{d}^4yJ(x)M(x,y)^{-1}J(y)} \tag{5.6}$$

where $A$ is a constant that cancels with the denominator and $M(x,y)^{-1}$ is given by

$$\int \mathrm{d}^4zM(x,z)M(z,y)^{-1} = \delta^{(4)}(x-y). \tag{5.7}$$

Note that the rigorous mathematics are more complicated than presented here since Eq. (5.3) is a functional instead of an ordinary integral which requires a more careful treatment. However, for introductory purposes and to outline the idea, the above suffices. Since one has an explicit expression for the free generating functional, the calculation of the functional derivatives that appear in Eq. (5.5) is straightforward. Introducing the short-hand notation $M_{lk} \equiv M(x_l, x_k)$, it is

$$\frac{\delta}{\delta J(x_1)}...\frac{\delta}{\delta J(x_n)}\mathcal{Z}_0[J]\Big|_{J=0} = A\begin{cases}M_{12}^{-1}M_{34}^{-1}...M_{n-1,n}^{-1} + M_{13}^{-1}M_{24}^{-1}...M_{n-1,n} + ..., & n \text{ even},\\ 0, & n \text{ odd}.\end{cases} \tag{5.8}$$

The even case is the sum over all permutations of matrix elements where each index $1, ..., n$ is included exactly once. For example, a free four-point function in this theory is

$$\langle\phi(x_1)\phi(x_2)\phi(x_3)\phi(x_4)\rangle_0 = M_{12}^{-1}M_{34}^{-1} + M_{13}^{-1}M_{24}^{-1} + M_{14}^{-1}M_{23}^{-1}. \tag{5.9}$$

This is a major achievement since it is an exact result for the free theory. Nevertheless, the interacting part of the theory is of interest as well. Following the same consideration as in the free case, one can write the full correlator as

$$\begin{aligned}\langle\phi(x_1)...\phi(x_n)\rangle &= \frac{1}{\mathcal{Z}[0]}\frac{\delta}{\delta J(x_1)}...\frac{\delta}{\delta J(x_n)}\mathcal{Z}[J]\Big|_{J=0}\\ &= \frac{1}{\mathcal{Z}[0]}\frac{\delta}{\delta J(x_1)}...\frac{\delta}{\delta J(x_n)}e^{-S_{\text{int}}\left[\frac{\delta}{\delta J}\right]}\mathcal{Z}_0[J]\Big|_{J=0}\\ &= \frac{1}{\mathcal{Z}[0]}\frac{\delta}{\delta J(x_1)}...\frac{\delta}{\delta J(x_n)}\sum_{i=0}^{\infty}\frac{(-1)^i}{i!}\Big(S_{\text{int}}[\frac{\delta}{\delta J}]\Big)^i\mathcal{Z}_0[J]\Big|_{J=0}\\ &= \frac{1}{\mathcal{Z}[0]}\frac{\delta}{\delta J(x_1)}...\frac{\delta}{\delta J(x_n)}\sum_{i=0}^{\infty}\frac{1}{i!}\Big(-\lambda\int \mathrm{d}^4x\frac{\delta^3}{\delta^3J(x)}\Big)^i\mathcal{Z}_0[J]\Big|_{J=0}.\end{aligned} \tag{5.10}$$

In the first and second step, the interchangeability of integral and derivative was again used. In the third step, the smallness of $\lambda$ in the interacting action Eq. (5.1) allowed the expansion of the exponential. In the last step, the interacting action of this specific example was inserted. Further, note two things: First of all, the derivatives can be again computed explicitly using Eq. (5.8). Secondly, the expansion of the exponential in the second-to-last step produces a sum of terms with increasing power in the coupling constant $\lambda$, and the correlation function can be calculated order by order. This is the core of perturbation theory. To get a feeling of the implication of this equation, consider a two-point function $\langle\phi(x_1)\phi(x_2)\rangle$. Its value $\langle\phi(x_1)\phi(x_2)\rangle_0$ at order $\mathcal{O}(\lambda^0)$ corresponds to the addend with $i = 0$ and coincides with the free value, $M(x_1, x_2)^{-1}$. At order $\mathcal{O}(\lambda)$, $i$ equals 1 and there is an odd number of derivatives - two from the correlator itself and three from the interaction - so that $\langle\phi(x_1)\phi(x_2)\rangle_1$ vanishes according to Eq. (5.8). Furthermore, order $\mathcal{O}(\lambda^2)$ is given by the addend $i = 2$. Here, eight derivatives emerge in total and the next-to-leading order contribution to the two-point function is

$$\langle\phi(x_1)\phi(x_2)\rangle_2 = \lambda^2\int \mathrm{d}^4x\mathrm{d}^4y\big(M(x_1,x)^{-1}M(x,y)^{-1}M(x,y)^{-1}M(y,x_2)^{-1} + \text{permutations}\big)/2!. \tag{5.11}$$

Disconnected permutations where the external points $x_1$ and $x_2$ appear in one matrix element and are factorized from those that are integrated over do not contribute as they are cancelled out by the denominator $\mathcal{Z}[0]$. They are called vacuum bubbles. Furthermore, the integrals in Eq. (5.11) diverge for most theories and correlators. This seems like a problem at first, but it is a manifest property of quantum field theories and physical observables can still be extracted via renormalization. Note that all the quantities $M(x,y)^{-1}$ and $\lambda$ that emerge in the perturbative expansion can be read off almost immediately from the action, so looking at the action is sufficient to determine correlation functions in this framework. This way, one can also calculate vacuum expectation values for more complicated theories such as QED or QCD.

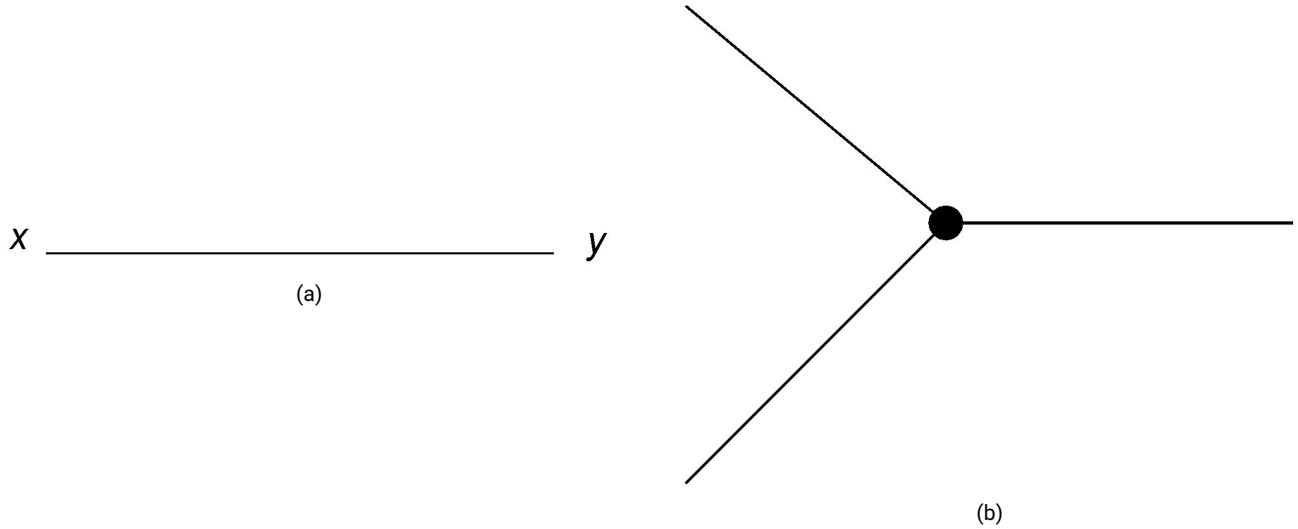


Figure 4: The graphical representation of the objects that appear in the perturbative expansion of the correlator. These diagrams allow one to construct contributions. (a) The propagator $M(x,y)^{-1}$. (b) The vertex $-\lambda$. Feynman diagrams drawn with Ref. [17].

## 5.1. Feynman diagrams

Keeping an overview of the involved combinatorics can turn somewhat complicated. Therefore, Feynman diagrams were introduced as a graphical visualisation. The matrix elements $M(x,y)^{-1}$ are called propagators and the factor $\lambda$ in the action is called a vertex. In the presented theory, each vertex is associated with three propagators since the interaction term is of cubic order. Therefore, one draws the propagator as a line and the vertex as a knot connecting three lines as shown in Fig. 4. One can now use these building blocks for perturbation theory using the following Feynman rules: Each line gets a propagator $M(x,y)^{-1}$. Each vertex gets the negative coupling constant and an integral $\int \mathrm{d}^4 z$. A $n$-point function has $n$ external lines. Feynman diagrams of order $\lambda^2$ - one that is contributing to the correlator and a cancelled vacuum bubble - for the two-point function are shown in Fig. 5. Note that this is not the only contributing diagram, but other permutations as well. Most of the time, it is easier to determine Feynman rules in momentum space as derivatives turn into momenta and therefore ordering of terms plays no role.

## 5.2. Feynman rules for gluons

The results from the previous section can be translated into QCD [1, 3]. Consider the continuum gluon action Eq. (2.15). It contains terms quadratic, cubic and quartic in the gluon fields $A_\mu(x)$. Therefore, this theory has apart from the propagator a three- and a four-gluon vertex. These quantities are not scalars but tensors in Lorentz and colour space. Therefore, Feynman rules will carry these indices as well. For gauge theories such as QCD, one needs to fix the gauge before the perturbative series can be performed. This is because in the path integral, many configurations differ only by a gauge transformation. Due to the gauge invariance of the action, plenty of equivalent integrations are performed and the path integral is redundant. More specifically, the problematic configurations are those that are flat, that is they can be gauge transformed to a configuration with $F_{\mu\nu}(x) = 0$. The integrand in the path integral is 1 for those. Since there is an continuously infinite amount of them, the path integral consequently diverges. A gauge condition is

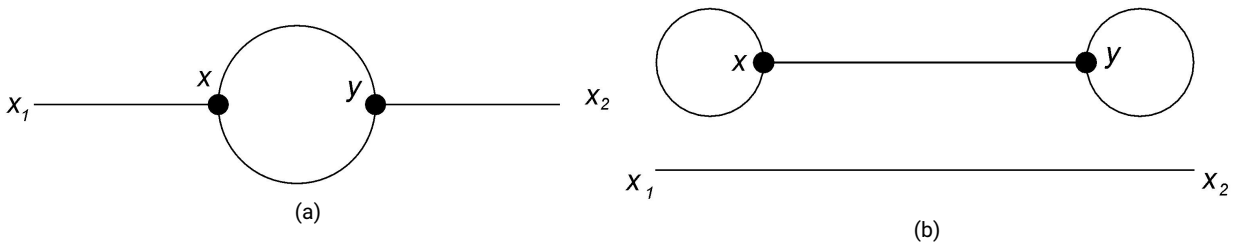


Figure 5: Feynman diagrams of $\mathcal{O}(\lambda^2)$. All lines can be matched to a propagator and all dots can be matched to vertices. (a) The diagram contributing to $\langle\phi(x_1)\phi(x_2)\rangle_2$. The interior lines form a loop. (b) A non-contributing vacuum bubble.

therefore necessary to remove this overabundance of physically equivalent configurations. If a generalised Lorentz gauge

$$\partial_\mu A^B_\mu(x) - \omega^B(x) = 0 \tag{5.12}$$

with arbitrary scalar fields $\omega^B(x)$ is employed, the gauge condition can be elegantly implemented in a gauge fixing action $S_{\text{gf}}$ by the Fadeev-Popov trick. This action reads

$$S^{\text{cont}}_{\text{gf}}[A] = \frac{1}{2\alpha}\sum_{B=1}^{8}\int \mathrm{d}^4x\big(\partial_\mu A^B_\mu(x)\big)^2 \tag{5.13}$$

with the gauge fixing parameter $\alpha$ and needs to be considered when deriving the Feynman rules. Unfortunately, this trick comes at the cost of having to introduce additional scalar fields, the Fadeev-Popov ghost fields $c/\bar{c}$. They carry colour indices and are coupled to the gauge field via the action

$$S^{\text{cont}}_{\text{FP}}[c, A] = -\int \mathrm{d}^4x\bar{c}^B(x)\partial_\mu\big(\partial_\mu + ig_0 f^{BCD}A^D_\mu(x)\big)c^C(x). \tag{5.14}$$

These fields do not describe physical particles but do contribute to correlation functions. The gauge fixed pure gluon action

$$S^{\text{cont}}_{g,\text{gf}}[A] = S^{\text{cont}}_g[A] + S^{\text{cont}}_{\text{gf}}[A] \tag{5.15}$$

may now be split into terms that are quadratic, cubic or quartic in the fields respectively. By Fourier transforming the quadratic term into the form

$$S^{\text{cont}}_{(2)}[A] = \int_p\int_q \tilde{A}^A_\mu(p)K^{AB}_{\mu\nu}(p,q)\tilde{A}^B_\nu(q), \tag{5.16}$$

one can read off the propagator

$$D^{AB}_{\mu\nu}(p,q) = \big(K^{-1}\big)^{AB}_{\mu\nu}(p,q) = (2\pi)^4\delta^{(4)}(p+q)\frac{1}{p^2}\Big(\delta_{\mu\nu} - (1-\alpha)\frac{p_\mu p_\nu}{p^2}\Big)\delta^{AB}. \tag{5.17}$$

Note the dependence on $\alpha$ that is introduced by the gauge fixing action. Not fixing the gauge would correspond to $\alpha \to \infty$ and the propagator would be ill-defined, corroborating the necessity of gauge fixing. The inverse in Eq. (5.17) is defined by

$$\int_r K^{AC}_{\mu\rho}(p,r)\big(K^{-1}\big)^{CB}_{\rho\nu}(r,q) = \delta^{AB}\delta_{\mu\nu}\delta^{(4)}(p-q). \tag{5.18}$$

The diagram for the gluon propagator is a curled line. Meanwhile, the cubic part of the gluon action is part of the interaction and can be cast into

$$S^{\text{cont}}_{(3)}[A] = \int_p\int_q\int_r \Gamma^{ABC}_{\mu\nu\rho}(p,q,r)\tilde{A}^A_\mu(p)\tilde{A}^B_\nu(q)\tilde{A}^C_\rho(r), \tag{5.19}$$

where the three-gluon vertex

$$\Gamma^{ABC}_{\mu\nu\rho}(p,q,r) = ig_0(2\pi)^4\delta^{(4)}(p+q+r)f^{ABC}\big[(r-q)_\mu\delta_{\nu\rho} + (p-r)_\nu\delta_{\mu\rho} + (q-p)_\rho\delta_{\mu\nu}\big] \tag{5.20}$$

can be read off. Following the same procedure for the quartic part of the action, the four-gluon vertex

$$\begin{aligned}\Gamma^{ABCD}_{\mu\nu\rho\sigma}(p,q,r,s) = -g_0^2\big[&f^{ABE}f^{CDE}(\delta_{\mu\rho}\delta_{\nu\sigma} - \delta_{\mu\sigma}\delta_{\nu\rho})\\ &+ f^{ACE}f^{BDE}(\delta_{\mu\nu}\delta_{\rho\sigma} - \delta_{\mu\sigma}\delta_{\nu\rho})\\ &+ f^{ADE}f^{BCE}(\delta_{\mu\nu}\delta_{\rho\sigma} - \delta_{\mu\sigma}\delta_{\nu\rho})\big]\end{aligned} \tag{5.21}$$

is found. The Feynman diagrams corresponding to these expressions are shown in Fig. 6 and can be used to construct correlation functions order by order. Note that one integrates over momenta in closed loops. An additional remark can be made about the delta functions appearing in the Feynman rules: They describe conservation of energy and momentum in vertices. It is also important to keep in mind that since QCD is a gauge theory, only observables that are gauge independent are physical.

## 5.3. Perturbative lattice QCD

At first sight, it might seem paradoxical to treat a lattice theory perturbatively. After all, the lattice was introduced to measure correlation functions non-perturbatively. However, this treatment can still give valuable insight, for example about renormalization and running coupling [18] or restoration of symmetries in the continuum limit that are broken on the lattice [2]. Furthermore, each lattice theory comes with its own action and hence its own Feynman rules. Therefore, if a new theory is introduced to improve numerical calculations - for example the improved action from Sect. 4.2 - it is insightful to do perturbation theory first to get a rough understanding what to expect and interpret results properly. The results from Sect. 7 of this work however will be used for tree-level improvement, a method first described in Ref. [19]. The assumption is that lattice cut-off effects are mainly included in the leading

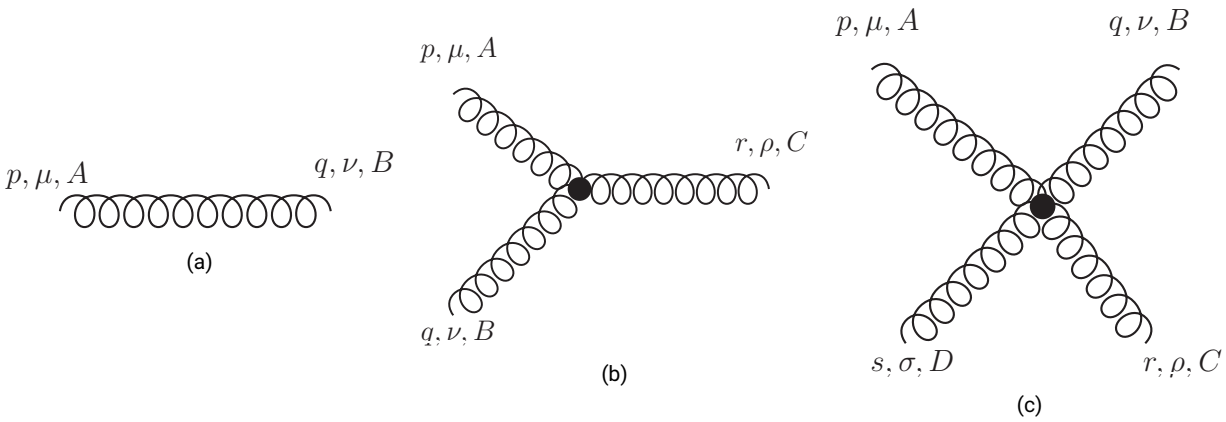


Figure 6: The Feynman diagrams for the gluon in the continuum. (a) Propagator. (b) Three-gluon vertex. (c) Four-gluon vertex.

order contributions to observables. Therefore, the ratio of full and perturbative lattice results approaches the continuum limit faster than the full result itself. Written as an equation,

$$\frac{\langle \mathcal{O}^{\text{latt}} \rangle_{\text{full}}}{\langle \mathcal{O}^{\text{latt}} \rangle_{\text{pert}}} \overset{a \to 0}{\to} \frac{\langle \mathcal{O}^{\text{cont}} \rangle_{\text{full}}}{\langle \mathcal{O}^{\text{cont}} \rangle_{\text{pert}}} \tag{5.22}$$

has a better convergence than $\langle \mathcal{O}^{\text{latt}} \rangle_{\text{full}}$ itself for some observable $\mathcal{O}$. Therefore, after measuring an observable on the lattice, having perturbative expressions for the expectation values both on the lattice and the continuum facilitates continuum extrapolation. This in turn allows a more precise determination of the full continuum expression - which is where real-world physics information are encoded. The subsequent discussion on lattice perturbation theory will follow Refs. [2, 8]. On the lattice, Feynman rules are derived equivalently to the continuum. In the derivation, position space integrals are replaced by sums and delta functions by the Kronecker delta. However, there are significant differences between the perturbative treatment of QCD in the continuum and on the lattice: A lot more vertices emerge that have no analogue in the continuum. This will be explained in the following. In lattice perturbation theory, the links need to be parametrized in terms of the gluon fields $A_\mu$. The new vertices are produced because the gluon fields appear in the power of the link variables $U_\mu(n)$. A small $g_0$ expansion of a link reads

$$U_\mu(n) = 1 + iag_0 A_\mu(n) - \frac{a^2 g_0^2}{2} A_\mu(n)^2 - \frac{ia^3 g_0^3}{6} A_\mu(n)^3 + \mathcal{O}(g_0^4), \tag{5.23}$$

so as a product of links, the action will contain terms with any natural power of $A_\mu(n)$ except 1. Correspondingly, there will be vertices with any number of lines attached. The ones without a corresponding continuum vertex - those who are quintic or higher - vanish in the $a \to 0$ limit but play a role in renormalization. Another problem arises at the lattice: As mentioned in Sect. 3, the integration stretches over the SU(3) group manifold instead of the Lie algebra. In the derivation of perturbation theory however, one integrates over the latter. The solution to this problem is the formulation of the measure

$$\begin{aligned} DU &= ag_0 \prod_{n,\mu} \sqrt{\det\left[\frac{1}{2} M^\dagger\big(A'_\mu(n)\big) M\big(A'_\mu(n)\big)\right]}\, DA, \\ M\big(A'_\mu(n)\big) &= \frac{1 - e^{-iag_0 A'_\mu(n)}}{iag_0 A'_\mu(n)}, \\ A'_\mu(n) &= t^B A^B_\mu(n), \end{aligned} \tag{5.24}$$

which relates the group integration measure to the Lie algebra measure. The $t^B$ in the last line of Eqs. (5.24) are the group generators in the adjoint representation as defined by Eq. (2.10). Similar to the gauge fixing procedure, the measure can be incorporated in another action $S_{\text{meas}}$, reading

$$S_{\text{meas}}[A] = -\frac{1}{2} \sum_{n,\mu} \operatorname{Tr} \ln\left[\frac{2\big(1 - \cos ag_0 A_\mu(n)\big)}{\big(ag_0 A_\mu(n)\big)^2}\right]. \tag{5.25}$$

A small $g_0$ expansion needs to be performed for the cosine and the logarithm to find polynomials of the gluon field. Note that this action contains an infinite number of natural powers of the field as well, contributing to vertices with vanishing continuum limit. Now the total lattice action is

$$S^{\text{latt}}_{g,\text{tot}}[A] = S^{\text{latt}}_g[A] + S^{\text{latt}}_{\text{gf}}[A] + S_{\text{meas}}[A] \tag{5.26}$$

where $S_g^{\text{latt}}$ is any linear combination of actions from Eq. (3.13) with normalization for the right continuum limit, $S_{\text{gf}}^{\text{latt}}$ is the lattice gauge fixing action

$$S_{\text{gf}}^{\text{latt}}[A] = \frac{1}{2\alpha} \sum_{n,B} \left( \partial_\mu^L A_\mu^B(n) \right)^2 \tag{5.27}$$

with the left-handed lattice derivative

$$\partial_\mu^L f(n) = \frac{f(n) - f(n - \hat{\mu})}{a}, \tag{5.28}$$

and $S_{\text{meas}}$ given by Eq. (5.25). This expression can now be used to derive Feynman rules. These are obviously dependent on the choice of the lattice action.

### 5.3.1. Feynman rules for lattice QCD

Using the Fourier transforms defined in Sect. 3.2 one can now derive the propagators and vertices completely analogously to the continuum. The diagrams are drawn the same way. Performing the small $g_0$ expansion of the Wilson action as outlined in Appendix A, one finds

$$S_g^W[A] = \frac{1}{2} \int_{pp'} \tilde{A}_\mu^C(p)(2\pi)^4 \delta^{(4)}(p + p') \delta^{CD} (\hat{p}^2 \delta_{\mu\nu} - \hat{p}_\mu \hat{p}_\nu) A_\nu^D(p') + \mathcal{O}(g_0) \tag{5.29}$$

Inverting the kernel between the two gluon fields and considering the gauge fixing term, the propagator for the Wilson action is

$$(\hat{D}^{\text{W}})_{\mu\nu}^{AB}(p, q) = (2\pi)^4 \delta^{(4)}(p + q) \delta^{AB} \frac{1}{\hat{p}^2} \left( \delta_{\mu\nu} - (1 - \alpha) \frac{\hat{p}_\mu \hat{p}_\nu}{\hat{p}^2} \right) \tag{5.30}$$

with the lattice momenta $\hat{p}_\mu$ from Eq. (4.15) and $\hat{p}^2 = \hat{p}_\mu \hat{p}_\mu$. This expression of course returns the continuum limit as $\hat{p}_\mu \to p_\mu$ for $a \to 0$. There is no contribution from $S_{\text{meas}}$ despite it having a quadratic term in the fields. This is because this term is also proportional to $g_0^2$, so it is considered a part of the interaction. This two-gluon vertex reads

$$\hat{\Gamma}_{\mu\nu}^{AB}(p, q) = -(2\pi)^4 \delta^{(4)}(p + q) \delta^{AB} \frac{g_0^2}{4a^2} \delta_{\mu\nu} \tag{5.31}$$

and actually diverges in the continuum limit instead of vanishing. This is surprising at first sight, but this vertex plays a role at removing other $a \to 0$ divergences appearing in other $\mathcal{O}(g_0^2)$ Feynman diagrams. This shows the importance of considering all vertices, even those without continuum analogue. The three-gluon vertex for the Wilson action reads

$$\hat{\Gamma}_{\mu\nu\rho}^{ABC}(p, q, r) = i g_0 (2\pi)^4 \delta^{(4)}(p + q + r) f^{ABC} \left[ \widehat{(r - q)}_\mu \cos \frac{p_\nu a}{2} \delta_{\nu\rho} + \widehat{(p - r)}_\nu \cos \frac{q_\mu a}{2} \delta_{\mu\rho} + \widehat{(q - p)}_\lambda \cos \frac{r_\mu a}{2} \delta_{\mu\nu} \right] \tag{5.32}$$

and approaches the continuum limit as well for $a \to 0$. Expressions for further vertices are very lengthy and will not be given here. The lattice four-gluon vertex for the Wilson action can be taken from Ref. [8]. Weisz and Wohlert derived Feynman rules for improved lattice actions involving plaquettes, rectangles, chairs and parallelograms in Ref. [20]. The small coupling expansion of the Lüscher-Weisz action, for example, is

$$\begin{aligned} S_g^{\text{LW}}[A] = \frac{1}{2} \int_{pp'} \tilde{A}_\mu^C(p)(2\pi)^{(4)} \delta^{(4)}(p + p') \delta^{CD} \Bigg( & \left( \frac{5}{3} \hat{p}^2 - \frac{1}{3} \hat{c}_\mu^2 \hat{p}^2 - \frac{1}{3} \sum_\lambda \hat{c}_\lambda^2 \hat{p}_\lambda^2 \right) \delta_{\mu\nu} \\ & - \left( \frac{5}{3} - \frac{1}{3} (\hat{c}_\mu^2 + \hat{c}_\nu^2) \right) \hat{p}_\mu \hat{p}_\nu \Bigg) \tilde{A}_\nu^D(p') + \mathcal{O}(g_0) \end{aligned} \tag{5.33}$$

where

$$\hat{c}_\mu = \cos \frac{p_\mu a}{2}. \tag{5.34}$$

Adding the gauge fixing term and inverting the kernel returns the Lüscher-Weisz gluon propagator which, of course, differs from the Wilson propagator. Its explicit expression is very unwieldy and will not be given here. The derivation of the above expression is given in Appendix A. How leading order correlation functions are built from the propagators will be seen in Sect. 7 and 8.

## 6. Gradient flow

Quantities obtained by lattice calculations are often very noisy because some of them are very sensitive to small distance correlations. This is due to momentum integrals that diverge for large $p$. These $p \to \infty$ divergences are called ultraviolet (UV). As the momenta are restricted to the Brillouin zone on the lattice, these integrals are finite, but still very large since they scale with $a^{-2}$. Consequently, a dilemma arises: To extrapolate to the continuum, a small lattice spacing is necessary. On the other hand, this leads to a decrease of the signal-to-noise ratio of correlators. This makes it hard to actually extract physical information from the data. Techniques to reduce the noise are therefore very helpful. In the last years, gradient flow has been proven to be a useful tool for this and other

problems such as setting a reference scale on the lattice [21] or defining the renormalized coupling [22]. For a review of the latter use see Ref. [23]. It will also be discussed briefly in the beginning of Sect. 8. The idea of gradient flow was first introduced in Ref. [24] and fleshed out by M. Lüscher in Ref. [22]. Gradient flow adds an additional flow-time dimension $\tau$ to the gauge field. For $\tau = 0$, the initial unflowed field $A_\mu(x)$ should be reproduced, while for large values of $\tau$, the field will be suppressed. The flow time is of dimension length squared. Flowed fields in the continuum are defined by the flow equation

$$\dot{B}_\mu(\tau, x) = D_\nu G_{\nu\mu}(\tau, x) \tag{6.1}$$

with initial condition

$$B_\mu(0, x) = A_\mu(x). \tag{6.2}$$

The dot in Eq. (6.1) represents the derivative with respect to the flow time and $G_{\mu\nu}(\tau, x)$ is the flowed field strength tensor defined similar to Eq. (2.16) but with the unflowed fields $A_\mu(x)$ replaced with flowed fields $B_\mu(\tau, x)$. This equation is invariant under $\tau$-independent gauge transformations. In the following, perturbation theory of gradient flow will be discussed, and equivalently to the QCD case, the gauge needs to be fixed. This can be achieved by adding a gauge fixing term to the flow equation

$$\dot{B}_\mu(\tau, x) = D_\nu G_{\nu\mu}(\tau, x) + \lambda D_\mu \partial_\nu B_\nu(\tau, x), \tag{6.3}$$

where $\lambda$ is the gauge fixing parameter. The solution with $\lambda = 0$ is related to the ones with $\lambda \neq 0$ via

$$B_\mu(\tau, x) = \Lambda(\tau, x) B_\mu(\tau, x)|_{\lambda=0} \Lambda^{-1}(\tau, x) + \Lambda(\tau, x)\partial_\mu \Lambda^{-1}(\tau, x). \tag{6.4}$$

The gauge transformation $\Lambda(\tau, x)$ satisfies

$$\dot{\Lambda}(\tau, x) = -\lambda \partial_\nu B_\nu(\tau, x)\Lambda(\tau, x), \quad \Lambda(0, x) = 1. \tag{6.5}$$

This flow gauge fixing is independent of the QCD gauge fixing. To get an understanding of the effect of the flow equation, it is sensible to write the flowed field as a power series

$$B_\mu(\tau, x) = \sum_{k=0}^{\infty} g_0^k B_{\mu,k}(\tau, x), \quad B_{\mu,k}(0, x) = \delta_{k0} A_\mu(x). \tag{6.6}$$

The initial conditions mean that all terms in the series vanish for $\tau = 0$ except for the first one. Inserting the series into Eq. (6.4) gives a set of equations

$$\dot{B}_{\mu,k}(\tau, x) - \partial_\nu \partial_\nu B_{\mu,k}(\tau, x) - (\lambda - 1)\partial_\mu \partial_\nu B_{\mu,k}(\tau, x) = R_{\mu,k}(\tau, x) \tag{6.7}$$

with a rest term $R_{\mu,k}$ that depends on the previous solutions. Each single equation is a heat equation where the rest term is an inhomogeneity so known tools such as the fundamental solution or Duhamel's principle may be used [25]. Since $R_{\mu,0}(\tau, x) = 0$, the first term is actually the homogenous heat equation which, for $\lambda = 1$, gives the solution

$$B_{\mu,0}(\tau, x) = \int \mathrm{d}^4 y \frac{e^{-(x-y)^2/4\tau}}{(4\pi\tau)^2} A_\mu(y). \tag{6.8}$$

From this expression it is evident that to leading order, the gradient flow is a smearing operation that convolutes the unflowed fields with a function with radius $r_f = \sqrt{8\tau}$. In momentum space, this term reads

$$\tilde{B}_{\mu,0}(\tau, p) = e^{-\tau p^2} \tilde{A}_\mu(p). \tag{6.9}$$

Here, one can clearly recognize why gradient flow is a suitable tool to remove UV divergences. The field is wrapped in a gaussian envelope that exponentially suppresses large momenta. Therefore, it renders affected momentum integrals finite. Even higher orders of the solution can be written in an explicit form due to the simplicity of the heat equation. Introducing the heat kernel

$$\begin{aligned} K_{\mu\nu}(\tau, x) &= \int_p e^{ipx} \tilde{K}_{\mu\nu}(\tau, p), \\ \tilde{K}_{\mu\nu}(\tau, p) &= \frac{1}{p^2}\left((\delta_{\mu\nu} p^2 - p_\mu p_\nu) e^{-tp^2} + p_\mu p_\nu e^{-\lambda t p^2}\right), \end{aligned} \tag{6.10}$$

the heat equation Eq. (6.7) is solved via

$$\begin{aligned} B_{\mu,k}(\tau, x) &= \int \mathrm{d}^4 y \left[\delta_{k0} K_{\mu\nu}(\tau, x - y) A_\nu(y) + \int_0^\tau \mathrm{d}s K_{\mu\nu}(\tau - s, x - y) R_{\nu,k}(s, y)\right], \\ \tilde{B}_{\mu,k}(\tau, p) &= \delta_{k0} \tilde{K}_{\mu\nu}(\tau, p)\tilde{A}_\nu(p) + \int_0^\tau \mathrm{d}s \tilde{K}_{\mu\nu}(\tau - s, p)\tilde{R}_{\nu,k}(s, p). \end{aligned} \tag{6.11}$$

The first term arises from the initial condition which vanishes for $k \neq 0$, the second one from Duhamel's principle that is a tool to take source terms in the heat equation into account. As it depends on the lower order solutions, one can solve the equation iteratively.

Note that Eq. (6.11) reproduces Eq. (6.9) as the source term $R_{\mu,0}$ vanishes and the heat kernel takes on a simple form for $\lambda = 1$. One can now deduce the propagator for flowed fields. Only the first term $B_{\mu,0}$ contributes since it is of order $g_0^0$. The propagator for two flowed fields is now

$$\begin{aligned}(D^{\text{flow}})^{CD}_{\mu\nu}(\tau_1,\tau_2,p,q) &= \left\langle \tilde{B}^C_\mu(\tau_1,p)\tilde{B}^D_\nu(\tau_2,q)\right\rangle_0 \\ &= \left\langle \tilde{B}^C_{\mu,0}(\tau_1,p)\tilde{B}^D_{\nu,0}(\tau_2,q)\right\rangle \\ &= \tilde{K}_{\mu\rho}(\tau,p)\tilde{K}_{\nu\sigma}(\tau,q)\left\langle \tilde{A}^C_\rho(p)\tilde{A}^D_\sigma(q)\right\rangle_0 \\ &= (2\pi)^4\delta^{(4)}(p+q)\delta^{CD}\frac{1}{(p^2)^2}\left[(\delta_{\mu\nu}p^2 - p_\mu p_\nu)e^{-(\tau_1+\tau_2)p^2} + \alpha p_\mu p_\nu e^{-\lambda(\tau_1+\tau_2)p^2}\right].\end{aligned} \tag{6.12}$$

Here, $\alpha$ is still the gauge fixing parameter of the gluon action. Note that this result includes both the unflowed propagator with $\tau_1 = \tau_2 = 0$ as well as the mixed propagator where exactly one of the fields is flowed. Choosing Feynman gauge for both flow and gluons, $\alpha = \lambda = 1$, reduces this expression greatly to

$$(D^{\text{flow}})^{CD}_{\mu\nu}(\tau_1,\tau_2,p,q)\Big|_{\alpha=\lambda=1} = (2\pi)^4\delta^{(4)}(p+q)\delta^{CD}\delta_{\mu\nu}\frac{e^{-(\tau_1+\tau_2)p^2}}{p^2} \tag{6.13}$$

where the exponential suppression is again evident. Lüscher also discussed gradient flow for fermions [26] but again, those will play no role in this work.

## 6.1. Perturbation theory of gradient flow

Introducing gradient flow obviously has an effect on correlation functions. Previously derived Feynman rules do not suffice any more. To include the impact of gradient flow in perturbation theory, a rigorous systematic approach is helpful. For this, a 4+1-dimensional theory is introduced with the flow time $\tau > 0$ as the additional dimension. The flow equation is enforced in this theory via a Lagrange multiplier field $L_\mu(\tau,x)$ in a new action

$$S^{\text{cont}}_{\text{flow}}[L,B] = 2\int_0^\infty \mathrm{d}\tau \int \mathrm{d}^4x\, \mathrm{Tr}\left[L_\mu(\tau,x)\big(\dot{B}_\mu(\tau,x) - D_\nu G_{\nu\mu}(\tau,x) - \lambda D_\mu\partial_\nu B_\nu(\tau,x)\big)\right]. \tag{6.14}$$

The flow equation is then the Euler Lagrange equation obtained by varying the multiplier field. Similar to the Fadeev-Popov ghost field, the newly introduced degree of freedom does not describe a physical particle but still plays a role in Feynman rules. The 4+1-dimensional theory's total action is therefore

$$S^{\text{cont}}_{4+1}[A,L,B] = S^{\text{cont}}_{g,\text{gf}}[A] + S^{\text{cont}}_{\text{flow}}[L,B] \tag{6.15}$$

with the known gauge fixed gluonic action $S_{g,\text{gf}}$. Here, the flowed and unflowed fields are treated as separate and only connected by the boundary condition $B_\mu(0,x) = A_\mu(x)$. After transforming into momentum space and inserting the solution Eq. (6.11), the time derivative can be computed and the Feynman rules for flow can be read off. The propagator derived this way is consistent with Eq. (6.12). The action gives rise to multiple different Feynman rules, such as a $LB$ propagator - the flow propagator - or $LB^2$ and $LB^3$ flow vertices. They were derived by Lüscher and Weisz in Ref. [27]. The flowed gluon propagator is given by Eq. (6.12). The $LB$ flow line reads

$$(D_{LB})^{CD}_{\mu\nu}(\tau_1,\tau_2,p,q) = (2\pi)^4\delta^{(4)}(p+q)\delta^{CD}\theta(\tau_1-\tau_2)\left[\left(\delta_{\mu\nu} - \frac{p_\mu p_\nu}{p^2}\right)e^{-(\tau_1-\tau_2)p^2} + \frac{p_\mu p_\nu}{p^2}e^{-\lambda(\tau_1-\tau_2)p^2}\right]. \tag{6.16}$$

Here, $\tau_1$ is always associated with the gauge field and $\tau_2$ with the multiplier field. The theta function then ensures that $\tau_1 > \tau_2$. The flow lines are either external operators or connect flow vertices sitting at flow times $\tau_2$ and $\tau_1$, so the flow time increases along the line. Therefore, $LB$ propagators are drawn as directed solid lines. To write down the flow vertices, the flow equation is Fourier transformed, integrated and then reads

$$\tilde{B}_\mu(\tau,p) = \tilde{K}_{\mu\nu}(\tau,p)\tilde{A}_\nu(p) + \int_0^t \mathrm{d}s\tilde{K}_{\mu\nu}(\tau-s,p)\tilde{R}_\nu(s,p) \tag{6.17}$$

with rest term

$$\begin{aligned}\tilde{R}^C_\mu(\tau,p) = &\frac{1}{2}\int_{q_1q_2}(2\pi)^4\delta^{(4)}(p+q_1+q_2)(X_2)^{CDE}_{\mu\nu\rho}(q_1,q_2)B^D_\nu(\tau,-q_1)B^E_\rho(\tau,-q_2) \\ &+ \frac{1}{3}\int_{q_1q_2q_3}(2\pi)^4\delta^{(4)}(p+q_1+q_2+q_3)(X_3)^{CDEF}_{\mu\nu\rho\sigma}(q_1,q_2,q_3)B^D_\nu(\tau,-q_1)B^E_\rho(\tau,-q_2)B^F_\sigma(\tau,-q_3).\end{aligned} \tag{6.18}$$

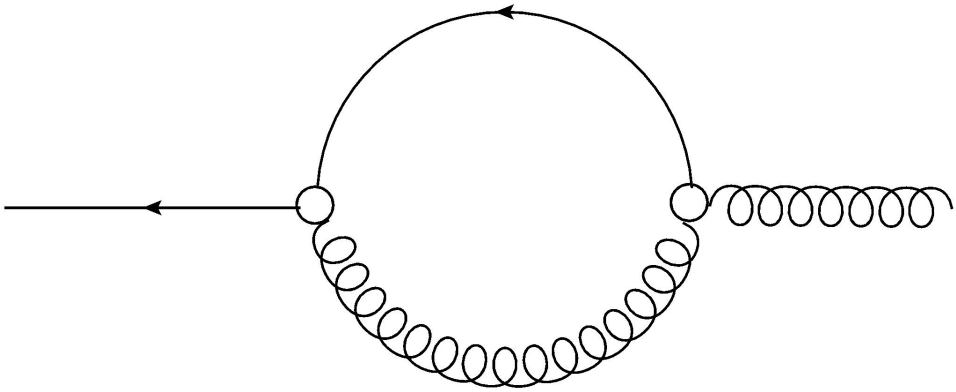

Figure 7: A Feynman graph contributing to the $\langle LB \rangle$ correlation function. On the right, a gluon line connects to a flow vertex. Then, a loop consisting of a flowed gluon and a flow line emerges which recombine in flow vertex to an outgoing flow line. Of course, many other diagrams contribute to this correlator as well.

Note that Eq. (6.17) is similar to Eq. (6.11) but without expanding the flowed gauge field in a series. The expressions $X_n$ are the $LB^2$ and $LB^3$ flow vertices. For better legibility, unlike in previous Feynman rules, some factors such as delta functions and the heat kernel are factored out from the vertices. Their explicit expressions are

$$(X_2)^{CDE}_{\mu\nu\rho}(q_1,q_2) = if^{CDE}\big[(q_1-q_2)_\mu\delta_{\nu\rho} + 2(q_1)_\rho\delta_{\mu\nu} - 2(q_2)_\nu\delta_{\mu\rho} + (\lambda-1)((q_1)_\nu\delta_{\mu\rho} - (q_2)_\rho\delta_{\mu\nu})\big] \tag{6.19}$$

and

$$\begin{aligned}(X_3)^{CDEF}_{\mu\nu\rho\sigma}(q_1,q_2,q_3) = {} & f^{CDG}f^{EFG}(\delta_{\mu\sigma}\delta_{\nu\rho} - \delta_{\mu\rho}\delta_{\nu\sigma}) \\ & + f^{CFG}f^{DEG}(\delta_{\nu\rho}\delta_{\nu\sigma} - \delta_{\mu\nu}\delta_{\rho\sigma}) \\ & + f^{CEG}f^{DFG}(\delta_{\mu\nu}\delta_{\rho\sigma} - \delta_{\mu\sigma}\delta_{\nu\rho}).\end{aligned} \tag{6.20}$$

The flow vertices always contain exactly one outgoing flow line arising from the heat kernel in the second term of Eq. (6.17). The two or three other lines can be either gluon or an incoming flow lines, so the $X_n$ actually describe $n+1$ different vertices. The reason is that a gauge field associated with a vertex can be either connected with a gluon propagator or a flow line. To distinguish them from gluon vertices, flow vertices are drawn as empty dots in Feynman diagrams. A diagram contributing to the $\langle LB \rangle$ correlator is shown in Fig. 7. It contains (flowed) gluons, flow lines and flow vertices. Each flow vertex is defined at a flow time $s$ that is integrated over. The theta function $\theta(\tau - s)$ of the outgoing flow line restricts this integral to the integration range $[0, \tau]$.

## 6.2. Gradient flow on the lattice

As mentioned previously, gradient flow is a powerful tool to reduce noise when calculating correlation functions on the lattice. In this setting, as mentioned above, it also has further applications in renormalization and measurement of the gauge coupling which motivates Sect. 8. The flowed lattice is of course different than the physical world in two ways. To extract physical information, one first needs to extrapolate to the continuum and then take the limit $\tau \to 0$. On the lattice, one needs to redefine the flow equation as it contains spatial derivatives. Introducing the flowed link variables $V_\mu(\tau, n)$ with initial condition $V_\mu(0, n) = U_\mu(n)$, a possible discretization of the flow equation Eq. (6.1) is [21]

$$a^2\dot{V}_\mu(\tau,x) = -g_0^2\big(\partial_{n,\mu}S_g^{\text{latt}}[V]\big)V_\mu(\tau,x) \tag{6.21}$$

where $S_g^{\text{latt}}[V]$ is again a linear combination of closed-path actions as in Eq. (3.13) that is normalized so that the continuum limit is achieved. Note that here, no sum over the Lorentz indices $\mu$ is understood. The algebra-valued derivative $\partial_{n,\mu}$ of a scalar function is defined via

$$\partial_{n,\mu}f(V_\mu(n)) = iT^A\frac{\mathrm{d}}{\mathrm{d}\epsilon}f(e^{i\epsilon T^A}U_\mu(n))\big|_{\epsilon=0}. \tag{6.22}$$

There is a structural difference between the continuum and lattice flow equation: While on the continuum, it is a single partial differential equation with respect to $x$ and $\tau$, on the lattice, it is a set of ordinary differential equations with respect only to $\tau$. As an example, for the plaquette action, one finds [28]

$$g_0^2\partial_{n,\mu}S_P[V] = 2\sum_\nu \mathrm{Tr}\big[T^A(P_{\mu\nu}(\tau,n) + P_{\mu,-\nu}(\tau,n))\big]T^A. \tag{6.23}$$

Note that here the plaquettes are defined as products of flowed links. From this expression one can see how the lattice flow equation evolves $V_\mu(\tau, n)$: A sample of the two plaquettes in the same plane that both contain this link is taken. One can consider the right-hand

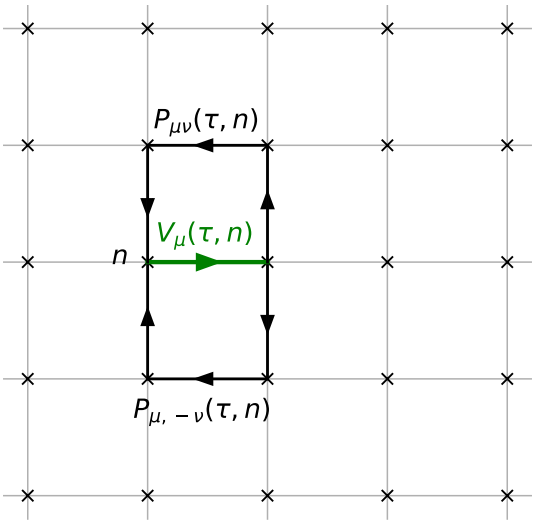


Figure 8: The evolution of the flowed link $V_\mu(\tau, n)$ is governed by the difference of the plaquettes $P_{\mu\nu}(\tau, n)$ and $P_{\mu,-\nu}(\tau, n)$. It is the only link these two plaquettes share. This way, the link approaches the average of the surrounding ones with increasing $\tau$. Doing this for every link hence smoothes the overall field. Note that the plaquettes are expressed in terms of flowed links.

side of Eq. (6.23) as a difference despite the plus operator since one loop runs clockwise while the other one runs counter-clockwise. Therefore, the larger the difference between these fields, the more the link decreases with $\tau$, reducing the difference between these plaquettes and hence smoothing the field. This is sketched in Fig. 8. In Sect. 6.2.2, it will be shown to leading order that the $a \to 0$ limit of the lattice flow equation reproduces the continuum one which is not obvious by merely looking at continuum and lattice flow equation. The lattice gradient flow defined with the Wilson plaquette action is referred to as Wilson flow. Choosing another lattice action to define flow, flow evolution is governed by sampling not only plaquettes but the respective loops appearing in the action, for example rectangles if the Lüscher-Weisz action defines flow.

### 6.2.1. Improved gradient flow

As the lattice flow equation is a discretization, lattice cut-off artefacts similar to those described in Sect. 4 remain and can be analysed by inserting the Schwinger line integral. Again, one can push back their order by modifying the discrete version in a clever way. Considering Eq. (6.21), the obvious idea is to construct a lattice action to remove first deviations. These are of $\mathcal{O}(a^2)$ if the center of the links is again chosen to be between to lattice sites. However, Ramos and Sint found in Ref. [29] that this approach is not sufficient: Actions including paths of length $6a$ such as rectangles, chairs and parallelograms are not enough to remove $\mathcal{O}(a^2)$ terms in the flow. It has to be modified even further. They presented a solution to this problem in Ref. [28], the Zeuthen flow defined by

$$a^2 \dot{V}_\mu(\tau, x) = -g_0^2 \left[ \left( 1 + \frac{a^2}{12} \nabla_\mu^* \nabla_\mu \right) \partial_{n,\mu} S_{\text{impr}}[V] \right] V_\mu(\tau, x) \tag{6.24}$$

with the forward and backward covariant lattice derivatives acting on matrix-valued functions as

$$a \nabla_\mu f(\tau, n) = V_\mu(\tau, n) f(\tau, n + \hat{\mu}) V_\mu^\dagger(\tau, n) - f(\tau, n) \tag{6.25}$$

$$a \nabla_\mu^* f(\tau, n) = f(\tau, n) - V_\mu^\dagger(\tau, n - \hat{\mu}) f(\tau, n - \hat{\mu}) V_\mu(\tau, n - \hat{\mu}). \tag{6.26}$$

The action $S_{\text{impr}}$ is the improved lattice action from Eq. (4.22). The additional term including the covariant derivatives counters the remaining $\mathcal{O}(a^2)$ contributions but still vanishes in the continuum limit since it is proportional to $a^2$. Why Zeuthen flow is required for improvement and Lüscher-Weisz flow is not sufficient will be made clear in Sect. 8.

The 4+1-dimensional lattice theory can be established equivalently to the continuum. To the four-dimensional unflowed lattice action one adds a discrete flow action

$$S_{\text{flow}}^{\text{latt}}[L, V] = 2a \int_0^\infty \mathrm{d}\tau \sum_n \mathrm{Tr}\big( L_\mu(\tau, n) H_\mu(\tau, n) \big) \tag{6.27}$$

where the flow equation is written in the form $H_\mu(\tau, n) = 0$. For the Wilson flow, for example, one has

$$H_\mu(\tau, n) = a^2 \dot{V}_\mu(\tau, n) + g_0^2 \big(\partial_{n,\mu} S_P[V]\big) V_\mu(\tau, x), \tag{6.28}$$

and the flow equation is again enforced by the Euler Lagrange equation with respect to the Lagrange multiplier. For other discretizations of the flow equation, $H_\mu(\tau, x)$ obviously takes on a different form. The total action of the 4+1-dimensional theory is now

$$S_{4+1}^{\text{latt}}[U, L, V] = S_g^{\text{latt}}[U] + S_{\text{flow}}^{\text{latt}}[L, V]. \tag{6.29}$$

It is important to emphasize at this point that the action of the gauge fields on the four-dimensional boundary is not necessarily equal to the one defining the flow equation. For the discretization of the 4+1-dimensional action, two choices therefore need to be made. Also, when going from $U$ to $A$ or from $V$ to $B$ fields to make use of perturbation theory, the gauge needs to be fixed and the integration measure modified as summarized in Sect. 5.3.

### 6.2.2. Solving the the lattice flow equation to leading order

The continuum flow equation was already solved to leading order in Sect. 6, however, a slightly different approach to do so is helpful as it can be generalized to the lattice flow equation. The leading order continuum flow equation is Eq. (6.7) with $k = 0$ and, via transformation to momentum space, reads

$$\partial_\tau \tilde{B}_\mu(\tau, p) = -K_{\mu\nu}^{\text{cont}}(p) \tilde{B}_\nu(\tau, p) \tag{6.30}$$

with the continuum flow kernel

$$K_{\mu\nu}^{\text{cont}}(p) = p^2 \delta_{\mu\nu} - (1 - \lambda) p_\mu p_\nu. \tag{6.31}$$

Note that this is related but not equal to the heat kernel from Eq. (6.10) as will shown in the following. The leading order flow equation in this form is a set of four homogenous ordinary differential equations of first order with initial condition $\tilde{B}_\mu(0, p) = \tilde{A}_\mu(p)$ which is easy to solve. Here, the advantage of the Fourier transform is evident: A set of partial differential equations turns into a set of ordinary ones. The solution reads

$$\tilde{B}_\mu(\tau, p) = \left(e^{-\tau K^{\text{cont}}(p)}\right)_{\mu\nu} \tilde{A}_\nu(p). \tag{6.32}$$

The exponential of the flow kernel is

$$\left(e^{-\tau K^{\text{cont}}(p)}\right)_{\mu\nu} = \frac{1}{p^2} \left(p^2 e^{-\tau p^2} \delta_{\mu\nu} + (e^{-\lambda \tau p^2} - e^{-\tau p^2}) p_\mu p_\nu\right) \tag{6.33}$$

which is the heat kernel from Eq. (6.10). Therefore, one finds that Eq. (6.32) corresponds to the second line of Eq. (6.11) with $k = 0$ and both approaches are in accordance. Fittingly, inserting this solution of the flow equation in the leading order two-point function gives the flowed propagator from Eq. (6.12).

To see what happens on the lattice, consider the Wilson flow equation Eq. (6.21) where the right-hand side is given by Eq. (6.23). Expanding the flowed links according to $V_\mu(\tau, n) = \exp iag_0 B_\mu(\tau, n)$ to linear order in $B_\mu(\tau, p)$ to make use of perturbation theory, transforming to momentum space and fixing the gauge, one finds the leading order Wilson flow equation

$$\partial_\tau \tilde{B}_\mu(\tau, p) = -K_{\mu\nu}^{\text{W}}(p) \tilde{B}_\nu(\tau, p) \tag{6.34}$$

with the Wilson flow kernel

$$K_{\mu\nu}^{\text{W}}(p) = \hat{p}^2 \delta_{\mu\nu} - (1 - \lambda) \hat{p}_\mu \hat{p}_\nu. \tag{6.35}$$

Obviously, this can be solved completely analogously to the continuum case as presented previously, leading to

$$\tilde{B}_\mu(\tau, p) = \left(e^{-\tau K^{\text{W}}(p)}\right)_{\mu\nu} \tilde{A}_\nu(p). \tag{6.36}$$

The exponential of the Wilson flow kernel is the same as the continuum one in Eq. (6.33) with the replacements $p^2 \to \hat{p}^2$ and $p_\mu \to \hat{p}_\mu$. It is easy to see that the Wilson kernel approaches the continuum flow kernel for $a \to 0$ and therefore it is shown that the continuum limit of the leading order solution of Wilson flow is indeed the leading solution of continuum gradient flow which has not been made clear so far. In general, lattice gradient flows defined with any action to define flow according to Eq. (6.21) can be treated the same way: Expanding the lattice flow equation to leading order, Fourier transforming and gauge fixing always gives an expression of the form

$$\partial_\tau \tilde{B}_\mu(\tau, p) = -K_{\mu\nu}^{(f)}(p) \tilde{B}_\nu(\tau, p) \tag{6.37}$$

and its solution is given analogously to Eq. (6.36) where $K^{\text{W}}$ needs to be replaced by the respective flow kernel $K^{(f)}$. It always approaches the continuum kernel for $a \to 0$. If flow is defined with the Lüscher-Weisz action, one finds

$$K_{\mu\nu}^{\text{LW}}(p) = \left(\frac{5}{3}\hat{p}^2 - \frac{1}{3}\hat{c}_\mu^2 \hat{p}^2 - \frac{1}{3}\sum_\lambda \hat{c}_\lambda^2 \hat{p}_\lambda^2\right) \delta_{\mu\nu} - \left(\frac{5}{3} - \frac{1}{3}\left(\hat{c}_\mu^2 + \hat{c}_\nu^2\right) - \lambda\right) \hat{p}_\mu \hat{p}_\nu \tag{6.38}$$

with $\hat{c}_\mu = \cos(p_\mu a/2)$. The right continuum limit is again evident. Note that the Wilson and Lüscher-Weisz kernels are the same as appearing in the actions in Sect. 5.3.1. This is no coincidence and comes in handy: Expanding the lattice flow equation in $\tilde{B}_\mu(\tau, p)$ can be quite tedious for elaborate actions even to leading order. However, the flow kernel $K^{(f)}$ can always be found by expanding the flow action itself in $\tilde{B}_\mu$ which gives an expression like

$$S_g^{\text{latt}}[V] = \frac{1}{2}\int_{pq} (2\pi)^4 \delta^{(4)}(p+q)\tilde{B}^A_\mu(\tau,p)K^{(f)}_{\mu\nu}(p)\tilde{B}^A_\nu(\tau,q) + \mathcal{O}(B^3) \tag{6.39}$$

where the flow kernel can be read off. This procedure is often simpler than the more direct approach and is detailed in Appendix A for Wilson and Lüscher-Weisz flow. Zeuthen flow, while not defined by only an action, can still be treated the same way: To leading order, the additional operator $1 + \frac{a^2}{12}\nabla^*_\mu\nabla_\mu$ simply turns into $1 - \frac{a^2}{12}\hat{p}^2_\mu$ after expanding and Fourier transforming. Hence, the Zeuthen flow kernel is

$$K^{\text{Z}}_{\mu\nu}(p) = \left(1 - \frac{a^2}{12}\hat{p}^2_\mu\right) K^{\text{LW}}_{\mu\nu}(p). \tag{6.40}$$

Finalizing this discussion, flowed propagators can be expressed in terms of the flow kernel. If $D^{CD}_{\mu\nu}$ is the unflowed propagator for some lattice action, then the flowed propagator reads

$$\begin{aligned}(D^{\text{flow}})^{CD}_{\mu\nu}(\tau_1,\tau_2,p,q) &= \left\langle \tilde{B}^C_\mu(\tau_1,p)\tilde{B}_\nu(\tau_2,q)\right\rangle_0 \\ &= \left\langle \left(e^{-\tau_1 K^{(f)}(p)}\right)_{\mu\sigma}\tilde{A}^C_\sigma(p)\left(e^{-\tau_2 K^{(f)}(q)}\right)_{\nu\rho}\tilde{A}^D_\rho(q)\right\rangle_0 \\ &= \left(e^{-\tau_1 K^{(f)}(p)}\right)_{\mu\sigma}\left(e^{-\tau_2 K^{(f)}(q)}\right)_{\nu\rho} D^{CD}_{\sigma\rho}(p,q).\end{aligned} \tag{6.41}$$

In the last step, the linearity of the expectation value was used. This is a generalization of Eq. (6.12) to an arbitrary discretization of gauge action and flow on the lattice. Unfortunately, in general, there is no handy expression for the exponential of the flow kernel, most notably for Zeuthen flow. Calculations therefore need to be performed numerically. In the following, the framework sketched above and especially Eq. (6.41) will be used to determine leading order expectation values of flowed operators on the lattice with numerical momentum integration. Note that the propagators described here are not observables by themselves as they depend on the gauge and bear no immediate physical information. However, they will be part of the expression for gauge-invariant observables.

## 7. Color-electric and color-magnetic correlation functions on the lattice

At low temperatures, quarks do not occur freely but are bound in hadrons since under these conditions, the coupling of strong interaction is large. However, at high temperatures - for example briefly after the big bang or in heavy-ion collisions - a new phase of strong interacting matter, the quark-gluon plasmas (QGP) arises. After its existence has been speculated for years, it was finally observed at the beginning of the century at the Relativistic Heavy Ion Collider (RHIC) of the Brookhaven National Laboratory [30, 31, 32]. Since it exists only on short time and length scales, the properties of the QGP can be measured only indirectly, for example by its effect on the behaviour of heavy quarks such as charm and bottom quarks. Their diffusion has been shown to be anisotropic, a phenomenon which is called elliptic flow [30, 32]. As it turns out, the QGP shows properties of a fluid [33]. This allows a modelling by hydrodynamics. Hydrodynamics in turn require input parameters, so-called transport coefficients. This section summarizes how one of them, the momentum diffusion coefficient, depends on QCD correlation functions and how to calculate those perturbatively. First, however, the implementation of the surrounding medium in perturbation theory is outlined briefly.

### 7.1. Thermal baths as a time cut-off

To treat correlators used in the description of the QGP, one further step that has not been described yet needs to be taken: Previously, only vacuum expectation values have been described, however, the QGP is a thermal bath with temperature $T$. Luckily, for purposes of this work, incorporating a temperature is easy: It is sufficient to introduce a time periodicity of extent $\beta = L_\tau = 1/T$ for Euclidean correlators. The justification for that is that the partition function - an important tool in statistical physics - has a formula that is similar to the Euclidean path integral outlined in Sect. 2 but with time integration of the action in the exponential restricted to $\beta$ [34, 35]. From here on, the symbol $\tau$ will be used for Euclidean time while for flow time, $\tau_F$ will be used. The boundary conditions following from the periodicity renders the temporal momentum coefficient $p_0$ not continuous, instead, it is discrete and takes values

$$p_0 = \frac{2\pi}{L_\tau}n = 2\pi n T \tag{7.1}$$

with any integer $n$. Consequently, the momentum integration over the $p_0$ component of the Fourier transform turns into a sum over allowed momenta,

$$\int_{-\infty}^{\infty}\frac{\mathrm{d}p_0}{2\pi} \to T\sum_{n\in\mathbb{Z}}. \tag{7.2}$$

The factor of $2\pi$ cancels, it occurs in the numerator due to the momentum step size as well as in the denominator because of the Fourier transform. On the lattice, the finite step size in position space also leads to a cutoff of the sum in the same way the momentum integral is restricted to the Brillouin zone in the vacuum. Allowed values of the momentum or the summation index $n$ arise from

$$\begin{aligned} -\frac{\pi}{a} &\leqslant p_0 < \frac{\pi}{a} \\ \Leftrightarrow -\frac{\pi N_\tau}{L_\tau} &\leqslant 2\pi n T < \frac{\pi N_\tau}{L_\tau} \\ \Leftrightarrow -\frac{N_\tau}{2} &\leqslant n < \frac{N_\tau}{2} - 1. \end{aligned} \tag{7.3}$$

In the first step, the number of lattice sites in temporal direction $N_\tau = L_\tau / a$ was introduced while in the last step, $L_\tau = 1/T$ was used. Consequently, in a heat bath on the lattice,

$$\int_{-\pi/a}^{\pi/a} \frac{\mathrm{d}p_0}{2\pi} \to T \sum_{n=-N_\tau/2}^{N_\tau/2-1}. \tag{7.4}$$

For a more detailed look into thermal field theory, refer to Refs. [34, 35].

## 7.2. Relevance of color-electric and color-magnetic correlators for heavy quark behaviour in the QGP

The theory of describing the dynamics of heavy particles suspended in a bath of lighter ones while not in equilibrium is not new. Einstein and Langevin laid its groundwork at the beginning of last century independently of each other when modelling Brownian motion [36, 37]. While the general concept translates to heavy quarks in the QGP in heavy-ion collisions - massive particles suspended in lighter ones disturbed from equilibrium -, of course a more careful treatment is needed here. The framework for that was developed by Kubo in the 1950s in Refs. [38, 39] by calculating the response of a thermal system to a perturbation. In a classical picture of processes like these, force-force correlation functions at different times of the forces that act on the suspended particles are often paramount [33]. Similar to electrodynamics, the strong force on quarks is mediated by color-electric and color-magnetic fields so it is to be expected that they play a role in the diffusion of heavy quarks in the QGP. Indeed, in Ref. [40], heavy quark effective theory is used to relate the momentum diffusion coefficient $\kappa$ to Euclidean color-electric correlation functions. In the continuum, the electric field components are components of the field strength tensor,

$$E_i = F_{0i},\ i = 1, 2, 3.$$

This is in line with the definition of electric fields in in QED. On the lattice, a discretization of this operator needs to be chosen. The authors found that in the heavy quark limit, $\kappa$ is encrypted in the spectral function of the operator

$$G_E^{\text{cont}}(\tau) = -\frac{1}{3} \sum_i \frac{\left\langle \mathrm{Re\,Tr}[U_\tau^\beta(\vec{0}) E_i(\tau, \vec{0}) U_0^\tau(\vec{0}) E_i(0, \vec{0})] \right\rangle}{\left\langle \mathrm{Re\,Tr}[U_0^\beta(\vec{0})] \right\rangle} \tag{7.5}$$

where $U_{\tau_1}^{\tau_2}(\vec{x}) = \exp\left(i g_0 \int_{\tau_1}^{\tau_2} A_0(\tau, \vec{x}) \mathrm{d}\tau\right)$ is a Wilson line from $\tau_1$ to $\tau_2$ at spatial position $\vec{x}$ that only runs in time direction. The spatial position can be chosen to be the origin because of translational invariance. The operator in Eq. (7.5) takes the correlation between two electrical fields that have a time-separation of $\tau$ connected by time-direction only Wilson lines so as foreshadowed, this is the force-force correlator necessary for the description of heavy quark propagation in the QGP. The denominator serves as gauge-invariant normalization. Having determined the color-electric operator, its spectral function $\rho_E(\omega)$ can be found by inverting

$$G_E(\tau) = \int_0^\infty \frac{\mathrm{d}\omega}{\pi} \rho_E(\omega) \frac{\cosh\left(\frac{\beta}{2} - \tau\right)\omega}{\sinh\left(\frac{\beta\omega}{2}\right)}. \tag{7.6}$$

This is a highly non-trivial task and its execution will not be addressed in this work. The momentum diffusion coefficient is encoded in the zero-frequency limit of $\rho_E(\omega)$ via

$$\kappa = \lim_{\omega \to 0} \frac{2T}{\omega} \rho_E(\omega). \tag{7.7}$$

The authors also provide a lattice discretization of Eq. (7.5) which is simplified by their use of Wilson lines which translate to the lattice easily. The electric field is discretized as

$$E_i(\tau, \vec{x}) = U_0(\tau, \vec{x} + \hat{\imath}) U_i(\tau, \vec{x}) - U_i(\tau + a, \vec{x}) U_0(\tau, \vec{x}). \tag{7.8}$$

The color-electric correlator on the lattice is then

$$G_E^{\text{latt}}(\tau) = -\frac{1}{3} \sum_i \frac{\left\langle \mathrm{Re\,Tr}[U_{\tau+a}^\beta(\vec{0}) E_{-i}(\tau, \hat{\imath}) U_a^\tau(\hat{\imath}) E_i(0, \vec{0})] \right\rangle}{\left\langle \mathrm{Re\,Tr}[U_0^\beta(\vec{0})] \right\rangle} \tag{7.9}$$

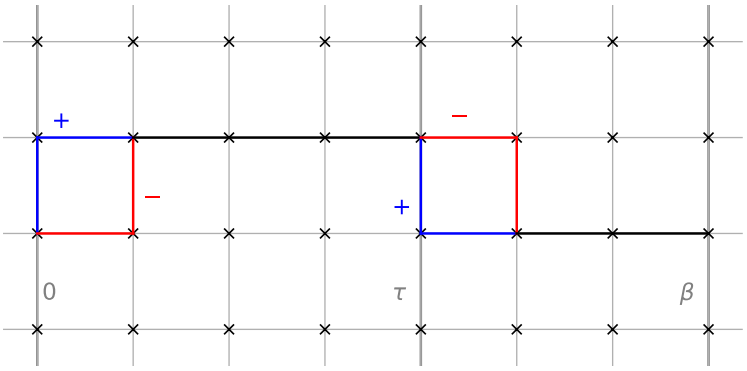


Figure 9: The color-electric correlator on the lattice. Time runs from left to right while the vertical axis corresponds to the spatial direction $i$. Blue links have a positive sign, red links a negative one. The black segments are the Wilson lines $U_{\tau_1}^{\tau_2}(\vec{x})$. The grey line in the middle indicates the temporal separation $\tau$. Time periodicity makes the operator a closed loop and therefore gauge invariant.

which is sketched in Fig. 9. Note that this is dimensionless while $G_E^{\text{cont}}$ has units of length$^{-4}$ so they differ by a factor of $a^4$. To avoid clutter of notation, this factor will be omitted for perturbative results so that those are of the same dimension as the continuum ones to simplify comparison. The color-electric correlator was measured under Zeuthen flow on the lattice with Wilson action in Ref. [41]. The authors use leading order lattice perturbation theory at flow time $\tau_F = 0$ to facilitate the continuum extrapolation via tree-level improvement as outlined in Sect. 5.3. However, normalization with the leading order lattice correlator with the right flow-time dependence is to be preferred since this simplifies not only continuum but also flow-time-to-zero extrapolation. Since the authors did not have any data to do so; one of the goals of this work is to provide precisely that.

The consideration above is a leading order result of heavy quark effective theory. The expansion parameter is proportional to the inverse heavy quark mass. In Ref. [42], the next-to-leading order contribution to $\kappa$ was figured out. It is determined by the spectral function of the expectation value of color-magnetic instead of color-electric fields. In an illustrative sense, color-magnetic fields contribute to the force on heavy quarks as well albeit to a smaller degree than their electric counterparts. In the continuum, the magnetic field relates to the components of the field strength tensor via

$$B_i = -\frac{1}{2}\varepsilon_{ijk}F_{jk}. \tag{7.10}$$

Unfortunately, the same symbol for the magnetic field operators and the flowed gluon fields is used. However, it will be clear from context which one is meant. The rest of the consideration is equivalent for electric and magnetic correlation functions. Defining the operator

$$G_B^{\text{cont}}(\tau) = \frac{1}{3}\sum_i \frac{\left\langle \operatorname{Re}\operatorname{Tr}[U_\tau^\beta(\vec{0})B_i(\tau,\vec{0})U_0^\tau(\vec{0})B_i(0,\vec{0})]\right\rangle}{\left\langle \operatorname{Re}\operatorname{Tr}[U_0^\beta(\vec{0})]\right\rangle} \tag{7.11}$$

that correlates two magnetic fields separated in time by $\tau$, the spectral function $\rho_B(\omega)$ defined by

$$G_B(\tau) = \int_0^\infty \frac{\mathrm{d}\omega}{\pi}\rho_B(\omega)\frac{\cosh\left(\frac{\beta}{2}-\tau\right)\omega}{\sinh\left(\frac{\beta\omega}{2}\right)} \tag{7.12}$$

contains the next-to-leading order contribution to the momentum diffusion coefficient in its infrared limit according to

$$\kappa' = \lim_{\omega\to 0}\frac{2T}{\omega}\rho_B(\omega). \tag{7.13}$$

On the lattice, the magnetic field can be discretized as

$$B_i(\tau,\vec{x}) = \varepsilon_{ijk}U_k(\tau,\vec{x}+\hat{\jmath})U_j(\tau,\vec{x}). \tag{7.14}$$

This definition leads to the lattice color-magnetic correlator

$$G_B^{\text{latt}}(\tau) = \frac{1}{3}\sum_i \frac{\left\langle \operatorname{Re}\operatorname{Tr}[U_\tau^\beta(\vec{0})B_{-i}(\tau,\hat{\jmath}+\hat{k})U_0^\tau(\hat{\jmath}+\hat{k})B_i(0,\vec{0})]\right\rangle}{\left\langle \operatorname{Re}\operatorname{Tr}[U_0^\beta(\vec{0})]\right\rangle} \tag{7.15}$$

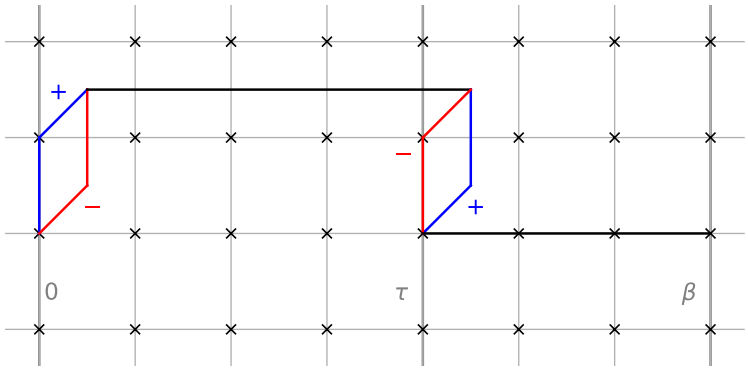


Figure 10: The color-magnetic correlator on the lattice. Again, time runs from left to right. The vertical direction and the one orthogonal to the drawing plane correspond to $j$ and $k$ appearing in Eq. (7.15) respectively. The colour-code and the vertical lines are the same as in Fig. 9.

where the indices $j, k$ are the summation indices that arise from inserting Eq. (7.14) into the correlator. Fig. 10 is a sketch of $G_B^{\text{latt}}$. In Ref. [43], it was measured on the lattice analogously to the color-electric correlator. Again, proper flow-time dependent normalization is missing, providing the necessary data is also goal of this work.

## 7.3. Leading order analysis of color-electric and -magnetic correlators under flow

The gradient-flowed lattice correlators described in the previous section shall now be calculated in leading order perturbation theory. For flowed operators $\mathcal{O}$ that contain two gluonic fields, the leading order contribution to the expectation value can be expressed as

$$\begin{aligned}\langle \mathcal{O} \rangle_0 &= \sum\!\!\!\!\!\!\int_{pq} O_{\mu\nu}^{CD}(p) (D^{\text{flow}})_{\mu\nu}^{CD}(\tau_{F,1}, \tau_{F,2}, p, q) \\ &= \sum\!\!\!\!\!\!\int_{pq} O_{\mu\nu}^{CD}(p) \left(e^{-\tau_F K^{(f)}(p)}\right)_{\mu\sigma} \left(e^{-\tau_F K^{(f)}(q)}\right)_{\nu\rho} D_{\sigma\rho}^{CD}(p,q) \\ &= \sum\!\!\!\!\!\!\int_{p} O_{\mu\nu}^{CD}(p) \left(e^{-\tau_F K^{(f)}(p)}\right)_{\mu\sigma} \left(e^{-\tau_F K^{(f)}(p)}\right)_{\nu\rho} D_{\sigma\rho}^{CD}(p)\end{aligned} \tag{7.16}$$

where $O_{\mu\nu}^{CD}(p)$ is an operator-dependent matrix. In the second step, the general flowed propagator from Eq. (6.41) was inserted and it was chosen that both fields are flowed to the same depth $\tau_F = \tau_{F,1} = \tau_{F,2}$. In the last step, the delta distribution in the propagator was integrated over and $D_{\mu\nu}^{CD}(p)$ was defined by factoring $(2\pi)^4 \delta^{(4)}(p+q)$ out from the propagator according to

$$D_{\mu\nu}^{CD}(p,q) = (2\pi)^4 \delta^{(4)}(p+q) D_{\mu\nu}^{CD}(p). \tag{7.17}$$

In Eq. (7.16), the three discretization choices on the lattice are evident: The operator kernel $O_{\mu\nu}^{CD}$ depends on the discretization choice of the observable, the flow kernel $K^{(f)}$ depends on the lattice implementation of gradient flow while the propagator $D_{\mu\nu}^{CD}$ depends on the underlying gauge action. A leading order calculation of an expectation value hence requires determining the operator kernel $O_{\mu\nu}^{CD}$ and, after having chosen a specific lattice action and flow, performing the momentum integration and summation. For the first step, the operator expressed in terms of links is expanded to $\mathcal{O}(B^2)$. The second step is in general performed numerically, however, for Wilson action and flow, often an analytical solution exists.

### 7.3.1. Flowed color-electric correlator in leading order perturbation theory

The color-electric lattice correlator Eq. (7.9) is now expanded to squared order in $B_\mu$ as mentioned above. The details of this calculation can be found in Appendix B. One finds

$$\begin{aligned} G_E^{\text{latt}}(\tau,\tau_F) &= -\frac{g_0^2}{18}\sum\!\!\!\!\!\!\int_p \cos(p_0\tau)\delta^{CD}\sum_i\Big[\hat{p}_i^2(D^{\text{flow}})_{00}^{CD}(\tau_F,p)+\hat{p}_0^2(D^{\text{flow}})_{ii}^{CD}(\tau_F,p)-2\hat{p}_0\hat{p}_i(D^{\text{flow}})_{0i}^{CD}(\tau_F,p)\Big]+\mathcal{O}(g_0^3) \\ &= -\frac{g_0^2T}{18}\sum_{n=-\frac{N_\tau}{2}}^{\frac{N_\tau}{2}-1}\cos(2\pi n\tau T)\delta^{CD}\times \\ &\quad \int_p\Big[\hat{p}_i^2(D^{\text{flow}})_{00}^{CD}(\tau_F,p)+\hat{p}_0^2(D^{\text{flow}})_{ii}^{CD}(\tau_F,p)-2\hat{p}_0\hat{p}_i(D^{\text{flow}})_{0i}^{CD}(\tau_F,p)\Big]+\mathcal{O}(g_0^3). \end{aligned} \tag{7.18}$$

For Wilson flow and Wilson action, an analytical solution for the momentum integrals exists that will be presented shortly. For other choices, the momentum integration is performed numerically. The focus for the numerical calculations will lie on Wilson action and Zeuthen flow as this combination is used in Refs. [41, 43]. Choosing Feynman gauge for both flow and action, $\lambda=\alpha=1$, the Wilson-Wilson propagator reduces to

$$(D^{\text{latt}})_{\mu\nu}^{CD}(\tau_F,p)=\frac{1}{\hat{p}^2}e^{-2\tau_F\hat{p}^2}\delta_{\mu\nu}\delta^{CD}. \tag{7.19}$$

Inserting this into Eq. (7.18) and performing the sum over the Lie algebra indices $C,D$ gives

$$\begin{aligned} G_E^{\text{WW}}(\tau,\tau_F) &= -\frac{g_0^2C_FT}{3}\sum_{n=-\frac{N_\tau}{2}}^{\frac{N_\tau}{2}}\cos(2\pi n\tau T)\int_p e^{-2\tau_F\hat{p}^2}\frac{1}{\hat{p}^2}\left(\sum_i\hat{p}_i^2+3\hat{p}_0^2\right)+\mathcal{O}(g_0^3) \\ &= -\frac{g_0^2C_FT}{3}\sum_{n=-\frac{N_\tau}{2}}^{\frac{N_\tau}{2}}\cos(2\pi n\tau T)\int_p e^{-2\tau_F\hat{p}^2}\left(3-2\frac{\sum_i\hat{p}_i^2}{\hat{p}^2}\right)+\mathcal{O}(g_0^3) \end{aligned} \tag{7.20}$$

where $C_F=(N_c^2-1)/(2N_c)=4/3$ with the number of colours $N_c$. In the second step, $\hat{p}_0^2=\hat{p}^2-\sum_i\hat{p}_i^2$ was used. To solve the momentum integral, one requires the modified Bessel functions $I_\gamma(z)$ of the first kind and order $\gamma$. They can be expressed in terms of integrals [44],

$$I_\gamma(z)=\frac{1}{\pi}\int_0^\pi e^{z\cos\theta}\cos(\gamma\theta)\mathrm{d}\theta-\frac{\sin(\pi\gamma)}{\pi}\int_0^\infty e^{-z\cosh(t)-\gamma t}\mathrm{d}t, \tag{7.21}$$

where the second term vanishes for $\gamma\in\mathbb{N}_0$. The integration is detailed in Appendix B.1 and yields [41]

$$\begin{aligned} G_E^{\text{WW}}(\tau,\tau_F) &= -g_0^2C_FT^4N_\tau^3\sum_{n=-N_\tau/2}^{N_\tau/2-1}\cos(2\pi n\tau T)\times \\ &\Bigg[e^{-8\tau_FT^2N_\tau^2\sin^2(\frac{\pi n}{N_\tau})}e^{-12\tau_FT^2N_\tau^2}I_0\left(4\tau_FT^2N_\tau^2\right)^3-\int_{8\tau_FT^2N_\tau^2}^\infty \mathrm{d}x e^{-x\sin^2(\frac{\pi n}{N_\tau})}e^{-\frac{3}{2}x}I_0\left(\frac{x}{2}\right)^2\left(I_0\left(\frac{x}{2}\right)-I_1\left(\frac{x}{2}\right)\right)\Bigg]+\mathcal{O}(g_0^3). \end{aligned} \tag{7.22}$$

The integration over $x$ needs to be performed numerically. If $n\neq0$, this is easy since then, the first exponential factor makes the integrand converge exponentially. However, for $n=0$, this factor vanishes and the integrand only converges like $x^{-\frac{3}{2}}$ since

$$I_\gamma(x)\sim\frac{e^x}{\sqrt{2\pi x}} \tag{7.23}$$

for large $x$ [45]. Therefore, it converges very slowly which exacerbates the evaluation of this integral. Luckily, this addend can be rewritten since $n=0$ leads to $\hat{p}_0=0$ and therefore, $\sum_i\hat{p}_i^2=\hat{p}^2$. Therefore, the $n=0$ addend of Eq. (7.20) reduces to

$$\begin{aligned} \left(G_E^{\text{WW}}(\tau,\tau_F)\right)\Big|_{n=0} &= -\frac{g_0^2C_FT}{3}\int_p e^{-2\tau_F\sum_i\hat{p}_i^2} \\ &= -\frac{g^2C_FT^4N_\tau^3}{3}e^{-12\tau_FT^2N_\tau^2}I_0\left(4\tau_FT^2N_\tau^2\right)^3 \end{aligned} \tag{7.24}$$

which can be evaluated without any additional integration. The second step is equivalent to what is outlined in Eq. (B.22) in Appendix B.1. Note that due to the lattice character, allowed values for the temporal separation $\tau$ in Eq. (7.22) are given by

$$\tau T=\frac{\tau}{L_\tau}=\left\{\frac{1}{N_\tau},\frac{2}{N_\tau},...,\frac{1}{2}-\frac{1}{N_\tau},\frac{1}{2}\right\}. \tag{7.25}$$

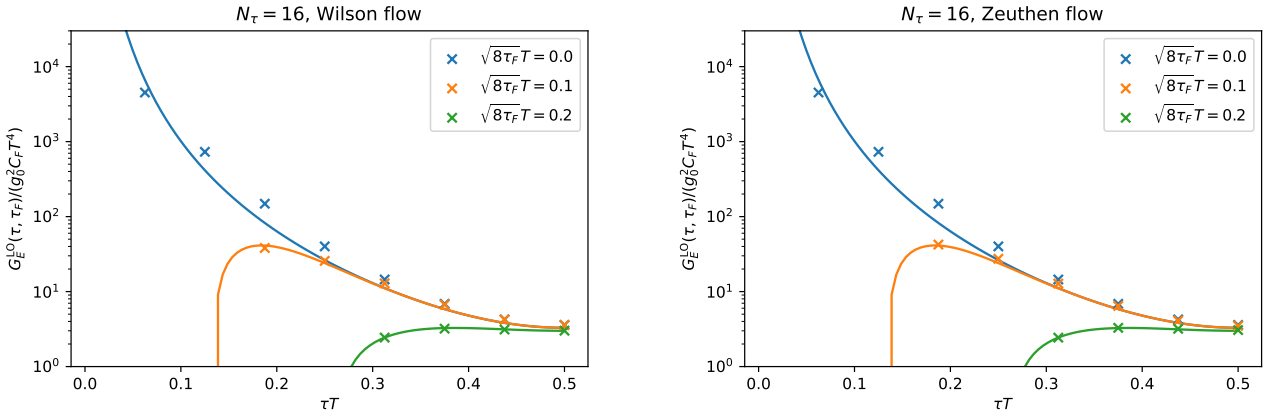


(a) (b)

Figure 11: The leading order color-electric correlator under gradient flow in the continuum (solid lines) and on the lattice (markers), the latter with Wilson action and (a) Wilson or (b) Zeuthen flow. It is easy to see that flow brings lattice correlators closer to their continuum counterparts. The steep drop at small separations indicates the unphysical region produced by too much gradient flow. Both flow choices yield similar results.

Values larger than $1/2$ are redundant as they are equivalent to smaller separations because of the periodic time boundary. Under gradient flow, the continuum leading order color-electric correlator, that is the leading order expansion of Eq. (7.5), was calculated in Ref. [46] as

$$G_{\mathrm{E}}^{\mathrm{cont}}(\tau, \tau_F) = \frac{g^2 C_F T^4}{\pi^2} \sum_{n \in \mathbb{Z}} \frac{1}{\tilde{t}_n^4} \left[ \left( \tilde{\xi}_n^4 + \tilde{\xi}_n^2 + 1 \right) e^{-\tilde{\xi}_n^2} - 1 \right] + \mathcal{O}(g_0^3) \tag{7.26}$$

with the dimensionless quantities $\tilde{t}_n = t_n T$ and $\xi_n^2 = t_n^2 T^2 / \tilde{\tau}_F$ where $t_n = \tau + n/T$ and $\tilde{\tau}_F = 8\tau_F T^2$. Note that here, the sum has no cut-off: It arises from the method of images since in the continuum, each copy in position space caused by the time periodicity contributes to the correlator. This is where the shift $n/T$ in $t_n$ comes from; each $n$ describes one copy. The Wilson-Wilson color-electric correlator from Eq. (7.22) is compared to the continuum result in Fig. 11a for both the flowed and unflowed case. It is evident that the larger the flow time, the closer the lattice correlator is to the continuum one. However, the disadvantage of gradient flow is equally obvious: At small separations, the flowed correlator drops severely. The reason is that the smearing of the fields gets too large compared to the separation $\tau$ so that the two 'bends' in the color-electric correlator contaminate each other, creating an unphysical region where no useful information can be extracted.

For Wilson action and Zeuthen flow, Eq. (7.18) needs to be integrated numerically since the flowed propagator has to be calculated numerically as well according to Eq. (6.41). 64 sampling positions whose density is larger close to the origin were chosen for each spatial direction since this region dominates the integral. The sampling points were also chosen to satisfy a quadrature that is accurate up to $p^8$. The integration was performed for the Wilson-Wilson case as well to test its accuracy. It was in the order of $10^{-8}$ which is several orders of magnitude better than the statistical uncertainty in Refs. [41, 43] so this is suitable for tree-level improvement. However, for larger $N_\tau$, the accuracy gets worse so the sampling size needs to be increased. The color-electric correlator on the lattice with Wilson action and under Zeuthen flow is shown in Fig. 11b. The result is similar to the one with Wilson flow but of course not quite the same; for a representative flow time of $\sqrt{8\tau_F}T = 0.1$ and a temporal lattice extent of $N_\tau = 16$ they are compared in Fig. 12. This figure also exemplifies the success of improvement by using Zeuthen flow. Consider the horizontal axis to be function of the temperature $T$ instead of the separation $\tau$. At large temperatures - which correspond to fine lattices according to $a = 1/(N_\tau T)$ - the Zeuthen flowed observable is a better approximation to the continuum than the Wilson flowed observable. At small temperatures which correspond to coarse lattices, $\mathcal{O}(a^4)$ effects come into play so the advantage of Zeuthen flow is lost. The framework used for the numerical integration also allows for other combinations of action and flow to be calculated.

### 7.3.2. Flowed color-magnetic correlator in leading order perturbation theory

The color-magnetic lattice correlator Eq. (7.15) is now treated equivalently as the color-electric lattice correlator. First, a general leading-order expression dependent on action and flow is given. Choosing both as Wilson, an analytical solution for the integration over spatial momenta exists. For Wilson action and Zeuthen flow, values are calculated numerically. After performing the small

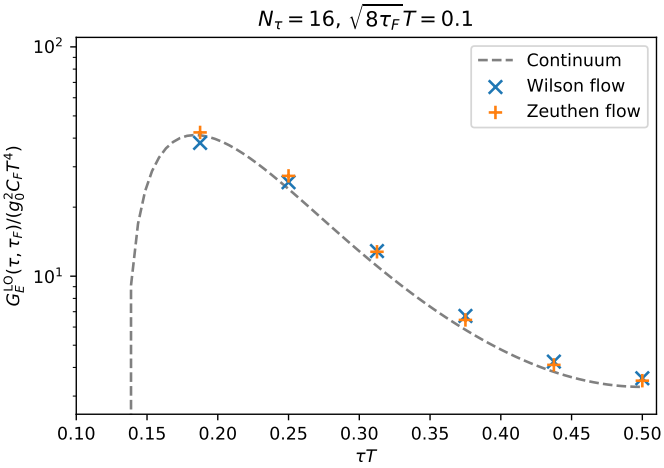


Figure 12: Comparison of Wilson and Zeuthen flow. While similar, they are not equal. At large temperatures, the Zeuthen flowed correlator is closer to the continuum value than the Wilson flowed one.

coupling expansion as outlined in Appendix B, one finds

$$\begin{aligned} G_B^{\text{latt}}(\tau,\tau_F) &= \frac{g_0^2}{18}\sum\!\!\!\!\!\!\int_p \cos(p_0\tau)\delta^{CD}\sum_{jk}\Big[\sum_i \hat{p}_i^2\delta_{jk} - \hat{p}_j\hat{p}_k\Big](D^{\text{flow}})_{jk}^{CD}(\tau_F,p) + \mathcal{O}(g_0^3) \\ &= \frac{g_0^2 T}{18}\sum_{n=-\frac{N_\tau}{2}}^{\frac{N_\tau}{2}-1}\cos(2\pi n\tau T)\delta^{CD}\int_p\sum_{jk}\Big[\sum_i \hat{p}_i^2\delta_{jk} - \hat{p}_j\hat{p}_k\Big](D^{\text{flow}})_{jk}^{CD}(\tau_F,p) + \mathcal{O}(g_0^3). \end{aligned} \tag{7.27}$$

This is a new result. After inserting the Wilson-Wilson propagator with Feynman gauge in flow and action, Eq. (7.19), performing the sum over the Lie algebra indices $C, D$ and the spatial indices $j, k$ gives

$$G_B^{\text{WW}}(\tau,\tau_F) = \frac{2g_0^2 C_F T}{3}\sum_{n=-\frac{N_\tau}{2}}^{\frac{N_\tau}{2}-1}\cos(2\pi n\tau T)\int_p e^{-2\tau_F\hat{p}^2}\frac{\sum_i \hat{p}_i^2}{\hat{p}^2} + \mathcal{O}(g_0^3). \tag{7.28}$$

This is equivalent to the second term in Eq. (7.20) whose evaluation is detailed in Appendix B.1 and finally gives

$$G_B^{\text{WW}}(\tau,\tau_F) = g_0^2 C_F T^4 N_\tau^3\sum_{n=-\frac{N_\tau}{2}}^{\frac{N_\tau}{2}-1}\cos(2\pi n\tau T)\int_{8\tau_F T^2 N_\tau^2}^{\infty}\mathrm{d}x e^{-x\sin^2(\frac{\pi n}{N_\tau})}e^{-\frac{3}{2}x}I_0\left(\frac{x}{2}\right)^2\left(I_0\left(\frac{x}{2}\right) - I_1\left(\frac{x}{2}\right)\right) + \mathcal{O}(g_0^3). \tag{7.29}$$

Again, the problem of bad convergence of the $n = 0$ term arises which can be solved by rewriting it to

$$\begin{aligned} \left(G_B^{\text{WW}}(\tau,\tau_F)\right)\Big|_{n=0} &= \frac{2g_0^2 C_F T}{3}\int_p e^{-2\tau_F\sum_i\hat{p}_i^2} \\ &= \frac{2g_0^2 C_F T^4 N_\tau^3}{3}e^{-12\tau_F T^2 N_\tau^2} I_0\left(4\tau_F T^2 N_\tau^2\right)^3 \end{aligned} \tag{7.30}$$

which is the twice the expression as for $G_E^{\text{WW}}$. Interestingly, if $\tau_F$ vanishes, the color-electric correlator coincides with the color-magnetic one both in the continuum [42] and on the lattice with Wilson action [43]. The latter can be seen by considering that the first term in the second line of Eq. (7.22) turns to unity if $\tau_F = 0$ which leaves the sum over the cosine which vanishes. Then, only the second term remains which is the same expression as $G_E^{\text{WW}}(\tau, 0)$. Due to the lack of analytical expressions, it is unclear if they are the same under different actions, for example Lüscher-Weisz, as well. The color-magnetic correlator with Wilson action and Wilson or Zeuthen flow is shown in Figs. 13a and 13b respectively, again compared to the continuum. The latter was calculated in Ref. [47] and reads

$$G_B^{\text{cont}}(\tau,\tau_F) = \frac{g^2 C_F T^4}{\pi^2}\sum_{n\in\mathbb{Z}}\frac{1}{\tilde{t}_n^4}\left[1 - \left(\xi_n^2+1\right)e^{-\xi_n^2}\right] \tag{7.31}$$

with the same dimensionless quantities as in Eq. (7.26). For the lattice correlators, the same integration technique as for $G_E^{\text{latt}}$ was used. Again, the analytical result Eq. (7.29) for Wilson flow was used to test the numerical accuracy which, for small lattices, turned

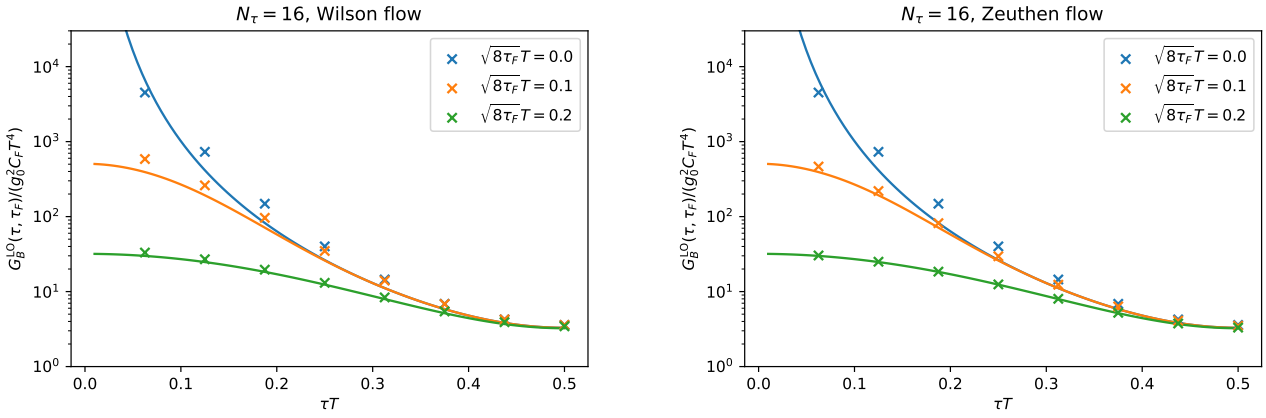


(a) (b)

Figure 13: The leading order color-magnetic correlator under gradient flow on the lattice (markers), the latter with Wilson action and (a) Wilson or (b) Zeuthen flow. The solid line are the continuum results. The one with $\tau_F = 0$ is the same as for the color-electric correlator. As expected, both flow choices yield similar but not equal results.

out to be around $10^{-8}$ as well which allows this data to be used for tree-level improvement. While the unphysical region is less evident as for the color-electric correlator since there is no sharp decline for too small separations, it still exists. The precise reason for this is that at zero flow, $G_E$ at $\tau = 0$ has an opposite sign compared to finite separation. This does not hold for $G_B$. At finite flow, the effect of this contact term is 'smeared' so that is contaminates the finite-separation correlators. For $G_E$, this leads to the observed sign flip.

## 8. Lattice deviations of action density

Finishing the discussion on color-electric and color-magnetic correlators in the QGP, there is another observable that deserves discussion due to its relevance in lattice simulations. The gradient-flowed action density $\varepsilon(\tau_F)$ is often used to determine the gauge coupling $g_0$ [21]. Its measurement is necessary since it is not an input parameter of these simulations. In the continuum, the action density is the expectation value of the pure gauge term of the QCD Lagrangian Eq. (2.15),

$$\varepsilon^{\text{cont}}(\tau_F) = \frac{g_0^2}{4} G^A_{\mu\nu}(x) G^A_{\mu\nu}(x) \tag{8.1}$$

where the field strength tensor $G^A_{\mu\nu}(x)$ is expressed in terms of flowed fields $B_\mu(x)$. Translation invariance allows to choose $x = 0$. Note that the subsequent discussion takes place in a vacuum, not in a thermal bath like $G_E$ and $G_B$. The idea of measuring the gauge coupling is explained in the following. As outlined in Appendix C, the leading order contribution to the continuum action density is [21]

$$\left\langle \varepsilon^{\text{cont}}(\tau_F) \right\rangle = \frac{3(N_c^2 - 1) g_0^2}{128 \pi^2 \tau_F^2} + \mathcal{O}(g_0^4) \tag{8.2}$$

which diverges in the $\tau_F \to 0$ limit. Measuring it at a finite flow time $\tau_F$ hence allows to determine the gauge coupling with two different methods: One can solve for the coupling and use this to define the renormalized coupling $g_{\text{flow}}$ at scale given by the flow depth,

$$g^2_{\text{flow}} = \frac{128\pi^2}{3(N_c^2 - 1)} \tau_F^2 \left\langle \varepsilon^{\text{cont}}(\tau_F) \right\rangle. \tag{8.3}$$

Alternatively, one can measure the action density and match it with perturbative schemes, for example $\overline{\text{MS}}$. By this matching, the perturbative coupling $g_{\text{pert}}$ can be extracted. A problem of these methods is that their validity is restricted to the continuum while in fact lattice observables are measured. Therefore, discretization errors of order $a^2$ and higher arise that need to be accounted for in the leading order expectation value. Doing so gives the general expression

$$\left\langle \varepsilon^{\text{latt}}(\tau_F) \right\rangle = \frac{g_0^2 (N_c^2 - 1)}{\pi^2 \tau_F^2} \left[ \frac{3}{128} + \sum_{n=1}^{\infty} \frac{c_{2n} a^{2n}}{\tau_F^n} \right] + \mathcal{O}(g_0^4). \tag{8.4}$$

In accordance with Eq. (7.16), the expansion parameters $c_m,\ m = 2, 4, 6, \ldots$ depend on the discretization of the observable - in this case action density -, the lattice action and the choice of gradient flow procedure. Considering them allows for a superior extraction of the gauge coupling compared to using only the continuum expression or to find a combination that is most advantageous for specific purposes. While they have been calculated to some order for different discretizations [28, 48], some combinations, especially those involving Zeuthen flow, have not been determined to order $\mathcal{O}(a^4)$. This will be done in this work.

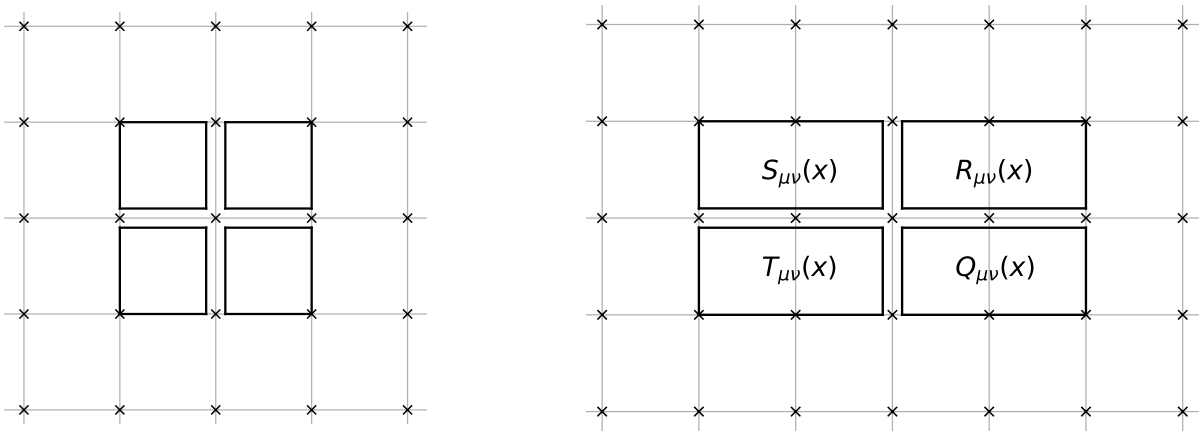


Figure 14: The (a) naive and (b) rectangle clover discretization of the field strength. For the rectangle, only one part is shown, a clover where the rectangles extend one link in the horizontal and two in the vertical direction is needed as well. The orientation of the loops is in a way so that the contour of the entire combination runs counter-clockwise, same as the plaquette operator. A superposition of both naive and rectangle clover can be used to define an improved field strength.

## 8.1. Definitions of the action density on the lattice

There are different popular methods to discretize the action density. The easiest one is again using a single plaquette which is called Wilson discretization,

$$\varepsilon^{\mathrm{W}}(\tau_F) = \frac{1}{a^4}\sum_{\mu\nu}\mathrm{Re}\,\mathrm{Tr}\big[1 - P_{\mu\nu}(\tau_F, x)\big]. \tag{8.5}$$

Similar to the continuum, it is the action but not summed or integrated over all positions. In the same sense, the improved Lüscher-Weisz action density

$$\begin{aligned}\varepsilon^{\mathrm{LW}}(\tau_F) &= \frac{1}{a^4}\sum_{\mu\nu}\mathrm{Re}\,\mathrm{Tr}\left[\frac{5}{3}\left(1 - P_{\mu\nu}(\tau_F, x)\right) - \frac{1}{12}\left(1 - R_{\mu\nu}(\tau_F, x)\right)\right] \\ &= \frac{1}{a^4}\sum_{\mu\nu}\mathrm{Re}\,\mathrm{Tr}\left[\frac{19}{12} - \frac{5}{3}P_{\mu\nu}(\tau_F, x) + \frac{1}{12}R_{\mu\nu}(x, \tau_F)\right]\end{aligned} \tag{8.6}$$

that consists of squares and rectangles can be defined. A couple observable choices that are not immediately given by an action shall be explained now, so called clover discretizations. Their advantage is that unlike the two previously discussed ones, they respect the lattice symmetry $O(4)$. While the Wilson and Lüscher-Weisz definitions can be used only for action densities, so the summed square of field strengths, clovers define lattice analogues of $F_{\mu\nu}$ itself. Therefore, they are a popular choice to measure quantities that depend on the field strength in a different way such as the topological charge which is proportional to $\varepsilon_{\mu\nu\sigma\rho}F_{\mu\nu}F_{\sigma\rho}$ [49]. For the clover observable, four plaquettes in the $\mu - \nu$ plane are considered, sketched in Fig. 14a. They can be used to define a lattice analogue to the field strength tensor

$$F^{\mathrm{cl}}_{\mu\nu}(\tau_F, x) = \frac{1}{2a^2}\,\mathrm{Tr}\left[T^A\big(P_{\mu\nu}(\tau_F, x) + P_{\nu,-\mu}(\tau_F, x) + P_{-\mu,-\nu}(\tau_F, x) + P_{-\nu,\mu}(\tau_F, x)\big)\right]T^A \tag{8.7}$$

which in turn can be used to define the clover action density operator

$$\varepsilon^{\mathrm{cl}}(\tau_F) = -\frac{1}{2}\,\mathrm{Tr}\left[F^{\mathrm{cl}}_{\mu\nu}(\tau_F, x)F^{\mathrm{cl}}_{\mu\nu}(\tau_F, x)\right]. \tag{8.8}$$

Starting from this, the authors of Ref. [50] found an improved clover by choosing a superposition with a clover consisting of rectangles instead of plaquettes. Hence, define the rectangle clover field strength

$$F^{\text{r-cl}}_{\mu\nu}(\tau_F, x) = \frac{1}{8a^2}\,\mathrm{Tr}\left[T^A\big(R_{\mu\nu}(\tau_F, x) + S_{\mu\nu}(\tau_F, x) + T_{\mu\nu}(\tau_F, x) + Q_{\mu\nu}(\tau_F, x) + (\mu \leftrightarrow \nu)\big)\right]T^A \tag{8.9}$$

| Discretization | Kernel $K_{\mu\nu}(p)$ |
|---|---|
| Wilson | $\hat{p}^2\delta_{\mu\nu} - \hat{p}_\mu\hat{p}_\nu$ |
| Lüscher-Weisz | $\big(\frac{5}{3}\hat{p}^2 - \frac{1}{3}\hat{c}_\mu^2\hat{p}^2 - \frac{1}{3}\sum_\lambda \hat{c}_\lambda^2\hat{p}_\lambda^2\big)\delta_{\mu\nu} - \big(\frac{5}{3} - \frac{1}{3}(\hat{c}_\mu^2 + \hat{c}_\nu^2)\big)\hat{p}_\mu\hat{p}_\nu$ |
| Zeuthen | $(1 - a^2\hat{p}_\mu^2/12)\big($ Lüscher-Weisz $\big)$ |
| Clover | $\hat{c}_\mu^2\mathring{p}^2\delta_{\mu\nu} - \hat{c}_\mu\dot{p}_\mu\hat{c}_\nu\dot{p}_\nu$ |
| Rectangle clover | $\frac{1}{4}((\mathring{p}^2\mathring{c}_\mu^2 + 2\sum_\lambda \mathring{p}_\lambda\check{p}_\lambda\mathring{c}_\mu + \check{p}^2)\hat{c}_\mu^2\delta_{\mu\nu} - (\mathring{p}_\mu\mathring{p}_\nu\mathring{c}_\mu\mathring{c}_\nu + \check{p}_\mu\mathring{p}_\nu\mathring{c}_\mu + \mathring{p}_\mu\check{p}_\nu\mathring{c}_\nu + \check{p}_\mu\check{p}_\nu)\hat{c}_\mu\hat{c}_\nu)$ |
| Improved clover | $\frac{25}{9}\big($ Clover $\big) + \frac{4}{9}\big($ Rectangle clover $\big)$<br>$-\frac{20}{9}\big(\frac{1}{2}(\mathring{p}^2\mathring{c}_\mu + \sum_\lambda \mathring{p}_\lambda\check{p}_\lambda)\hat{c}_\mu^2\delta_{\mu\nu} - \frac{1}{4}(\check{p}_\mu\mathring{p}_\nu + \mathring{p}_\mu\check{p}_\nu + (\mathring{c}_\mu + \mathring{c}_\nu)\mathring{p}_\mu\mathring{p}_\nu)\hat{c}_\mu\hat{c}_\nu\big)$ |

Table 1: Kernels for some discretizations. The gauge can be fixed by adding the usual term $\gamma\hat{p}_\mu\hat{p}_\nu$ where $\gamma$ is either the action or flow gauge fixing parameter. Notation is explained in Appendix C.1.

where $\mu \leftrightarrow \nu$ indicates that it is symmetrized in these Lorentz indices. It is shown in Fig. 14b where the unexplained operators in Eq. (8.9) are sketched as well. The first link in the loop is always the one going away from the center. The linear combination

$$F_{\mu\nu}^{\text{i-cl}}(\tau_F, x) = \frac{5}{3}F_{\mu\nu}^{\text{cl}}(\tau_F, x) - \frac{2}{3}F_{\mu\nu}^{\text{r-cl}}(\tau_F, x) \tag{8.10}$$

is free of $\mathcal{O}(a^2)$ contributions and can be used to define the improved clover action density

$$\begin{aligned}\varepsilon^{\text{i-cl}}(\tau_F) &= -\frac{1}{2}\operatorname{Tr}\left[F_{\mu\nu}^{\text{i-cl}}(\tau_F, x)F_{\mu\nu}^{\text{i-cl}}(\tau_F, x)\right] \\ &= \frac{25}{9}\varepsilon^{\text{cl}}(\tau_F) - \frac{20}{9}\varepsilon^{\text{m-cl}}(\tau_F) + \frac{4}{9}\varepsilon^{\text{r-cl}}(\tau_F).\end{aligned} \tag{8.11}$$

Here, $\varepsilon^{\text{r-cl}}$ is defined purely by rectangles while $\varepsilon^{\text{m-cl}}$ is the contraction of a naive and rectangle clover field strength. To calculate the leading order contribution, one makes use of Eq. (7.16). For this, the operator matrices $O_{\mu\nu}^{CD}(p)$ need to be found by expanding the operator up to quadratic order in $A_\mu$, equivalent to the procedure for $G_E^{\text{latt}}$ and $G_B^{\text{latt}}$ in Appendix B. Luckily, the considered observables are action densities, therefore up to an overall factor and a Kronecker delta in Lie algebra space the operator matrices, flow kernels $K^{(f)}$ as well as action kernels $K^{(a)}$ are equal if the same combination of loops is used. The action kernels are the matrices that appear between two gluon fields when expanding the action as in Eqs. (5.29) and (5.33). After all, each of the three kernels is found the same way, that is by expanding an action consisting of some closed paths to second order in the gluon fields. Therefore, it is obvious that all three kernels are the same for the same considered loops. A minor asterisk needs to be added to the previous statement since flow and action kernels can be manipulated with a gauge fixing term which is not true for the operator kernel. In the following, it will not always be made explicit in text whether the momentum delta distribution and the Lie algebra Kronecker delta are included in the kernel but it will be clear in the notation by the kernels having Lie algebra indices or not and the number of momentum arguments. Following the prior discussion, Eq. (7.16) turns into [28, 48]

$$\left\langle \varepsilon^{\text{latt}}(\tau_F)\right\rangle_0 = \frac{g_0^2}{2}\int_p \left(K^{(o)}\right)_{\mu\nu}^{CD}(p)\left(e^{-\tau_F K^{(f)}(p)}\right)_{\mu\sigma}\left(e^{-\tau_F K^{(f)}(q)}\right)_{\nu\rho}\left((K^{(a)})^{-1}\right)_{\sigma\rho}^{CD}(p). \tag{8.12}$$

The kernels for considered choices without gauge fixing term are listed in Tab. 1. The Wilson and Lüscher-Weisz kernels were derived in Appendix A in terms of the action. The calculation of the the naive and improved clover kernels is detailed in Appendix D. Evidently, each kernel approaches the continuum kernel $p^2\delta_{\mu\nu} - p_\mu p_\nu$ as $a$ goes to zero. Similar to the color-electric and -magnetic correlators, an analytical solution exists for the easiest combination of discretizations - Wilson action, flow and observable. The calculation outlined in Appendix C.2 yields

$$\left\langle \varepsilon^{\text{W-W-W}}(\tau_F)\right\rangle_0 = \frac{3(N_c^2-1)g_0^2}{2a^4}e^{-16\frac{\tau_F}{a^2}}I_0\left(\frac{4\tau_F}{a^2}\right)^4. \tag{8.13}$$

As for $G_E^{\text{latt}}$ and $G_B^{\text{latt}}$, modified Bessel functions of the first kind appear. For other discretizations, the integral needs to be evaluated numerically or one is content with knowing the expansion coefficients $c_m$ defined in Eq. (8.4) up to some order.

## 8.2. Expansion of action density in the lattice spacing

To find the coefficients $c_m$, Eq. (8.12) is expanded in the lattice spacing by expanding the operator, action and flow part up to $\mathcal{O}(a^4)$ separately. Write a kernel matrix as

$$K(p) = K^{\text{cont}}(p) + a^2R(p) + a^4S(p) + \mathcal{O}(a^6) \tag{8.14}$$

| Kernel | $R_{\mu\nu}(p)$ | $S_{\mu\nu}(p)$ |
|---|---|---|
| Wilson | $-\frac{1}{12}p^4\delta_{\mu\nu}+\frac{1}{24}(p_\mu^3p_\nu+p_\mu p_\nu^3)$ | $\frac{1}{360}p^6\delta_{\mu\nu}-\frac{1}{5760}(3p_\mu^5p_\nu+3p_\mu p_\nu^5+10p_\mu^3p_\nu^3)$ |
| Lüscher-Weisz | $\frac{1}{12}p^2p_\mu^2\delta_{\mu\nu}+\frac{1}{12}(p_\mu^3p_\nu+p_\mu p_\nu^3)$ | $-\frac{1}{720}(5p^2p_\mu^4+5p^4p_\mu^2+8p^6)\delta_{\mu\nu}$ $+\frac{1}{1920}(19p_\mu^5p_\nu+19p_\mu p_\nu^5+10p_\mu^3p_\nu^3)$ |
| Zeuthen | $\frac{1}{24}(p_\mu^3p_\nu-p_\mu p_\nu^3)$ | $-\frac{1}{720}(5p^2p_\mu^4+5p^4p_\mu^2+8p^6)\delta_{\mu\nu}$ $+\frac{1}{5760}(35p_\mu^5p_\nu+57p_\mu p_\nu^5+50p_\mu^3p_\nu^3)$ |
| Clover | $-\frac{1}{12}(3p^2p_\mu^2+4p^4)\delta_{\mu\nu}+\frac{7}{24}(p_\mu^3p_\nu+p_\mu p_\nu^3)$ | $\frac{1}{720}(15p^2p_\mu^4+60p^4p_\mu^2+32p^6)\delta_{\mu\nu}$ $-\frac{1}{5760}(183p_\mu^5p_\nu+183p_\mu p_\nu^5+490p_\mu^3p_\nu^3)$ |
| Improved clover | $\frac{1}{12}p^2p_\mu^2\delta_{\mu\nu}-\frac{1}{24}(p_\mu^3p_\nu+p_\mu p_\nu^3)$ | $-\frac{1}{720}(45p^2p_\mu^4+40p^4p_\mu^2+48p^6)$ $+\frac{1}{5760}(377p_\mu^5p_\nu+377p_\mu p_\nu^5+310p_\mu^3p_\nu^3)$ |
| $\hat{p}_\mu\hat{p}_\nu$ | $-\frac{1}{24}(p_\mu^3p_\nu+p_\mu p_\nu^3)$ | $\frac{1}{5760}(3p_\mu^5p_\nu+3p_\mu p_\nu^5+10p_\mu^3p_\nu^3)$ |

Table 2: Expansion terms of different kernels in the lattice spacing without gauge fixing. In the last line, the expansion of the standard gauge fixing term is given to obtain the expansion terms $R_{\mu\nu}$ and $S_{\mu\nu}$ in other gauges. Terms of the form $p^n$ are defined as $\sum_\mu p_\mu^n$.

with the continuum kernel

$$K_{\mu\nu}^{\text{cont}}(p)=p^2\delta_{\mu\nu}-(1-\gamma)p_\mu p_\nu \tag{8.15}$$

where $\gamma$ is either the action or flow gauge fixing parameter or zero for the operator kernel. The latter appears linearly in the leading order expectation value of the action density so no further work needs to be done there. For the flow part of Eq. (8.12), the exponential of the kernel matrix needs to be expanded. Doing so gives

$$\begin{aligned}\left(e^{-\tau_F K(p)}\right)_{\mu\nu}&=\left(e^{-\tau_F(K^{\text{cont}}(p)+a^2R(p)+a^4S(p)}\right)_{\mu\nu}+\mathcal{O}(a^6)\\&\overset{\lambda=1}{=}\left(e^{-\tau_F K^{\text{cont}}(p)}e^{-\tau_F(a^2R(p)+a^4S(p))}\right)_{\mu\nu}+\mathcal{O}(a^6)\\&=e^{-\tau_F p^2}\left(e^{-\tau_F(a^2R(p)+a^4S(p))}\right)_{\mu\nu}+\mathcal{O}(a^6)\\&=e^{-\tau_F p^2}\left(1-a^2\tau_F R(p)+a^4\tau_F\left(\frac{\tau_F}{2}(R(p))^2-S(p)\right)\right)_{\mu\nu}+\mathcal{O}(a^6)\\&=e^{-\tau_F p^2}\left(1-a^2\tau_F R_{\mu\nu}(p)+a^4\tau_F\left(\frac{\tau_F}{2}R_{\mu\rho}(p)R_{\rho\nu}(p)-S_{\mu\nu}(p)\right)\right)+\mathcal{O}(a^6).\end{aligned} \tag{8.16}$$

In second step, flow gauge invariance was taken advantage of: Feynman gauge renders the continuum kernel diagonal, therefore, it commutes with $R(p)$ and $S(p)$ and the exponential can be factorized. The last expression hence holds only in flow Feynman gauge and can be used in Eq. (8.12). In the second-to-last step, the second exponential was expanded. This expression again showcases that the lattice modifies the suppression of large momenta by leading order gradient flow. Instead of a purely gaussian envelope, correction terms in the lattice spacing appear. Furthermore, the inverse of the action kernel which is the propagator needs to be expanded. One finds that

$$\begin{aligned}\left(K^{-1}(p)\right)_{\mu\nu}^{CD}&=\delta^{CD}\left(D^{\text{cont}}(p)(1-a^2R(p)D^{\text{cont}}(p)+a^4(R(p)D^{\text{cont}}(p)R(p)-S(p))D^{\text{cont}}(p)\right)_{\mu\nu}+\mathcal{O}(a^6)\\&=\delta^{CD}D_{\mu\rho}^{\text{cont}}(p)\left(\delta_{\rho\nu}-a^2R_{\rho\sigma}(p)D_{\sigma\nu}^{\text{cont}}(p)+a^4(R_{\rho\sigma}(p)D_{\sigma\gamma}^{\text{cont}}(p)R_{\gamma\alpha}(p)-S_{\rho\alpha}(p))D_{\alpha\nu}^{\text{cont}}(p)\right)+\mathcal{O}(a^6)\end{aligned} \tag{8.17}$$

satisfies the defining equation

$$\left(K^{-1}\right)_{\mu\rho}^{CE}(p)K_{\rho\nu}^{ED}(p)=\delta_{\mu\nu}\delta^{CD}+\mathcal{O}(a^6) \tag{8.18}$$

for the propagator. In Eq. (8.17), $D^{\text{cont}}(p)$ is the continuum propagator from Eq. (5.17). Now the expansions of all parts of Eq. (8.12) up to order including $\mathcal{O}(a^4)$ are found and can be put together. What is left to do is determine the expansion terms $R_{\mu\nu}$ and $S_{\mu\nu}$ for the considered discretizations. This is done via straightforward Taylor series of the kernels $K_{\mu\nu}$ in the lattice spacing $a$. The results are listed in Table 2. It is now instructive to have a closer look at some $R_{\mu\nu}$ to get a better understanding of how improvement works. Lüscher-Weisz is an improved observable and action but not flow. This is because while it is possible for the second term, there is no gauge where the first term of $R_{\mu\nu}^{\text{LW}}$ vanishes. It happens to cancel out when inserting the Lüscher-Weisz kernel in Eq. (8.12) in the observable or action spot but not when choosing it as flow, so for flow it leaves $\mathcal{O}(a^2)$ lattice artefacts. The same happens for the improved clover but it is used only as an observable anyway so it is irrelevant. For Zeuthen flow, things are different: $R_{\mu\nu}^{\text{Z}}$ is actually zero in some gauge - while it cannot vanish by merely adding a multiple of the standard gauge fixing term $\hat{p}_\mu\hat{p}_\nu$, gauge fixing can actually get more elaborate by adding more complicated terms. In the Zeuthen case, the additional term $\hat{p}_\mu\hat{p}_\nu(4-\hat{c}_\nu)$ with the right

| Observable | Action | Flow | $c_2$ | $c_4$ |
|---|---|---|---|---|
| Wilson | Wilson | Wilson | $\frac{3}{1024}$ | $\frac{9}{16384}$ |
| Wilson | Wilson | Zeuthen | $0$ | $\frac{101}{163840}$ |
| Clover | Wilson | Zeuthen | $-\frac{1}{256}$ | $\frac{343}{327680}$ |
| Lüscher-Weisz | Wilson | Zeuthen | $\frac{1}{768}$ | $\frac{17}{32768}$ |
| Improved clover | Wilson | Zeuthen | $\frac{1}{768}$ | $-\frac{21}{65536}$ |
| Lüscher-Weisz | Lüscher-Weisz | Zeuthen | $0$ | $\frac{101}{163840}$ |
| Improved clover | Lüscher-Weisz | Zeuthen | $0$ | $-\frac{72}{327680}$ |

Table 3: Expansion coefficients for different discretizations of $\left\langle \varepsilon^{\text{latt}}(\tau_F) \right\rangle_0$ defined by Eq. (8.4).

normalization cancels the rest of $R^{\text{Z}}_{\mu\nu}$. Because of gauge independence, Zeuthen flow will therefore not have any $\mathcal{O}(a^2)$ contribution and is indeed an improved flow. Another interesting observation is that the expansion terms of clover are larger than those of Wilson. This agrees with intuition: A discrete version of some continuum object - for example a derivative - is more precise the closer the sampling points are. A clover has a larger extent on the lattice than the plaquette, therefore it is a worse approximation of the continuum.

Inserting the expressions listed in Table 2 into the kernels, subsequently inserting the kernels themselves in Eqs. (8.16) and (8.17) gives the small $a$ expansion of Eq. (8.12) up to including $a^4$. Summing over Lorentz indices gives integrals of the form

$$\int_p e^{-2\tau_F p^2} \frac{\left(p^m\right)^{n_1}}{\left(p^2\right)^{n_2}} \tag{8.19}$$

where $m$ is even and $n_1, n_2 = 0, 1, 2$. If $n_2 = 0$, those are gaussian integrals that have a straightforward solution [51]. If it is not zero however, one can insert

$$1 = \int_0^\infty \mathrm{d}x p^2 e^{-x p^2} \tag{8.20}$$

into the integrand to cancel the denominator in Eq. (8.19). If $n_2 = 2$, this needs to done twice. After switching the order of $p$ and $x$ integration, the $p$ integrals are ordinary gaussians and, after solving them, the $x$ integration can be performed analytically as well. The resulting Taylor expansion coefficients of the action density are listed in Table 3 for some combinations. This overview is the main result of this section. Several observations are in order. The last two lines consist of purely improved parts. As expected, $c_2$ vanishes then. In principle, since the observable enters linearly in the action density, using the $c_4$ results for these combinations one can also define an observable which is $a^4$ improved by coosing Lüscher-Weisz action, Zeuthen flow and an appropriate superposition of Lüscher-Weisz and improved clover observable. Furthermore, the $a^2$ contributions of observable and action cancel out if both are chosen to be the same. This is visible in the Wilson-Wilson-Zeuthen case: Zeuthen flow does not contribute since it is improved and the remaining $a^2$ contributions cancel. In addition, the $a^4$ contributions from clover observables - both naive and improved - appear to be negative while contributions from the other kernels are positive. This comes in handy: While the expansion terms of clover observables are comparably large - see Table 2 - the negative sign leads to cancellations of different contributions to $c_4$. Therefore, the absolute value of $c_4$ is smaller in the Improved-clover-Lüscher-Weisz-Zeuthen case than in the Lüscher-Weisz-Lüscher-Weisz-Zeuthen case despite the improved clover having a larger extent on the lattice than the Lüscher-Weisz observable. Numerical cross-checks of some combinations have been done to confirm the validity of the presented results. Two of them are shown in Fig. 15. For those, Eq. (8.12) has been integrated numerically without expanding in the lattice spacing. The analytical result for the Wilson-Wilson-Wilson action density can serve as a more robust cross-check as well. Using the asymptotic expansion [45]

$$I_\gamma(z) \overset{z\to\infty}{\sim} \frac{e^z}{\sqrt{2\pi z}} \left(1 - \frac{4\gamma^2 - 1}{8z} + \frac{(4\gamma^2 - 1)(4\gamma^2 - 9)}{128 z^2} + \mathcal{O}\left(z^{-3}\right)\right) \tag{8.21}$$

in Eq. (8.13), one obtains the same coefficients as listed in Table 3. The used framework also allows for easy calculation of $c_2$ and $c_4$ for different combinations of the used kernels. For other loops, using chairs and parallelograms for example, their kernel needs to found and expanded in $a$ first.

## 9. Conclusion and Outlook

Color-electric and color-magnetic correlation functions bear insight to the propagation of heavy quarks in the QGP, a high-energy phase of strong interacting matter where quarks are not restricted by confinement. While these correlators can be measured on the

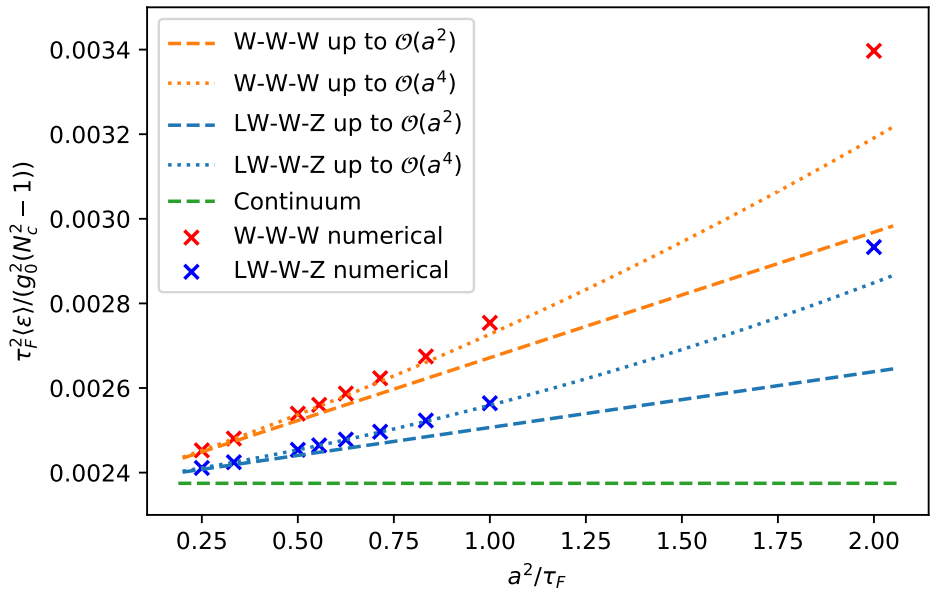


Figure 15: Action density for the everything-Wilson case as well as Lüscher-Weisz observable, Wilson action and Zeuthen flow as a function of the lattice spacing. It is multiplied by the squared flow time to make it dimensionless. The dashed green horizontal line is the continuum value which is constant due to the multiplication with $\tau_F^2$. Numerical results are compared to small $a$ expansions up to $\mathcal{O}(a^2)$ and $\mathcal{O}(a^4)$. The comparison confirms the validity of the expansion parameters listed in Table 3. It is also well visible that, as expected, the combination with improved discretizations approaches the continuum faster.

lattice, a method to study QCD non-perturbatively following the path integral approach to quantization, several obstacles need to be resolved. One of those is a bad signal-to-noise ratio. Since its brute-force increase is computationally costly, gradient flow, a versatile tool in lattice gauge theories, has been introduced and studied in the last decade. Continuum extrapolation of observables measured in lattice calculations can be simplified by using improved observables, actions and flow. For this, clever linear combinations of different loops on the lattice are considered. Improved gradient flow is called Zeuthen flow. To obtain physical correlation functions, the data measured on the lattice needs to be extrapolated to both the continuum and zero flow time. Both procedures can be simplified with tree-level improvement, that is by normalizing with leading order perturbative results of the correlators under the assumption that a large fraction of lattice and flow effects are included in leading order.

The presented data allows tree-level improved flow-time-to-zero extrapolation of the color-electric and color-magnetic correlation functions under Zeuthen flow by providing numerical data of the leading order term. It remains to be seen how this influences the respective spectral functions and finally the momentum diffusion coefficient. The results also confirm that to leading order, Zeuthen flow approaches the continuum limit faster than Wilson flow. The next-to-leading order behaviour of $G_E$ and $G_B$ under Zeuthen flow might be interesting to see. Unfortunately, since both lattice and gradient flow perturbation theory are required to determine them, it would be a very intricate endeavour, especially when renormalization comes into play. In principle, lattice studies of these correlators can also be improved by constructing operator discretizations that are free of $\mathcal{O}(a^2)$ lattice effects. A desirable enhancement would also be to make the numerical integration used for the perturbative result more robust for larger $N_\tau$ to reduce computational cost.

On a different note, gradient flow can not only serve as a tool to reduce noise, but the gradient-flowed action density can help to measure the gauge coupling on the lattice. Its extraction can be simplified by knowing the dependence of its leading order term on the lattice spacing. The expansion coefficients depend on operator, action and flow. The first two, $c_2$ and $c_4$, are calculated in this work for various discretizations with emphasis on Zeuthen flow. With the results, a superposition of Lüscher-Weisz and improved clover observable can be constructed that is free of both $a^2$ and $a^4$ deviations from the continuum. Furthermore, the improved clover observable turns out to cancel discretization effects of action and flow of some extent due to opposite signs. Therefore, despite its larger size, implementing it leads to smaller $a^4$ contributions than the Lüscher-Weisz observable. The used framework can be easily applied to further combinations of the considered kernels. For other discretizations, for example including chairs or parallelograms, their kernel needs to be found and expanded in $a$. Then, the presented framework can be applied as well.

## A. Expansion of Wilson and Lüscher-Weisz action to leading order

For lattice perturbation theory, the action needs to be expanded in the gauge coupling. Here, the Wilson and Lüscher-Weisz kernels whose inverses are the respective propagators are derived. Begin with the Wilson action, Eq. (3.15). The plaquette operator can be written in terms of the gluon fields as

$$P_{\mu\nu}(n) = \exp\big[iag_0\big(A_\mu(n) + A_\nu(n+\hat{\mu}) - A_\mu(n+\hat{\nu}) - A_\nu(n)\big) + \mathcal{O}(g_0^2)\big]. \tag{A.1}$$

Expanding the exponential to second order gives

$$\begin{aligned} S_P[A] &= \frac{1}{g_0^2}\sum_{n\mu\nu}\mathrm{Re}\,\mathrm{Tr}\Big[\mathcal{O}(A) + \frac{a^2g_0^2}{2}\big(A_\mu(n) + A_\nu(n+\hat{\mu}) - A_\mu(n+\hat{\nu}) - A_\nu(n)\big)^2\Big] + \mathcal{O}(g_0) \\ &= \frac{a^2}{2}\sum_{n\mu\nu}\mathrm{Re}\,\mathrm{Tr}\Big[\big(A_\mu(n) + A_\nu(n+\hat{\mu}) - A_\mu(n+\hat{\nu}) - A_\nu(n)\big)^2\Big] \end{aligned} \tag{A.2}$$

The linear term of the expansion in the exponential does not contribute since it is a Lie algebra element which is traceless. This still holds when expanding the exponent up to $\mathcal{O}(A^2)$ according to the Baker-Campbell-Hausdorff formula Eq. (4.10) since the commutator of Lie algebra elements is a Lie algebra element itself. Fourier transforming this expression gives

$$\begin{aligned} S_P[A] &= \frac{a^2}{2}\sum_{n\mu\nu}\mathrm{Re}\,\mathrm{Tr}\bigg(\int_p e^{ipan}\Big(\big(e^{ip_\mu a/2} - e^{i(p_\mu/2+p_\nu)a}\big)\tilde{A}_\mu(p) + \big(e^{i(p_\mu+p_\nu/2)a} - e^{ip_\nu a/2}\big)\tilde{A}_\nu(p)\Big)\bigg)^2 + \mathcal{O}(g_0) \\ &= \frac{a^2}{2}\sum_{n\mu\nu}\mathrm{Re}\,\mathrm{Tr}\bigg(\int_p e^{ipan}e^{i(p_\mu+p_\nu)a/2}\Big(\big(e^{-ip_\nu a/2} - e^{ip_\nu a/2}\big)\tilde{A}_\mu(p) + \big(e^{ip_\mu a/2} - e^{ip_\mu a/2}\big)\tilde{A}_\nu(p)\Big)\bigg)^2 + \mathcal{O}(g_0) \\ &= \frac{a^4}{2}\sum_{n\mu\nu}\mathrm{Re}\,\mathrm{Tr}\bigg(\int_p e^{ipan}e^{i(p_\mu+p_\nu)a/2}\Big(-i\hat{p}_\nu\tilde{A}_\mu(p) + \hat{p}_\mu\tilde{A}_\nu(p)\Big)\bigg)^2 + \mathcal{O}(g_0) \\ &= -\frac{a^4}{2}\sum_{n\mu\nu}\mathrm{Re}\,\mathrm{Tr}\bigg(\int_p e^{ipan}e^{i(p_\mu+p_\nu)a/2}\Big(\hat{p}_\mu\tilde{A}_\nu(p) + \hat{p}_\nu\tilde{A}_\mu(p)\Big)\bigg)^2 + \mathcal{O}(g_0). \end{aligned} \tag{A.3}$$

The last line emphasizes that the plaquette action approaches the right continuum limit since the expression in the integral looks like the Fourier transform of the leading order of the continuum field strength tensor Eq. (2.16) with the replacement $p \to \hat{p}$. Executing the square gives

$$\begin{aligned} S_P[A] &= -\frac{a^4}{2}\,\mathrm{Re}\,\mathrm{Tr}\sum_{n\mu\nu}\int_{pp'} e^{i(p+p')an}e^{i(p_\mu+p_\nu+p'_\mu+p'_\nu)a/2}\Big(\hat{p}_\mu\hat{p}'_\mu\tilde{A}_\nu(p)\tilde{A}_\nu(p') - \hat{p}_\mu\hat{p}'_\nu\tilde{A}_\nu(p)\tilde{A}_\mu(p') \\ &\qquad - \hat{p}_\nu\hat{p}'_\mu\tilde{A}_\mu(p)\tilde{A}_\nu(p') + \hat{p}_\nu\hat{p}'_\nu\tilde{A}_\mu(p)\tilde{A}_\mu(p')\Big) + \mathcal{O}(g_0) \\ &= \frac{1}{2}\,\mathrm{Tr}\sum_{\mu\nu}\int_{pp'}(2\pi)^4\delta^{(4)}(p+p')\Big(\hat{p}_\mu^2\tilde{A}_\nu(p)\tilde{A}_\nu(p')\tilde{A} - \hat{p}_\mu\hat{p}_\nu\tilde{A}_\nu(p)\tilde{A}_\mu(p') \\ &\qquad - \hat{p}_\nu\hat{p}_\mu\tilde{A}_\mu(p)\tilde{A}_\nu(p') + \hat{p}_\nu^2\tilde{A}_\mu(p)\tilde{A}_\mu(p')\Big) + \mathcal{O}(g_0) \\ &= \mathrm{Tr}\sum_{\mu\nu}\int_{pp'}(2\pi)^4\delta^{(4)}(p+p')\Big(\hat{p}_\nu^2\tilde{A}_\mu(p)\tilde{A}_\mu(p') - \tilde{p}_\mu\tilde{p}_\nu\tilde{A}_\mu(\tilde{A}_\mu(p'))\Big) + \mathcal{O}(g_0) \\ &= \frac{1}{2}\sum_{\mu\nu}\int_{pp'}\tilde{A}_\mu^C(p)(2\pi)^4\delta^{(4)}(p+p')\delta^{CD}(\hat{p}^2\delta_{\mu\nu} - \hat{p}_\mu\hat{p}_\nu)\tilde{A}_\nu^D(p') + \mathcal{O}(g_0). \end{aligned} \tag{A.4}$$

In the second step, Eq. (3.20) was used while in the third step, a renaming of indices took place. From this expression, the kernel for the Wilson action can be read off.

To find the Lüscher-Weisz action, the same procedure needs to be repeated for the rectangle since the Lüscher-Weisz action is defined in terms of plaquettes and rectangles. Expand its operator Eq. (3.16) in $g_0$ up to quadratic order,

$$\begin{aligned} R_{\mu\nu}(n) &= \exp\big[iag_0\big(A_\mu(n) + A_\mu(n+\hat{\mu}) + A_\nu(n+2\hat{\mu}) - A_\mu(n+\hat{\mu}+\hat{\nu}) - A_\mu(n+\nu) - A_\nu(n)\big) + \mathcal{O}(g_0^2)\big] \\ &= 1 + \mathcal{O}(A) - \frac{a^2g_0^2}{2}\big(A_\mu(n) + A_\mu(n+\hat{\mu}) + A_\nu(n+2\hat{\mu}) - A_\mu(n+\hat{\mu}+\hat{\nu}) - A_\mu(n+\nu) - A_\nu(n)\big)^2 + \mathcal{O}(g_0^3), \end{aligned} \tag{A.5}$$

so that after Fourier transforming and not normalising properly by choosing $c_R = 1$, the rectangle action reads

$$\begin{aligned}
S_R[A] &= a^2 \sum_{n\mu\nu} \mathrm{Re\,Tr}\Big( \int_p e^{ipan} \Big( \big(e^{ip_\mu a/2} + e^{i3p_\mu a/2} - e^{i(3p_\mu/2+p_\nu)} - e^{i(p_\mu/2+p_\nu)}\big)\tilde{A}_\mu(p) \\
&\qquad + \big(e^{i(2p_\mu+p_\nu/2)a} - e^{ip_\nu a/2}\big)\tilde{A}_\nu(p)\Big)\Big)^2 + \mathcal{O}(g_0) \\
&= a^2 \sum_{n\mu\nu} \mathrm{Re\,Tr}\Big( \int_p e^{ipan} e^{i(p_\mu+p_\nu/2)a} \Big( \big(e^{-i(p_\mu+p_\nu)a/2} + e^{i(p_\mu-p_\nu)a/2} - e^{i(p_\mu+p_\nu)a/2} - e^{i(-p_\mu+p_\nu)a/2}\big)\tilde{A}_\mu(p) \\
&\qquad + \big(e^{ip_\mu a} - e^{ip_\mu a}\big)\tilde{A}_\nu(p)\Big)\Big)^2 + \mathcal{O}(g_0) \\
&= a^2 \sum_{n\mu\nu} \mathrm{Re\,Tr}\Big( \int_p e^{ipan} e^{i(p_\mu+p_\nu/2)a} \Big( -\big(e^{ip_\mu a/2} + e^{-ip_\mu a/2}\big)\big(e^{ip_\nu a/2} - e^{-ip_\nu a/2}\big)\tilde{A}_\mu(p) \\
&\qquad + \big(e^{ip_\mu a/2} + e^{-ip_\mu a/2}\big)\big(e^{ip_\mu a/2} - e^{-ip_\mu a/2}\big)\tilde{A}_\nu(p)\Big)\Big)^2 + \mathcal{O}(g_0) \\
&= -4a^4 \sum_{n\mu\nu} \mathrm{Re\,Tr}\Big( \int_p e^{ipan} e^{i(p_\mu+p_\nu/2))a} \hat{c}_\mu \Big( -\hat{p}_\nu \tilde{A}_\mu(p) - \hat{p}_\mu \tilde{A}_\nu(p)\Big)\Big)^2 + \mathcal{O}(g_0)
\end{aligned} \tag{A.6}$$

with $\hat{c}_\mu = \cos p_\mu a/2$. Executing the square gives

$$\begin{aligned}
S_R[A] &= -4a^4 \,\mathrm{Re\,Tr} \sum_{n\mu\nu} \int_{pp'} e^{i(p+p')an} e^{i(p_\mu+p'_\mu+p_\nu/2+p'_\nu/2)a} \hat{c}_\mu \hat{c}'_\mu \Big( \hat{p}_\mu \hat{p}'_\mu \tilde{A}_\nu(p)\tilde{A}_\nu(p') - \hat{p}_\mu \hat{p}'_\nu \tilde{A}_\nu(p)\tilde{A}_\mu(p') \\
&\qquad - \hat{p}_\nu \hat{p}'_\mu \tilde{A}_\mu(p)\tilde{A}_\nu(p') + \hat{p}_\nu \hat{p}'_\nu \tilde{A}_\mu(p)\tilde{A}_\mu(p')\Big) + \mathcal{O}(g_0) \\
&= 4\,\mathrm{Tr} \sum_{\mu\nu} \int_{pp'} (2\pi)^4 \delta^{(4)}(p+p') \hat{c}_\mu^2 \Big( \hat{p}_\mu^2 \tilde{A}_\nu(p)\tilde{A}_\nu(p') - \hat{p}_\mu \hat{p}_\nu \tilde{A}_\nu(p)\tilde{A}_\mu(p') \\
&\qquad - \hat{p}_\nu \hat{p}_\mu \tilde{A}_\mu(p)\tilde{A}_\nu(p') + \hat{p}_\nu^2 \tilde{A}_\mu(p)\tilde{A}_\mu(p')\Big) + \mathcal{O}(g_0) \\
&= 4\,\mathrm{Tr} \sum_{\mu\nu} \int_{pp'} (2\pi)^4 \delta^{(4)}(p+p') \Big( \big(\hat{c}_\mu + \hat{c}_\nu\big)\hat{p}_\nu^2 \tilde{A}_\mu(p)\tilde{A}_\mu(p') - \big(\hat{c}_\mu + \hat{c}_\nu\big)\hat{p}_\mu \hat{p}_\nu \tilde{A}_\mu(p)\tilde{A}_\nu(p')\Big) + \mathcal{O}(g_0) \\
&= 2 \sum_{\mu\nu} \int_{pp'} \tilde{A}^C_\mu(p) (2\pi)^4 \delta^{(4)}(p+p') \delta^{CD} \Big( \big(\hat{c}_\mu^2 \hat{p}^2 + \sum_\lambda \hat{c}_\lambda \hat{p}_\lambda\big)\delta_{\mu\nu} - \big(\hat{c}_\mu + \hat{c}_\nu\big)\hat{p}_\mu \hat{p}_\nu\Big) \tilde{A}^D_\nu(p') + \mathcal{O}(g_0).
\end{aligned} \tag{A.7}$$

The same methods as for the plaquette action were used. The linear combination

$$S_{\mathrm{LW}}[A] = \frac{5}{3} S_P[A] - \frac{1}{12} S_R[A] \tag{A.8}$$

that defines the improved Lüscher-Weisz action leads to Eq. (5.33).

## B. Expansion of $G_E$ and $G_B$ on the lattice

In this section, the color-electric correlator $G_E^{\mathrm{latt}}$ from Eq. (7.9) shall be expanded to bring it into the form of Eq. (7.16). Due to the difference in the electric field operator Eq. (7.8), the numerator consists of four parts

$$\big\langle \mathcal{O}_1^i \big\rangle = \mathrm{Re\,Tr} \big\langle U^\beta_{\tau+a}(\vec{0}) U_0(\tau,\vec{0}) U_i^\dagger(\tau,\vec{0}) U_a^\tau(i) U_0(0,i) U_i(0,\vec{0}) \big\rangle, \tag{B.1}$$

$$\big\langle \mathcal{O}_2^i \big\rangle = \mathrm{Re\,Tr} \big\langle U^\beta_{\tau+a}(\vec{0}) U_i^\dagger(\tau+a,0) U_0(\tau,i) U_a^\tau(i) U_0(0,i) U_i(0,\vec{0}) \big\rangle, \tag{B.2}$$

$$\big\langle \mathcal{O}_3^i \big\rangle = \mathrm{Re\,Tr} \big\langle U^\beta_{\tau+a}(\vec{0}) U_0(\tau,\vec{0}) U_i^\dagger(\tau,\vec{0}) U_a^\tau(i) U_i(a,\vec{0}) U_0(0,\vec{0}) \big\rangle, \tag{B.3}$$

$$\big\langle \mathcal{O}_4^i \big\rangle = \mathrm{Re\,Tr} \big\langle U^\beta_{\tau+a}(\vec{0}) U_i^\dagger(\tau+a,0) U_0(\tau,i) U_a^\tau(i) U_i(a,\vec{0}) U_0(0,\vec{0}) \big\rangle \tag{B.4}$$

for each $i$ so that the numerator is

$$\big\langle \mathcal{O}_{\mathrm{num}} \big\rangle = \big\langle \mathcal{O}_1^i \big\rangle - \big\langle \mathcal{O}_2^i \big\rangle - \big\langle \mathcal{O}_3^i \big\rangle + \big\langle \mathcal{O}_4^i \big\rangle. \tag{B.5}$$

The four operators are shown in Fig. B.1. Now expand these operators by parametrizing them as $U_\mu(x) = \exp i a g_0 A_\mu(x)$. Consider $\mathcal{O}_1^i$:

$$\begin{aligned}
\big\langle \mathcal{O}_1^i \big\rangle &= \big\langle \mathrm{Re\,Tr} \exp\big[ i a g_0 \big( A_0(\tau,\vec{0}) - A_i(\tau,\vec{0}) + A_0(0,\hat{\imath}) + A_i(0,\vec{0}) + A_{\mathrm{rest}}\big) + \mathcal{O}(g_0^2)\big] \big\rangle \\
&= \big\langle \mathrm{Re\,Tr} \Big[ 1 + \mathcal{O}(A) - \frac{a^2 g_0^2}{2} \big( A_0(\tau,\vec{0}) - A_i(\tau,\vec{0}) + A_0(0,\hat{\imath}) + A_i(0,\vec{0}) + A_{\mathrm{rest}}\big)^2 \Big] \big\rangle + \mathcal{O}(g_0^3).
\end{aligned} \tag{B.6}$$

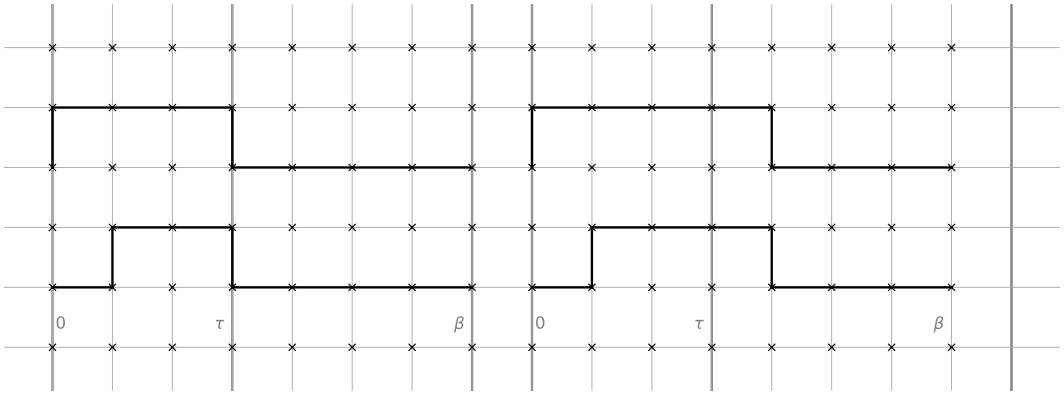


Figure B.1: The four operators $\mathcal{O}_1^i$ to $\mathcal{O}_4^i$ that constitute the numerator of $G_E^{\text{latt}}$ according to Eq. B.5. Upper left: $\mathcal{O}_1^i$. Upper right: $\mathcal{O}_2^i$. Lower left: $\mathcal{O}_3^i$. Lower right: $\mathcal{O}_4^i$. The horizontal axis indicates time direction, the vertical one the $i^{\text{th}}$ spatial direction.

All the fields on the Wilson line were summarized as $A_{\text{rest}}$ since they occur in each of the four operators and will subsequently cancel out. In the next steps, something similar will happen, and the notation will not be stringent. As in the previous appendix, the linear expansion term of the exponential will not contribute. Hence, solving the square gives

$$\begin{aligned}\langle \mathcal{O}_1^i \rangle = \big\langle \operatorname{Re}\operatorname{Tr}\Big[1 - a^2 g_0^2 \big(&A_0(\tau,\vec{0})A_0(0,\hat{\imath}) + A_0(\tau,\vec{0})A_i(0,\vec{0}) - A_i(\tau,\vec{0})A_0(0,\hat{\imath}) \\ &- A_i(\tau,\vec{0})A_i(0,\vec{0}) + A_{\text{rest}}^2\big)\Big]\big\rangle + \mathcal{O}(g_0^3)\end{aligned} \tag{B.7}$$

where multiple terms were absorbed in $A_{\text{rest}}^2$ since they arise in another operator with opposite sign. Essentially, only those terms where one factor stems from one 'bend' in the operator and the other one stems from the other 'bend' survive. The calculations for the other three operators are equivalent and only the results will be given here:

$$\begin{aligned}\langle \mathcal{O}_2^i \rangle &= \big\langle \operatorname{Re}\operatorname{Tr}\Big[1 - a^2 g_0^2 \big(-A_i(\tau+a,\vec{0})A_0(0,\hat{\imath}) - A_i(\tau+a,\vec{0})A_i(0,\vec{0}) + A_0(\tau,\hat{\imath})A_0(0,\hat{\imath}) \\ &\qquad + A_0(\tau,\hat{\imath})A_i(0,\vec{0}) + A_{\text{rest}}^2\big)\Big]\big\rangle + \mathcal{O}(g_0^3), \\ \langle \mathcal{O}_3^i \rangle &= \big\langle \operatorname{Re}\operatorname{Tr}\Big[1 - a^2 g_0^2 \big(A_0(\tau,\vec{0})A_i(a,\vec{0}) + A_0(\tau,\vec{0})A_0(0,\vec{0}) - A_i(\tau,\vec{0})A_i(a,\vec{0}) \\ &\qquad - A_i(\tau,\vec{0})A_0(0,\vec{0}) + A_{\text{rest}}^2\big)\Big]\big\rangle + \mathcal{O}(g_0^3), \\ \langle \mathcal{O}_4^i \rangle &= \big\langle \operatorname{Re}\operatorname{Tr}\Big[1 - a^2 g_0^2 \big(-A_i(\tau+a,\vec{0})A_i(a,\vec{0}) - A_i(\tau+a,\vec{0})A_0(0,\vec{0}) + A_0(\tau,\hat{\imath})A_i(a,\vec{0}) \\ &\qquad + A_0(\tau,\hat{\imath})A_0(0,\vec{0}) + A_{\text{rest}}^2\big)\Big]\big\rangle + \mathcal{O}(g_0^3).\end{aligned} \tag{B.8}$$

Inserting this into Eq. (B.5) gives the numerator of $G_E^{\text{latt}}$ as

$$\begin{aligned}\langle \mathcal{O}_{\text{num}} \rangle = -a^2 g_0^2 \big\langle \operatorname{Re}\operatorname{Tr}\Big[&A_0(\tau,\vec{0})A_0(0,\hat{\imath}) + A_0(\tau,\vec{0})A_i(0,\vec{0}) - A_i(\tau,\vec{0})A_0(0,\hat{\imath}) - A_i(\tau,\vec{0})A_i(0,\vec{0}) \\ &+A_i(\tau+a,\vec{0})A_0(0,\hat{\imath}) + A_i(\tau+a,\vec{0})A_i(0,\vec{0}) - A_0(\tau,\hat{\imath})A_0(0,\hat{\imath}) - A_0(\tau,\hat{\imath})A_i(0,\vec{0}) \\ &-A_0(\tau,\vec{0})A_i(a,\vec{0}) - A_0(\tau,\vec{0})A_0(0,\vec{0}) + A_i(\tau,\vec{0})A_i(a,\vec{0}) + A_i(\tau,\vec{0})A_0(0,\vec{0}) \\ &-A_i(\tau+a,\vec{0})A_i(a,\vec{0}) - A_i(\tau+a,\vec{0})A_0(0,\vec{0}) + A_0(\tau,\hat{\imath})A_i(a,\vec{0}) + A_0(\tau,\hat{\imath})A_0(0,\vec{0})\Big]\big\rangle + \mathcal{O}(g_0^3).\end{aligned} \tag{B.9}$$

The $A_0A_0$, $A_iA_i$ and mixed parts are now Fourier transformed separately for better overview. For the $A_0A_0$ part one finds

$$\begin{aligned}
&\mathrm{Tr}\big\langle A_0(\tau,\vec{0})A_(0,\hat{\imath}) - A_0(\tau,\hat{\imath})A_0(0,\hat{\imath}) - A_0(\tau,\vec{0})A_0(0,\vec{0}) + A_0(\tau,\hat{\imath})A_0(0,\vec{0})\big\rangle \\
=&\sum\!\!\!\!\!\!\int_{pp'} e^{i(p_0+p_0')a/2}\big(e^{ip_0\tau}e^{ip_i'a} - e^{i(p_0\tau+p_ia)}e^{ip_i'a} - e^{ip_0\tau} + e^{i(p_0\tau+p_ia)}\big)\,\mathrm{Tr}\big\langle\tilde{A}_0(p)\tilde{A}_0(p')\big\rangle \\
=&\frac{1}{2}\delta^{CD}\sum\!\!\!\!\!\!\int_{p}\big(e^{i(p_0\tau-p_ia)} - 2e^{ip_0\tau} + e^{i(p_0\tau+p_ia)}\big)D_{00}^{CD}(p) + \mathcal{O}(g_0) \\
=&\frac{1}{2}\delta^{CD}\sum\!\!\!\!\!\!\int_{p} e^{ip_0\tau}\big(e^{ip_ia/2} - e^{-ip_ia/2}\big)^2 D_{00}^{CD}(p) + \mathcal{O}(g_0) \\
=&-\frac{a^2}{2}\delta^{CD}\sum\!\!\!\!\!\!\int_{p} e^{ip_0\tau}\hat{p}_i^2 D_{00}^{CD}(p) + \mathcal{O}(g_0).
\end{aligned} \tag{B.10}$$

In the second step, the $A_0$ fields in the two-point function were expanded in the generators of SU(3) according to $A_0 = A_0^C T^C$ and subsequently, Eq. (2.8) was used. Considering that the real part is taken, the complex exponential simplifies to $\cos(p_0\tau)$. The $A_iA_i$ part is equivalent with $i \leftrightarrow 0$ except for the complex exponential so that it gives $-(a^2/2)\sum\!\!\!\!\!\!\int_p e^{ip_0\tau}\hat{p}_0^2 D_{ii}(p)$. For the mixed part one finds

$$\begin{aligned}
&\mathrm{Tr}\big\langle A_0(\tau,\vec{0})A_i(0,\vec{0}) - A_i(\tau,\vec{0})A_0(0,\hat{\imath}) + A_i(\tau+a,\vec{0})A_0(0,\hat{\imath}) - A_0(\tau,\hat{\imath})A_i(0,\vec{0}) \\
&\quad - A_0(\tau,\vec{0})A_i(a,\vec{0}) + A_i(\tau,\vec{0})A_0(0,\vec{0}) - A_i(\tau+a,\vec{0})A_0(0,\vec{0}) + A_0(\tau,\hat{\imath})A_i(a,\vec{0})\big\rangle \\
=&\sum\!\!\!\!\!\!\int_{pp'} e^{i(p_0+p_i')a/2}\Big(e^{ip_0\tau} - e^{ip_ia}e^{ip_0'\tau} + e^{ip_ia}e^{ip_0'(\tau+a)} - e^{i(p_0\tau+p_ia)} \\
&\qquad\qquad - e^{ip_0\tau}e^{ip_0'\tau} + e^{ip_0'\tau} - e^{ip_0'(\tau+a)} + e^{i(p_0\tau+p_ia)}e^{ip_0'a}\Big)\,\mathrm{Tr}\big\langle\tilde{A}_0(p)\tilde{A}_0(p')\big\rangle \\
=&\frac{1}{2}\delta^{CD}\sum\!\!\!\!\!\!\int_{p} e^{i(p_0a-p_ia)/2}\Big(e^{ip_0\tau} - e^{i(p_ia-p_0\tau)} + e^{i(p_ia-p_0(\tau+a))} - e^{i(p_0\tau+p_ia)} \\
&\qquad\qquad - e^{ip_0(\tau-a)} + e^{-ip_0\tau} - e^{-ip_0(\tau+a)} + e^{i(p_0(\tau-a)+p_ia)}\Big)D_{0i}^{CD}(p) + \mathcal{O}(g_0) \\
=&\frac{1}{2}\delta^{CD}\sum\!\!\!\!\!\!\int_{p}\Big(e^{ip_0\tau} + e^{-ip_0\tau}\Big)\Big(e^{ip_0a/2} - e^{-ip_0a/2}\Big)\Big(e^{-ip_ia/2} - e^{ip_ia/2}\Big)D_{0i}^{CD}(p) + \mathcal{O}(g_0) \\
=&a^2\delta^{CD}\sum\!\!\!\!\!\!\int_{p}\cos(p_0\tau)\hat{p}_0\hat{p}_i D_{0i}^{CD}(p) + \mathcal{O}(g_0).
\end{aligned} \tag{B.11}$$

Putting everything together, the numerator of $G_E^{\text{latt}}$ is

$$\big\langle\mathcal{O}_{\text{num}}\big\rangle = \frac{a^4 g_0^2}{2}\sum_i\sum\!\!\!\!\!\!\int_p \cos(p_0\tau)\Big[\hat{p}_i^2 D_{00}^{CD}(p) + \hat{p}_0^2 D_{ii}^{CD}(p) - 2\hat{p}_0\hat{p}_i D_{0i}^{CD}(p)\Big] + \mathcal{O}(g_0^3). \tag{B.12}$$

While these calculation were performed for an unflowed lattice, the flowed expression follows from simply replacing $D_{\mu\nu}^{CD} \to (D^{\text{flow}})_{\mu\nu}^{CD}$. The leading order expansion of the denominator $\mathrm{Re}\,\mathrm{Tr}\big\langle U_0^\beta(\vec{0})\big\rangle$ is considerably easier: The leading order contribution to the expansion of the links is the $N_c \times N_c$ unit matrix whose trace is $N_c = 3$, which is hence the leading term of the denominator. Omitting the factor of $a^4$ to give the perturbative result the dimension length$^{-4}$ and considering the overall factor of $-1/3$, one arrives at Eq. (7.18).

The same procedure as above shall be repeated for $G_B^{\text{latt}}$ to derive Eq. (7.27). First, realise that the numerator of Eq. (7.15) splits into two operators since

$$\begin{aligned}
\big\langle\mathcal{O}_{\text{num}}\big\rangle &= \sum_i \varepsilon_{ijk}\varepsilon_{imn}\,\mathrm{Re}\,\mathrm{Tr}\big\langle U_\tau^\beta(\vec{0})U_j^\dagger(\tau,\vec{0})U_k^\dagger(\tau,\hat{\jmath})U_0^\tau(\vec{0})U_m(0,\hat{n})U_n(0,\vec{0})\big\rangle \\
&= \sum_{jk}\Big[\mathrm{Re}\,\mathrm{Tr}\big\langle U_\tau^\beta(\vec{0})U_k^\dagger(\tau,\vec{0})U_j^\dagger(\tau,\hat{k})U_0^\tau(\vec{0})U_k(0,\hat{\jmath})U_j(0,\vec{0})\big\rangle \\
&\qquad - \mathrm{Re}\,\mathrm{Tr}\big\langle U_\tau^\beta(\vec{0})U_k^\dagger(\tau,\vec{0})U_j^\dagger(\tau,\hat{k})U_0^\tau(\vec{0})U_j(0,\hat{k})U_k(0,\vec{0})\big\rangle\Big] \\
&\overset{!}{=} \sum_{jk}\Big[\big\langle\mathcal{O}_1^{jk}\big\rangle - \big\langle\mathcal{O}_2^{jk}\big\rangle\Big].
\end{aligned} \tag{B.13}$$

In the second step,

$$\sum_i \varepsilon_{ijk}\varepsilon_{imn} = \delta_{jm}\delta_{kn} - \delta_{jn}\delta_{km} \tag{B.14}$$

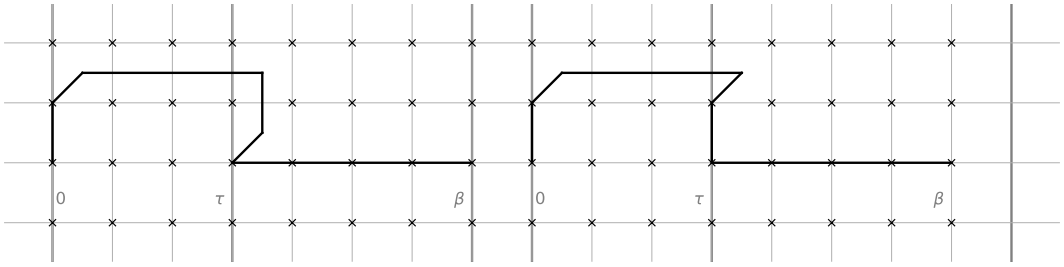


Figure B.2: The two operators that make up the numerator of $G_B^{\text{latt}}$. Left: $\mathcal{O}_1$. Right: $\mathcal{O}_2$. From left to right runs time, the vertical axis is the $j^{\text{th}}$ spatial direction while the axis orthogonal to the drawing plane is the $k^{\text{th}}$ one.

was used. While Eq. (7.15) or Fig. 10 appear to consist of four operators instead of only two, the two missing ones are included in the sum over $j$ and $k$. The two operators defined in Eq. (B.13) are sketched in Fig. B.2. Equivalent to the color-electric case, they are now expanded in $A_\mu$. This calculation will not be as detailed as for $G_E^{\text{latt}}$ since similar things occur: After expanding the exponential, the linear order disappears because of the tracelessness of Lie algebra elements. Also, after solving the square of the second quadratic order, only those products with one factor from the first and one factor from the second 'bend' survive if both operators are summed. The rest is therefore again summarized in $A_{\text{rest}}$. Begin with $\mathcal{O}_1^{jk}$:

$$\left\langle \mathcal{O}_1^{jk} \right\rangle = \operatorname{Re}\operatorname{Tr}\Big\langle \Big[1 - a^2 g_0^2 \big(A_j(0,\vec{0})A_j(\tau,\hat{k}) + A_j(0,\vec{0})A_k(\tau,\vec{0}) + A_k(0,\hat{\jmath})A_j(\tau,\hat{k}) + A_k(0,\hat{\jmath})A_k(\tau,\vec{0}) + A_{\text{rest}}^2\big)\Big]\Big\rangle + \mathcal{O}(g_0^3). \tag{B.15}$$

Continue with $\mathcal{O}_2^{jk}$:

$$\left\langle \mathcal{O}_2^{jk} \right\rangle = \operatorname{Re}\operatorname{Tr}\Big\langle \Big[1 - a^2 g_0^2 \big(A_j(0,\vec{0})A_k(\tau,\hat{\jmath}) + A_j(0,\vec{0})A_j(\tau,\vec{0}) + A_k(0,\hat{\jmath})A_k(\tau,\hat{\jmath}) + A_k(0,\hat{\jmath})A_j(\tau,\vec{0}) + A_{\text{rest}}^2\big)\Big]\Big\rangle + \mathcal{O}(g_0^3). \tag{B.16}$$

Subtracting them according to Eq. (B.13) gives

$$\begin{aligned} -\operatorname{Re}\operatorname{Tr}\big\langle & A_j(0,\vec{0})A_j(\tau,\hat{k}) + A_j(0,\vec{0})A_k(\tau,\vec{0}) + A_k(0,\hat{\jmath})A_j(\tau,\hat{k}) + A_k(0,\hat{\jmath})A_k(\tau,\vec{0}) \\ & - A_j(0,\vec{0})A_k(\tau,\hat{\jmath}) - A_j(0,\vec{0})A_j(\tau,\vec{0}) - A_k(0,\hat{\jmath})A_k(\tau,\hat{\jmath}) - A_k(0,\hat{\jmath})A_j(\tau,\vec{0})\big\rangle. \end{aligned} \tag{B.17}$$

Again, the $A_jA_j$ , $A_kA_k$ and mixed parts are transformed separately for better overview. For the $A_jA_j$ part one finds

$$\begin{aligned} & \operatorname{Tr}\big\langle A_j(0,\vec{0})A_j(\tau,\hat{k}) - A_j(0,\vec{0})A_j(\tau,\vec{0})\big\rangle \\ =& \sum\!\!\!\!\!\!\int_{pp'} e^{i(p_j+p'_j)a/2}\Big(e^{i(p'_0\tau+p'_k a)} - e^{ip'_0\tau}\Big)\operatorname{Tr}\big\langle \tilde{A}_j(p)\tilde{A}_j(p')\big\rangle \\ =& \frac{1}{2}\delta^{CD}\sum\!\!\!\!\!\!\int_p e^{-ip_0\tau}e^{-ip_k a/2}(e^{-ip_k a/2} - e^{ip_k a/2})D_{jj}^{CD}(p) + \mathcal{O}(g_0) \\ =& -\frac{ia}{2}\delta^{CD}\sum\!\!\!\!\!\!\int_p e^{-ip_0\tau}e^{-ip_k a/2}\hat{p}_k D_{jj}^{CD}(p) + \mathcal{O}(g_0). \end{aligned} \tag{B.18}$$

The $A_kA_k$ term is equivalent with $j \leftrightarrow k$ except for an overall sign so that it gives

$$\frac{ia}{2}\delta^{CD}\sum\!\!\!\!\!\!\int_p e^{-ip_0\tau}e^{ip_j a/2}\hat{p}_j D_{kk}^{CD}(p). \tag{B.19}$$

Renaming the indices, justified by the fact that they are summed over, the $A_jA_j$ and $A_kA_k$ parts together are therefore

$$\begin{aligned} & \frac{ia}{2}\delta^{CD}\sum\!\!\!\!\!\!\int_p e^{-ip_0\tau}\Big(-e^{-ip_k a/2} + e^{ip_k a/2}\Big)\hat{p}_k D_{jj}^{CD}(p) + \mathcal{O}(g_0) \\ & \qquad = -\frac{a^2}{2}\delta^{CD}\sum\!\!\!\!\!\!\int_p e^{-ip_0\tau}\hat{p}_k^2 D_{jj}^{CD}(p) + \mathcal{O}(g_0). \end{aligned} \tag{B.20}$$

Proceeding with the mixed part, one finds

$$
\begin{aligned}
&\mathrm{Tr}\big\langle A_k(0,\hat{\jmath})A_j(\tau,\hat{k}) - A_k(0,\hat{\jmath})A_j(\tau,\vec{0}) + A_j(0,\vec{0})A_k(\tau,\vec{0}) - A_j(0,\vec{0})A_k(\tau,\hat{\jmath})\big\rangle \\
=&\sum\!\!\!\!\!\!\int_{pp'}\Big[e^{ip_k a/2}e^{ip'_j a/2}\Big(e^{ip_j a}e^{i(p'_0\tau+p'_k a)} - e^{ip_j a}e^{ip'_0\tau}\Big)\,\mathrm{Tr}\big\langle\tilde{A}_k(p)\tilde{A}_j(p')\big\rangle \\
&\qquad e^{ip_j a/2}e^{ip'_k a/2}\Big(e^{ip'_0\tau} - e^{i(p'_0\tau+p'_j a)}\Big)\,\mathrm{Tr}\big\langle\tilde{A}_j(p)\tilde{A}_k(p')\big\rangle\Big] \\
=&\frac{1}{2}\delta^{CD}\sum\!\!\!\!\!\!\int_p e^{-ip_0\tau}\Big[e^{ip_j a/2}\Big(e^{-ip_k a/2} - e^{ip_k a/2}\Big) + e^{-ip_k a/2}\Big(e^{ip_j a/2} - e^{-ip_j a/2}\Big)\Big]D^{CD}_{jk}(p) + \mathcal{O}(g_0). \\
=&\frac{-ia}{2}\delta^{CD}\sum\!\!\!\!\!\!\int_p e^{-ip_0\tau}\hat{p}_j\Big(e^{ip_k a/2} - e^{-ip_k a/2}\Big)D^{CD}_{jk}(p) + \mathcal{O}(g_0) \\
=&\frac{a^2}{2}\delta^{CD}\sum\!\!\!\!\!\!\int_p e^{-ip_0\tau}\hat{p}_j\hat{p}_k D^{CD}_{jk}(p) + \mathcal{O}(g_0)
\end{aligned}
\tag{B.21}
$$

To put everything together, similar considerations to $G_E^{\text{latt}}$ need to be made: The exponential turns into into a cosine since one takes the real part, the overall factor of $1/3$ needs to be included while the leading order contribution of the denominator gives a factor of $N_c = 3$ . Replacing the flowed propagator by the unflowed one and renaming some summation indices finally gives Eq. (7.27).

## B.1. Analytical solution for $G_E$ and $G_B$ on the lattice with Wilson action and flow

In this section, the solution of Eq. (7.20) shall be derived. Consider its first term:

$$
\begin{aligned}
\int_p e^{-2\tau_F\hat{p}^2} &= e^{-8\frac{\tau_F}{a^2}\sin^2(\frac{p_0 a}{2})}\left(\int_{-\pi/a}^{\pi/a}\frac{\mathrm{d}p_i}{2\pi}e^{-8\frac{\tau_F}{a^2}\sin^2(\frac{p_i a}{2})}\right)^3 \\
&= e^{-8\tau_F T^2 N_\tau^2\sin^2(\frac{\pi n}{N_\tau})}\left(\frac{1}{TN_\tau}\int_{-\pi}^{\pi}\frac{\mathrm{d}u}{2\pi}e^{-8\tau_F T^2 N_\tau^2\sin^2(\frac{u}{2})}\right)^3 \\
&= e^{-8\tau_F T^2 N_\tau^2\sin^2(\frac{\pi n}{N_\tau})}\left(\frac{1}{TN_\tau}\int_{-\pi}^{\pi}\frac{\mathrm{d}u}{2\pi}e^{-4\tau_F T^2 N_\tau^2(1-\cos u)}\right)^3 \\
&= T^3 N_\tau^3 e^{-8\tau_F T^2 N_\tau^2\sin^2(\frac{\pi n}{N_\tau})}e^{-12\tau_F T^2 N_\tau^2}\left(\int_0^{\pi}\frac{\mathrm{d}u}{\pi}e^{4\tau_F T^2 N_\tau^2\cos u}\right)^3 \\
&= T^3 N_\tau^3 e^{-8\tau_F T^2 N_\tau^2\sin^2(\frac{\pi n}{N_\tau})}e^{-12\tau_F T^2 N_\tau^2} I_0\left(4\tau_F T^2 N_\tau^2\right)^3.
\end{aligned}
\tag{B.22}
$$

In the second step, $a = 1/(TN_\tau)$ and Eq. (7.1) were used. In the third step, the trigonometric relation

$$
\sin^2 x = \frac{1}{2}(1-\cos 2x) \tag{B.23}
$$

was taken advantage of while in the fourth step, the symmetry of the integrand was exploited. Finally, in the last step, Eq. (7.21) with $\gamma = 0$ and $z = 4\tau_F T^2 N_\tau^2$ was utilized. The second term of Eq. (7.20) requires slightly more work because of the $\hat{p}^2$ in the denominator. This can be resolved with the same trick as in Eq. (8.20), that is by inserting

$$
1 = a^2\int_0^\infty \mathrm{d}x\hat{p}^2 e^{-xa^2\hat{p}^2} \tag{B.24}
$$

into the integral so that the expression turns into

$$
\begin{aligned}
\int_p e^{-2\tau_F\hat{p}^2}\frac{\hat{p}_i^2}{\hat{p}^2} &= a^2\int_0^\infty \mathrm{d}x\int_p e^{-xa^2\hat{p}^2}e^{-2\tau_F\hat{p}^2}\hat{p}_i^2 \\
&= a^2 e^{-8\tau_F\sin^2(\frac{\pi n}{N_\tau})}\int_0^\infty \mathrm{d}x e^{-4x\sin^2(\frac{\pi n}{N_\tau})}\int_p e^{-(xa^2+2\tau_F)\sum_j\hat{p}_j}\hat{p}_i^2.
\end{aligned}
\tag{B.25}
$$

The momentum integration is now analytically possible. First, evaluate the integral over $p_i$:

$$\begin{aligned}
&a^2 \int_{-\pi/a}^{\pi/a} \frac{\mathrm{d}p_i}{2\pi} e^{-4(x+2\tau_F/a^2)\sum_j \sin^2\frac{p_j a}{2}} \hat{p_i^2} \\
=&\frac{4}{a} e^{-4(x+2\tau_F/a^2)\sum\limits_{j\neq i}\sin^2(\frac{p_j a}{2})} \int_0^{\pi} \frac{\mathrm{d}u}{\pi} e^{-4(x+2\tau_F/a^2)\sin^2\left(\frac{u}{2}\right)} \sin^2(\frac{u}{2}) \\
=&\frac{2}{a} e^{-4(x+2\tau_F T^2 N_\tau^2)\sum\limits_{j\neq i}\sin^2(\frac{p_j a}{2})} \int_0^{\pi} \frac{\mathrm{d}u}{\pi} e^{-2(x+2\tau_F T^2 N_\tau^2)(1-\cos u)} (1-\cos u) \\
=&\frac{2}{a} e^{-4(x+2\tau_F T^2 N_\tau^2)\sum\limits_{j\neq i}\sin^2(\frac{p_j a}{2})} e^{-2(x+2\tau_F T^2 N_\tau^2)} \Big( I_0\left(2x+4\tau_F T^2 N_\tau^2\right) - I_1\left(2x+4\tau_F T^2 N_\tau^2\right)\Big).
\end{aligned} \tag{B.26}$$

The same methods as previously were used. The $p_j$ integration is equivalent to Eq. (B.22) so that one finds

$$a^2 \int_p e^{-xa^2\sum_j \hat{p}_j^2} e^{-2\tau_F \sum_j \hat{p}_j^2} \hat{p}_i^2 = 2T^3 N_\tau^3 e^{-6(x+2\tau_F T^2 N_\tau^2)} I_0(2x+4\tau_F T^2 N_\tau^2)^2 \Big( I_0(2x+4\tau_F T^2 N_\tau^2) - I_1(2x+4\tau_F T^2 N_\tau^2)\Big). \tag{B.27}$$

Finally, after performing the summation over $j$ that simply amounts to a factor of 3 as well as substituting $2x + 4\tau_F T^2 N_\tau^2 \to x$ in the integration, tying everything together yields Eq. (7.22). Since the Wilson-Wilson case of the color-magnetic correlator $G_B^{\mathrm{WW}}$ is the same as the second term of $G_E^{\mathrm{WW}}$ with opposite sign, see Eqs. (7.20) and (7.28), the corresponding calculation from above can be copied and one arrives at Eq. (7.29).

## C. Action density integrations and notation

To understand the small $a$ deviations of the action densities, the leading order continuum expectation value under gradient flow needs to be derived first:

$$\begin{aligned}
\left\langle \varepsilon^{\mathrm{cont}}(\tau_F)\right\rangle_0 =&\frac{g_0^2}{4}\left\langle G^C_{\mu\nu}(x) G^C_{\mu\nu}(x)\right\rangle_0 \\
=&\frac{g_0^2}{4}\sum_{\mu\nu}\left\langle \left(\partial_\mu B^C_\nu(x) - \partial_\nu B^C_\mu(x)\right)^2\right\rangle_0 \\
=&\frac{g_0^2}{4}\left\langle \partial_\mu B^C_\nu(x) - 2\partial_\mu B^C_\nu(x)\partial_\nu B^C_\mu(x) + \partial_\nu B^C_\mu(x)\partial_\nu B^C_\mu(x)\right\rangle_0 \\
=&\frac{g_0}{2}\left\langle \partial_\mu B^C_\nu(x)\partial_\mu B^C_\nu(x) - \partial_\mu B^C_\nu(x)\partial_\nu B^C_\mu(x)\right\rangle_0 \\
=&-\frac{g_0^2}{2}\int_{pp'} e^{i(p+p')x}\left[p_\mu p'_\mu \left\langle \tilde{B}^C_\nu(p)\tilde{B}^C_\nu(p')\right\rangle_0 - p_\mu p'_\nu \left\langle \tilde{B}^C_\nu(p)\tilde{B}^C_\mu(p')\right\rangle_0\right] \\
=&\frac{g_0^2}{2}\int_p \left(p^2\delta_{\mu\nu} - p_\mu p_\nu\right)(D^{\mathrm{flow}})^{CC}_{\mu\nu}(p).
\end{aligned} \tag{C.1}$$

The argument $\tau_F$ of the flowed fields was omitted for brevity. In the second step, the quadratic term in the field strength was dropped since it only contributes to higher orders. In the fourth step, indices were renamed. In the second-to-last step, $p'$ was integrated over by considering the delta distribution in the propagator. Choosing flow and action Feynman gauge, the flowed continuum propagator in the last line turns into $\delta^{CC}\delta_{\mu\nu}\exp(-2\tau_F p^2)/p^2$. Inserting this gives

$$\begin{aligned}
\left\langle \varepsilon^{\mathrm{cont}}(\tau_F)\right\rangle_0 =&\frac{g_0^2}{2}\int_p \left(p^2\delta_{\mu\nu} - p_\mu p_\nu\right)\delta_{\mu\nu}\frac{e^{-2\tau_F p^2}}{p^2}\delta^{CC} \\
=&\frac{g_0^2}{2}\delta^{CC}\int_p \frac{e^{-2\tau p^2}}{p^2}\left(p^2\delta_{\mu\mu} - p_\mu p_\mu\right) \\
=&\frac{3g_0^2}{2}\delta^{CC}\int_p e^{-2\tau_F p^2} \\
=&\frac{3g_0^2}{2}\delta^{CC}\left(\int_{\mathbb{R}}\frac{\mathrm{d}p_\mu}{2\pi}e^{-2\tau_F p_\mu^2}\right)^4.
\end{aligned} \tag{C.2}$$

This is a gaussian integral which can be solved straightforwardly. The width of the gaussian function is $1/(\sqrt{4\tau_F})$ so the integral is $(\sqrt{2\pi}\sqrt{4\tau_F})^{-1}$. Inserting this and the sum over the Lie algebra indices $C$ which gives the factor $N_c^2 - 1$ returns Eq. (8.2).

## C.1. Notation of lattice momenta

Here, the notation of the lattice momenta appearing in Table 1 is summarized:

$$\begin{aligned}
\hat{p}_\mu &= \frac{2}{a}\sin\frac{p_\mu a}{2} \\
\mathring{p}_\mu &= \frac{1}{a}\sin p_\mu a \\
\check{p}_\mu &= \frac{1}{2a}\sin 2p_\mu a \\
\hat{p}^2 &= \sum_\mu \hat{p}_\mu^2 \\
\mathring{p}^2 &= \sum_\mu \mathring{p}_\mu^2 \\
\check{p}^2 &= \sum_\mu \check{p}_\mu^2 \\
\hat{c}_\mu &= \cos\frac{p_\mu a}{2} \\
\mathring{c}_\mu &= \cos p_\mu a \\
\check{c}_\mu &= \cos 2p_\mu a
\end{aligned} \tag{C.3}$$

It is clear that the first three approach $p_\mu$ with $a \to 0$ while the last three approach one.

## C.2. Analytical solution for Wilson-Wilson-Wilson

Choosing Wilson action, observable and flow allows an analytical solution for Eq. (8.12) that shall be derived in the following. The kernel is obviously the same for each part and can be taken from Table 1. The unflowed propagator which is the kernel's inverse is in Feynman gauge

$$\left(K^{-1}\right)^{\mathrm{CD}}_{\mu\nu}(p) = \frac{1}{\hat{p}^2}\delta_{\mu\nu}\delta^{CD}. \tag{C.4}$$

Choosing Feynman gauge for flow as well, inserting the three kernels into Eq. (8.12) gives

$$\begin{aligned}
\left\langle \varepsilon^{\text{W-W-W}}(\tau_F)\right\rangle_0 &= \frac{g_0^2}{2}\int_p (\hat{p}^2\delta_{\mu\nu} - \hat{p}_\mu\hat{p}_\nu)\delta^{CD} e^{-\tau_F\hat{p}^2}\delta_{\mu\sigma} e^{-\tau_F\hat{p}^2}\delta_{\nu\rho}\frac{1}{\hat{p}^2}\delta_{\sigma\rho}\delta^{CD} \\
&= \frac{g_0^2}{2}\delta^{CC}\int_p (\hat{p}^2\delta_{\mu\mu} - \hat{p}_\mu\hat{p}_\mu)\frac{e^{-2\tau_F\hat{p}^2}}{\hat{p}^2} \\
&= \frac{3g_0^2}{2}\delta^{CC}\int_p e^{-2\tau_F\hat{p}^2} \\
&= \frac{3g_0^2}{2}\delta^{CC}\left(\int_{-\pi/a}^{\pi/a}\frac{\mathrm{d}p_\mu}{2\pi}e^{-8\frac{\tau_F}{a^2}\sin^2\left(\frac{p_\mu a}{2}\right)}\right)^4 \\
&= \frac{3g_0^2}{2a^4}\delta^{CC}\left(\int_{-\pi}^{\pi}\frac{\mathrm{d}u}{2\pi}e^{-4\frac{\tau_F}{a^2}(1-\cos u)}\right)^4 \\
&= \frac{3g_0^2}{2a^4}\delta^{CC}e^{-16\frac{\tau_F}{a^2}}\left(\int_{-\pi}^{\pi}\frac{\mathrm{d}u}{2\pi}e^{4\frac{\tau_F}{a^2}\cos u}\right)^4 \\
&= \frac{3g_0^2}{2a^4}\delta^{CC}e^{-16\frac{\tau_F}{a^2}}I_0\left(\frac{4\tau_F}{a^2}\right)^4.
\end{aligned} \tag{C.5}$$

Performing the sum over $C$ yields Eq. (8.13).

## D. Derivation of naive and improved clover kernel

Here, the kernels of the naive and improved clover kernel given in Table 1 shall be derived. Start with the clover field strength Eq. (8.7). To leading order, each of the four plaquettes can be expanded like

$$\begin{aligned} P_{\sigma\rho}(n) &= \exp\Big[iag_0\big(A_\sigma(n) + A_\rho(n+\hat{\sigma}) - A_\sigma(n+\hat{\rho}) - A_\rho(n)\big) + \mathcal{O}(g_0^2)\Big] \\ &= 1 + iag_0\big(A_\sigma(n) + A_\rho(n+\hat{\sigma}) - A_\sigma(n+\hat{\rho}) - A_\rho(n)\big) + \mathcal{O}(g_0^2). \end{aligned} \tag{D.1}$$

Then, adding all four plaquettes contributing to the clover, only the eight links on the overall contour survive, those in the middle cancel out. Therefore, the clover field strength is

$$\begin{aligned} F^{\mathrm{cl}}_{\mu\nu}(x) &= \frac{ig_0}{2a}\,\mathrm{Tr}\Big[T^C\Big(\frac{4}{ig_0} + A_\nu(n+\hat{\mu}-\hat{\nu}) + A_\nu(n+\hat{\mu}) - A_\nu(x-\hat{\mu}) - A_\nu(n-\hat{\mu}-\hat{\nu}) - (\mu\leftrightarrow\nu)\Big)\Big]T^C + \mathcal{O}(g_0^2) \\ &= \frac{ig_0}{4a}\big(A_\nu(n+\hat{\mu}-\hat{\nu}) + A_\nu(n+\hat{\mu}) - A_\nu(n-\hat{\mu}) - A_\nu(n-\hat{\mu}-\hat{\nu}) - (\mu\leftrightarrow\nu)\big) + \mathcal{O}(g_0^2). \end{aligned} \tag{D.2}$$

Fourier transforming this leads to

$$\begin{aligned} F^{\mathrm{cl}}_{\mu\nu}(n) &= \frac{ig_0}{a}\int_p e^{ipan}\Big[e^{ip_\nu a/2}\big(e^{i(p_\mu-p_\nu)a} + e^{ip_\mu a} - e^{-ip_\mu a} - e^{-i(p_\mu+p_\nu)a}\big)\tilde{A}_\nu(p) - \big(\mu\leftrightarrow\nu\big)\Big] + \mathcal{O}(g_0^2) \\ &= \frac{ig_0}{a}\int_p e^{ipan}\Big[\big(e^{ip_\nu a/2} + e^{-ip_\nu a/2}\big)\big(e^{ip_\mu a} - e^{-ip_\mu a}\big)\tilde{A}_\nu(p) - \big(\mu\leftrightarrow\nu\big)\Big] + \mathcal{O}(g_0) \\ &= -g_0\int_p e^{ipan}\Big[\hat{c}_\nu\mathring{p}_\mu\tilde{A}_\nu(p) - \hat{c}_\mu\mathring{p}_\nu\tilde{A}_\mu(p)\Big] + \mathcal{O}(g_0^2). \end{aligned} \tag{D.3}$$

Notation is explained in Appendix C.1. Consequently, with Eq. (8.8), the clover action density is

$$\begin{aligned} \big\langle\varepsilon^{\mathrm{cl}}\big\rangle &= -\frac{g_0^2}{2}\sum_{\mu\nu}\int_{pp'} e^{i(p+p')an}\,\mathrm{Tr}\big\langle\hat{c}_\nu\mathring{p}_\mu\hat{c}'_\nu\mathring{p}'_\mu\tilde{A}_\nu(p)\tilde{A}_\nu(p') - \hat{c}_\nu\mathring{p}_\mu\hat{c}'_\mu\mathring{p}'_\nu\tilde{A}_\nu(p)\tilde{A}_\mu(p') \\ &\qquad - \hat{c}_\mu\mathring{p}_\nu\hat{c}'_\nu\mathring{p}'_\mu\tilde{A}_\mu(p)\tilde{A}_\nu(p') + \hat{c}_\mu\mathring{p}_\nu\hat{c}'_\mu\mathring{p}'_\nu\tilde{A}_\mu(p)\tilde{A}_\mu(p')\big\rangle + \mathcal{O}(g_0^3) \\ &= -g_0^2\sum_{\mu\nu}\int_{pp'} e^{i(p+p')an}\,\mathrm{Tr}\big\langle\hat{c}_\nu\mathring{p}_\mu\hat{c}'_\nu\mathring{p}'_\mu\tilde{A}_\nu(p)\tilde{A}_\nu(p') - \hat{c}_\nu\mathring{p}_\mu\hat{c}'_\mu\mathring{p}'_\nu\tilde{A}_\nu(p)\tilde{A}_\mu(p')\big\rangle + \mathcal{O}(g_0^3) \\ &= -\frac{g_0^2}{2}\sum_{\mu\nu}\int_{pp'} e^{i(p+p')an}\delta^{CD}\big\langle\hat{c}_\nu\mathring{p}_\mu\hat{c}'_\nu\mathring{p}'_\mu\tilde{A}^C_\nu(p)\tilde{A}^D_\nu(p') - \hat{c}_\nu\mathring{p}_\mu\hat{c}'_\mu\mathring{p}'_\nu\tilde{A}^C_\nu(p)\tilde{A}^D_\mu(p')\big\rangle + \mathcal{O}(g_0^3) \\ &= \frac{g_0^2}{2}\sum_{\mu\nu}\int_p \delta^{CD}\big(\hat{c}_\nu^2\mathring{p}_\mu^2 D^{CD}_{\nu\nu}(p) - \hat{c}_\nu\mathring{p}_\mu\hat{c}_\mu\mathring{p}_\nu D^{CD}_{\mu\nu}(p)\big) + \mathcal{O}(g_0^3) \\ &= \frac{g_0^2}{2}\sum_{\mu\nu}\int_p \delta^{CD}\big(\hat{c}_\mu\mathring{p}^2\delta_{\mu\nu} - \hat{c}_\nu\mathring{p}_\mu\hat{c}_\mu\mathring{p}_\nu\big)D^{CD}_{\mu\nu}(p) + \mathcal{O}(g_0^3). \end{aligned} \tag{D.4}$$

In the second step, indices were renamed. In the fourth step, the delta distribution in the propagator was integrated over. Under gradient flow, the propagator in the last line merely needs to be replaced by the flowed one. The clover kernel given in Table 1 can now easily be read off.

To obtain the improved clover, the rectangle clover field strength Eq. (8.9) needs to be considered first. When expanding the links to linear order and summing the loops, only the contour survives again. Therefore, the rectangle clover field strength reads

$$\begin{aligned} F^{\text{r-cl}}_{\mu\nu}(n) &= \frac{ig_0}{8a}\,\mathrm{Tr}\Big[T^C\Big(\frac{4}{ig_0} + A_\nu(n+2\hat{\mu}-\hat{\nu}) + A_\nu(n+2\hat{\mu}) - A_\mu(n+\hat{\mu}+\hat{\nu}) - A_\mu(n+\hat{\nu}) \\ &\qquad - A_\mu(n-\hat{\mu}+\hat{\nu}) - A_\mu(n-2\hat{\mu}+\hat{\nu}) - A_\nu(n-2\hat{\mu}) - A_\nu(n-2\hat{\mu}-\hat{\nu}) \\ &\qquad + A_\mu(n-2\hat{\mu}-\hat{\nu}) + A_\mu(n-\hat{\mu}-\hat{\nu}) + A_\mu(n-\hat{\nu}) + A_\mu(n+\hat{\mu}-\hat{\nu}) + (\mu\leftrightarrow\nu)\Big)\Big]T^C + \mathcal{O}(g_0^2) \\ &= \frac{ig_0}{16a}\big(A_\nu(n+2\hat{\mu}-\hat{\nu}) + A_\nu(n+2\hat{\mu}) - A_\mu(n+\hat{\mu}+\hat{\nu}) - A_\mu(n+\hat{\nu}) \\ &\quad - A_\mu(n-\hat{\mu}+\hat{\nu}) - A_\mu(n-2\hat{\mu}+\hat{\nu}) - A_\nu(n-2\hat{\mu}) - A_\nu(n-2\hat{\mu}-\hat{\nu}) \\ &\quad + A_\mu(n-2\hat{\mu}-\hat{\nu}) + A_\mu(n-\hat{\mu}-\hat{\nu}) + A_\mu(n-\hat{\nu}) + A_\mu(n+\hat{\mu}-\hat{\nu}) + (\mu\leftrightarrow\nu)\big) + \mathcal{O}(g_0^2). \end{aligned} \tag{D.5}$$

The $A_\mu$ and $A_\nu$ parts are Fourier transformed separately for better overview. However, note that the $\mu \leftrightarrow \nu$ part is then not included on which will be caught up afterwards. Begin with $A_\mu$:

$$\begin{aligned}
&- A_\mu(n+\hat{\mu}+\hat{\nu}) - A_\mu(n+\hat{\nu}) - A_\mu(n-\hat{\mu}+\hat{\nu}) - A_\mu(n-2\hat{\mu}+\hat{\nu}) \\
&+ A_\mu(n-2\hat{\mu}-\hat{\nu}) + A_\mu(n-\hat{\mu}-\hat{\nu}) + A_\mu(n-\hat{\nu}) + A_\mu(n+\hat{\mu}-\hat{\nu}) \\
=&\int_p e^{ipan} e^{ip_\mu a/2} \big(-e^{i(p_\mu+p_\nu)a} - e^{ip_\nu a} - e^{i(-p_\mu+p_\nu)a} - e^{i(-2p_\mu+p_\nu)a} \\
&\qquad + e^{-i(2p_\mu+p_\nu)a} + e^{-i(p_\mu+p_\nu)a} + e^{-ip_\nu a} + e^{i(p_\mu-p_\nu)a}\big)\tilde{A}_\mu(p) \\
=&-\int_p e^{ipan}\big(e^{ip_\mu a} + e^{-ip_\mu a}\big)\big(e^{ip_\mu a/2} + e^{-ip_\mu a/2}\big)\big(e^{ip_\nu a} - e^{ip_\nu a}\big)\tilde{A}_\mu(p) \\
=&-8ai\int_p e^{ipan}\mathring{c}_\mu\hat{c}_\mu\mathring{p}_\nu\tilde{A}_\mu(p).
\end{aligned} \tag{D.6}$$

Continue with $A_\nu$:

$$\begin{aligned}
&A_\nu(n+2\hat{\mu}-\hat{\nu}) + A_\nu(n+2\hat{\mu}) - A_\nu(n-2\hat{\mu}) - A_\nu(n-2\hat{\mu}-\hat{\nu}) \\
=&\int_p e^{ipan} e^{ip_\nu a/2}\big(e^{i(2p_\mu-p_\nu)a} + e^{i2p_\mu a} - e^{-i2p_\mu a} - e^{-i(2p_\mu+p_\nu)a}\big)\tilde{A}_\nu(p) \\
=&\int_p e^{ipan}\big(e^{i2p_\mu a} - e^{-i2p_\mu a}\big)\big(e^{ip_\nu a/2} + e^{-ip_\nu a/2}\big)\tilde{A}_\nu(p) \\
=&8ai\int_p e^{ipan}\hat{c}_\nu\check{p}_\mu\tilde{A}_\nu(p).
\end{aligned} \tag{D.7}$$

Inserting this into the rectangle clover field strength and symmetrizing by adding the $\mu \leftrightarrow \nu$ part, one obtains

$$F^{\text{r-cl}}_{\mu\nu}(n) = -\frac{g_0}{2}\int_p e^{ipan}\Big(\hat{c}_\nu(\mathring{c}_\nu\mathring{p}_\mu + \check{p}_\mu)\tilde{A}_\nu(p) - \hat{c}_\mu(\mathring{c}_\mu\mathring{p}_\nu + \check{p}_\nu)\tilde{A}_\mu(p)\Big) + \mathcal{O}(g_0^2). \tag{D.8}$$

This is used to find the rectangle and mixed clover action density by contracting it with itself or $F^{\text{cl}}_{\mu\nu}$ respectively. The steps to arrive at the result are the same as for the clover action density, see Eq. (D.4), so the first few steps, for example executing the delta distribution in the propagator, are not outlined explicitly. One finds

$$\begin{aligned}
\big\langle\varepsilon^{\text{r-cl}}\big\rangle &= \frac{g_0^2}{8}\sum_{\mu\nu}\int_p \delta^{CD}\Big(\hat{c}_\nu^2(\mathring{c}_\nu\mathring{p}_\mu + \check{p}_\mu)^2 D^{CD}_{\nu\nu}(p) - \hat{c}_\mu\hat{c}_\nu(\mathring{c}_\nu\mathring{p}_\mu + \check{p}_\mu)(\mathring{c}_\mu\mathring{p}_\nu + \check{p}_\nu)D^{CD}_{\mu\nu}(p)\Big) + \mathcal{O}(g_0^3) \\
&= \frac{g_0^2}{8}\sum_{\mu\nu}\int_p \delta^{CD}\Big(\hat{c}_\nu^2(\mathring{c}_\nu^2\mathring{p}_\mu^2 + 2\mathring{c}_\nu\mathring{p}_\mu\check{p}_\mu + \check{p}_\mu^2)D^{CD}_{\nu\nu}(p) - \hat{c}_\mu\hat{c}_\nu(\mathring{c}_\mu\mathring{c}_\nu\mathring{p}_\mu\mathring{p}_\nu + \mathring{c}_\nu\mathring{p}_\mu\check{p}_\nu + \mathring{c}_\mu\check{p}_\mu\mathring{p}_\nu + \check{p}_\mu\check{p}_\nu)D^{CD}_{\mu\nu}(p)\Big) + \mathcal{O}(g_0^3) \\
&= \frac{g_0^2}{8}\sum_{\mu\nu}\int_p \delta^{CD}\Big(\hat{c}_\mu^2(\mathring{c}_\mu^2\mathring{p}^2 + \check{p}^2 + 2\mathring{c}_\mu\sum_\lambda\mathring{p}_\lambda\check{p}_\lambda)\delta_{\mu\nu} - \hat{c}_\mu\hat{c}_\nu(\mathring{c}_\mu\mathring{c}_\nu\mathring{p}_\mu\mathring{p}_\nu + \mathring{c}_\nu\mathring{p}_\mu\check{p}_\nu + \mathring{c}_\mu\check{p}_\mu\mathring{p}_\nu + \check{p}_\mu\check{p}_\nu\Big)D^{CD}_{\mu\nu}(p) + \mathcal{O}(g_0^3).
\end{aligned} \tag{D.9}$$

The rectangle clover kernel given in Table 1 can be read off there. Now only the mixed term consisting of plaquette and rectangle clover field strength is missing. Again skipping the first few steps, one finds

$$\begin{aligned}
\big\langle\varepsilon^{\text{m-cl}}\big\rangle &= \frac{g_0^2}{8}\sum_{\mu\nu}\int_p \delta^{CD}\Big(2\hat{c}_\nu^2\mathring{p}_\mu(\mathring{c}_\nu\mathring{p}_\mu + \check{p}_\mu)D^{CD}_{\nu\nu}(p) - \hat{c}_\mu\hat{c}_\nu(\mathring{p}_\mu(\mathring{c}_\mu\mathring{p}_\nu + \check{p}_\nu) + (\mathring{c}_\nu\mathring{p}_\mu + \check{p}_\mu)\mathring{p}_\nu)D^{CD}_{\mu\nu}(p)\Big) + \mathcal{O}(g_0^3) \\
&= \frac{g_0^2}{8}\sum_{\mu\nu}\int_p \delta^{CD}\Big(2\hat{c}_\nu^2(\mathring{c}_\nu\mathring{p}_\mu^2 + \mathring{p}_\mu\check{p}_\mu)D^{CD}_{\nu\nu}(p) - \hat{c}_\mu\hat{c}_\nu((\mathring{c}_\mu + \mathring{c}_\nu)\mathring{p}_\mu\mathring{p}_\nu + \mathring{p}_\mu\check{p}_\nu + \check{p}_\mu\mathring{p}_\nu)D^{CD}_{\mu\nu}(p)\Big) + \mathcal{O}(g_0^3) \\
&= \frac{g_0^2}{8}\sum_{\mu\nu}\int_p \delta^{CD}\Big(2\hat{c}_\mu^2(\mathring{c}_\mu\mathring{p}^2 + \sum_\lambda\mathring{p}_\lambda\check{p}_\lambda)\delta_{\mu\nu} - \hat{c}_\mu\hat{c}_\nu((\mathring{c}_\mu + \mathring{c}_\nu)\mathring{p}_\mu\mathring{p}_\nu + \mathring{p}_\mu\check{p}_\nu + \check{p}_\mu\mathring{p}_\nu)\Big)D^{CD}_{\mu\nu}(p) + \mathcal{O}(g_0^3).
\end{aligned} \tag{D.10}$$

Together with Eq. (8.11), the improved clover kernel given in Table 1 is found.

## References


[1] M. Peskin and D. Schroeder, *An Introduction to Quantum Field Theory*. CRC Press, 1995.

[2] S. Capitani, "Lattice Perturbation Theory," *Phys.Rept. 382 (2003) 113-302*, Nov. 2002.

[3] O. Philipsen, *Quantenfeldtheorie und das Standardmodell der Teilchenphysik - Eine Einführung*. Springer Spektrum, 2018.

[4] H. Fritzsch, M. Gell-Mann, and H. Leutwyler, "Advantages of the Color Octet Gluon Picture," *Physical Letters B*, 1973.

[5] K. Wilson, "Confinement of quarks," *Physical Review D*, 1974.

[6] M. Creutz, *Quarks, gluons and lattices*. Cambridge University Press, 1983.

[7] C. Gattringer and C. Lang, *Quantum Chromodynamics on the Lattice*. Springer, 2010.

[8] H. Rothe, *Lattice Gauge Theories - An Introduction*. World Scientific Lecture Notes in Physics, 3. ed., 2005.

[9] G. L. Naber, *Topology, Geometry and Gauge fields: Foundations*. Springer, 2. ed., 2011.

[10] G. L. Naber, *Topology, Geometry and Gauge fields: Interactions*. Springer, 2. ed., 2011.

[11] K. Symanzik, "Continuum limit and improved action in lattice theories: (I). Principles and $\phi^4$ theory," *Nuclear Physics B*, 1983.

[12] K. Symanzik, "Continuum limit and improved action in lattice theories: (II). $\mathcal{O}(n)$ non-linear sigma model in perturbation theory," *Nuclear Physics B*, 1983.

[13] M. Lüscher and P. Weisz, "On-Shell Improved Lattice Gauge Theories," *Communications in Mathematical Physics*, 1985.

[14] P. Weisz, "Continuum Limit Improved Action for Pure Yang-Mills Theory (I)," *Nuclear Physics B*, 1983.

[15] B. Sheikholeslami and R. Wohlert, "Improved Continuum Limit Lattice Action for QCD with Wilson Fermions," *Nuclear Physics B*, 1986.

[16] D. Gross and F. Wilczek, "Ultraviolet Behavior of Non-Abelian Gauge Theories," *Physical Review Letters*, 1973.

[17] D. Binosi, J. Collins, C. Kaufhold, and L. Theussl, "JaxoDraw: A graphical user interface for drawing Feynman diagrams. Version 2.0 release notes," Nov. 2008.

[18] M. Lüscher and P. Weisz, "Two loop relation between the bare lattice coupling and the MS coupling in pure SU(N) gauge theories," *Physics Letters B*, 1995.

[19] R. Sommer, "A New Way to Set the Energy Scale in Lattice Gauge Theories and its Application to the Static Force and $\alpha_s$ in SU(2) Yang-Mills Theory," *Nuclear Physics B*, 1994.

[20] P. Weisz and R. Wohlert, "Continuum Limit Improved Action for Pure Yang-Mills Theory (II)," *Nuclear Physics B*, 1983.

[21] M. Lüscher, "Properties and uses of the Wilson flow in lattice QCD," *JHEP 1008:071,2010*, June 2010.

[22] M. Lüscher, "Trivializing maps, the Wilson flow and the HMC algorithm," *Journal of High Energy Physics*, 2010.

[23] A. Ramos, "The Yang-Mills gradient flow and renormalization," *Proceedings of Science*, 2015.

[24] R. Narayanan and H. Neuberger, "Infinite N phase transitions in continuum Wilson loop operators," *Journal of High Energy Physics*, 2006.

[25] D. Borthwick, *Introduction to Partial Differential Equations*. Springer, 2016.

[26] M. Lüscher, "Chiral symmetry and the Yang-Mills gradient flow," *Journal of High Energy Physics*, 2013.

[27] M. Lüscher and P. Weisz, "Perturbative analysis of the gradient flow in non-abelian gauge theories," *JHEP 1102:051,2011*, Jan. 2011.

[28] A. Ramos and S. Sint, "Symanzik improvement of the gradient flow in lattice gauge theories," *European Physics Journal*, Aug. 2015.

[29] A. Ramos and S. Sint, "On $\mathcal{O}(a^2)$ effects in gradient flow observables," *Proceedings of Science*, Nov. 2014.

[30] J. Adams *et al.*, "Azimuthal anisotropy in Au+Au collisions at $\sqrt{s_{NN}}$ = 200 GeV ," *Physical Review C*, 2005.

[31] A. Adare *et al.*, "$J\Psi$ Productionvs Centrality, Transverse Momentum, and Rapidity in Au+Au collisions at $\sqrt{s_{NN}}$ = 200 GeV," *Physical Review Letters*, 2007.

[32] S. Adler *et al.*, "Elliptic flow of identified hadrons in Au+Au collisions at $\sqrt{s_{NN}}$ = 200 GeV," *Physical Review Letters*, 2003.

[33] H. B. Meyer, "Transport Properties of the Quark-Gluon Plasma - A Lattice QCD Perspective," *Eur.Phys.J.A47:86,2011*, Apr. 2011.

[34] J. I. Kapusta and C. Gale, *Finite-Temperature Field Theory - Principles and Applications*. Cambridge University Press, 2. ed., 2006.

[35] M. Laine and A. Vuorinen, *Basics of Thermal Field Theory: A Tutorial on Perturbative Computations*. Springer International Publishing, 2016.

[36] A. Einstein, "Über die von der molekularkinetischen Theorie der Wärme geforderte Bewegung von in ruhenden Flüssigkeiten suspendierten Teilchen," *Annalen der Physik*, 1905.

[37] P. Langevin, "Sur la théorie du mouvement brownien," *C. R. Acad. Sci. Paris*, 1908.

[38] R. Kubo, "Statistical-Mechanical Theory of Irreversible Processes. I. General Theory and Simple Applications to Magnetic and Conduction Problems," *J. Phys. Soc. Jpn.*, 1957.

[39] R. Kubo, M. Yokota, and S. Nakajima, "Statistical-Mechanical Theory of Irreversible Processes. II. Response to Thermal Disturbance," *J. Phys. Soc. Jpn*, 1957.

[40] S. Caron-Huot, M. Laine, and G. D. Moore, "A way to estimate the heavy quark thermalization rate from the lattice," *JHEP*, Jan. 2009.

[41] L. Altenkort, A. M. Eller, O. Kaczmarek, L. Mazur, G. D. Moore, and H.-T. Shu, "Heavy quark momentum diffusion from the lattice using gradient flow," *Physical Review D*, Sept. 2020.

[42] A. Bouttefeux and M. Laine, "Mass-suppressed effects in heavy quark diffusion," *JHEP 12 (2020) 150*, Oct. 2020.

[43] L. Altenkort, A. M. Eller, O. Kaczmarek, L. Mazur, G. D. Moore, and H.-T. Shu, "Continuum extrapolation of the gradient-flowed color-magnetic correlator at $1.5T_c$," *Proceedings of Science*, Nov. 2021.

[44] G. N. Watson, *A Treatise on the Theory of Bessel functions*. Cambrige University Press, 2. ed., 1944.

[45] M. Abramowitz and I. A. Stegun, *Handbook of Mathematical Functions with Formulas, Graphs, and Mathematical Tables*. United States Department of Commerce, National Bureau of Standards, 9. ed., 1972.

[46] A. M. Eller and G. D. Moore, "Gradient-flowed thermal correlators: how much flow is too much?," *Physical Review D*, Feb. 2018.

[47] L. Altenkort, A. M. Eller, O. Kaczmarek, L. Mazur, G. D. Moore, and H. T. Shu, "Lattice QCD noise reduction for bosonic correlators through Blocking," Dec. 2021.

[48] Z. Fodor, K. Holland, J. Kuti, S. Mondal, D. Nogradi, and C. H. Wong, "The lattice gradient flow at tree-level and its improvement," *Journal of High Energy Physics*, June 2014.

[49] C. Alexandrou, A. Athenodorou, K. Cichy, A. Dromard, E. Garcia-Ramos, K. Jansen, U. Wenger, and F. Zimmermann, "Comparison of topological charge definitions in Lattice QCD," *European Physics Journal C*, Aug. 2017.

[50] S. O. Bilson-Thompson, D. B. Leinweber, and A. G. Williams, "Highly improved lattice field-strength tensor," *Annals of Physics*, 2003.

[51] D. B. Owen, "A table of normal integrals," *Communications in Statistics - Simulation and Computation*, 1980.